UNIVERSITÄT HOHENHEIM
Institute of Soil Science and Land Evaluation
Biogeophysics department (310d)
Prof. Dr. Thilo Streck

Measuring and modelling of soil water dynamics in two German landscapes.

Dissertation

for the acquisition of the degree "Doktor der Agrarwissenschaften"
(Dr. sc. agr. / Ph. D. in Agricultural Science)
to the Faculty of Agricultural Sciences

Presented by
Maksim Poltoradnev
from Moscow, Russia
2018

Date of thesis acceptance: 05.07.2017

Date of the oral examination: 04.04.2018

Examination Committee

Supervisor and Referee:	Prof. Dr. Thilo Streck
Co-Referee:	Prof. Dr. Volker Wulfmeyer
Additional examiner:	Prof. Dr. Andreas Fangmeier
Dean:	Prof. Dr. Stefan Böttinger

Contents

1. Summary

The soil water regime is focus of various disciplines including agricultural sciences, hydrology, weather forecast and climate modelling. As an inherent part of land surface exchange processes, the dynamics of soil water content (SWC) is simulated in distributed hydrological models and land surface models (LSM). The accuracy of the simulated SWC directly influences the simulation outcome and its performance. Biases in modelled temporal SWC dynamics and its spatial distribution lead to errors in evapotranspiration, runoff, cloud and precipitation simulations. The main objective of my thesis was to study the factors that control the SWC dynamics and its spatial variability. Long-term measurements from the soil moisture networks Kraichgau (KR) and Swabian Alb (SA) provided the data basis of this study.

SWC was sensed based on the Time Domain Transmission (TDT) technique. In each region, 21 measuring locations were distributed across three spatial domains: an inner domain 3 km × 3 km (5 stations), a middle 9 km × 9 km (8 stations), and an outer domain 27 km × 27 km (8 stations). The sizes of the three domains correspond with typical grid sizes of coupled atmosphere-LSM models. All stations were mounted on cropped agricultural sites. Each station was equipped with a TDT sensor, installed 15 cm deep into the soil, a rain gauge and a remote transfer unit. After adjusting the sensor networks, an in-situ field calibration was performed to derive pedotransfer and site-specific calibrations for TDT soil moisture sensors. The chemical and physical analysis of soil samples collected at each station revealed that soil bulk density influences in both regions the TDT readings. Moreover, the pedotransfer calibrations included electrical conductivity in KR and silt fraction and organic nitrogen content on SA. These variables are relatively easy to measure. Accordingly, the pedotransfer calibrations derived in this study are a quick possibility to calibrate TDT sensors in areas with similar soil properties as in KR and SA. Nevertheless, the site-specific calibrations performed the best and were therefore used for further data analysis.

In the second study, a three-year record of SWC and rainfall was evaluated. The response of the regional mean ($\langle\theta\rangle$) of SWC to a rain event was influenced by the seasonal water balance (SWB). In KR, the relation was more pronounced for positive SWB and less for neutral and negative SWB. On SA, where SWB was highly positive in all three years, the response of $\langle\theta\rangle$ to rainfall was always strong. At the seasonal scale, the relationship between the spatial standard

deviation of SWC (σ_θ) and $\langle\theta\rangle$ was investigated through σ_θ-$\langle\theta\rangle$ phase-space diagrams. The results show that with decreasing SWC σ_θ-$\langle\theta\rangle$ data pairs are approaching σ_θ at the permanent wilting point (σ_θ-$\langle\theta_{wp}\rangle$). With increasing SWC, in contrast, σ_θ-$\langle\theta\rangle$ data pairs are moving towards σ_θ at saturation (σ_θ-$\langle\theta_s\rangle$). These two points were termed anchor points. The σ_θ-$\langle\theta\rangle$ relationships formed combinations of concave and convex hyperbolas reflecting the variability of soil texture and depending on σ_θ in relation to the anchor points. At the event scale, hysteresis in the σ_θ-$\langle\theta\rangle$ was observed. Most σ_θ-$\langle\theta\rangle$ clockwise hysteresis cases occurred at an intermediate and intermediate/wet state of SWC. Among the factors that trigger the initiation of a σ_θ-$\langle\theta\rangle$ hysteretic loop, the present study revealed the following: rainstorms with spatially highly variable intensities (threshold rainfall intensity of 1.1 ± 0.6 mm and 2.9 ± 2.8 mm for KR and SA, respectively), preferential flow and, possibly, hysteresis in soil water retention curves. Based on these results, the following hypothesis was formulated: σ_θ-$\langle\theta\rangle$ phase space diagrams are useful to test whether hydrological models or land surface models (LSMs) capture the realistic range of spatial soil water variability.

The concept was tested with the Noah-MP LSM. Observations obtained from KR and SA soil moisture networks over a three-year period from 2010 to 2012 were used to build up the σ_θ-$\langle\theta\rangle$ phase-space. The study included two different setups used to compute the hydraulic conductivity and the diffusivity: 1) the default setting: the Clapp and Hornberger approach, and 2) the van Genuchten-Mualem functions. The default model parameterization was stepwise substituted with site-specific rainfall, soil texture, leaf area index (LAI) and green vegetation fraction (GVF) data. The atmospheric forcing was obtained from eddy covariance stations located in the regions. Although the model matched observed temporal $\langle\theta\rangle$ dynamics fairly well for the loess soils of KR, it performed poorly in the case of the shallow, clayey and stony soils of SA. The best match was achieved with the van Genuchten-Mualem functions and site-specific rainfall, soil texture, GVF and LAI. Nevertheless, the Noah-MP LSM failed to represent the spatial variability of SWC. In most cases, the simulated σ_θ-$\langle\theta\rangle$ data points were located below the bottom edge of the envelope, which indicates that the model smooths spatial variability of soil moisture. This smoothing can be mainly attributed to missing topography and terrain information, inadequate representation of the spatial variability of soil texture and hydraulic parameters, and the model assumption of a uniform root distribution.

2. Zusammenfassung

Der Bodenwasserhaushalt steht im Fokus verschiedener Disziplinen, wie zum Beispiel den Agrarwissenschaften, der Hydrologie, der Wettervorhersage und der Klimamodellierung. Als ein inhärenter Teil von Landoberflächenaustauschprozessen wird die Dynamik des Bodenwassergehalts (SWC) in verteilten hydrologischen Modellen und Landoberflächenmodellen (LSM) simuliert. Die Genauigkeit der simulierten Bodenwassergehalte beeinflusst direkt die Qualität des Simulationsergebnisses. Systematische Fehler in der modellierten zeitlichen Dynamik des SWC und seiner räumlichen Verteilung führen zu Fehlern in der Evapotranspirations-, Abfluss-, Wolken- und Niederschlagssimulation. Das Hauptziel meiner Dissertation war es, die Faktoren zu untersuchen, die die zeitliche Dynamik und die räumliche Variabilität des SWC kontrollieren. Die Basis hierfür lieferten Langzeitmessungen aus den Bodenwassermessnetzen Kraichgau (KR) und Schwäbische Alb (SA).

Der SWC wurde auf der Grundlage der TDT-Technik (Time Domain Transmission) gemessen. In jeder Region wurden 21 Messstellen über drei räumliche Domänen verteilt: eine innere Domäne 3 km × 3 km (5 Stationen), eine mittlere 9 km × 9 km (8 Stationen) und eine äußere Domäne 27 km × 27 km (8 Stationen). Die Größen der drei Domänen entsprechen typischen Rastergrößen von gekoppelten Atmosphären-LSM Modellen. Alle Messstationen wurden auf ackerbaulich genutzten Standorten installiert. Jede Messstation war mit einem Aquaflex TDT-Sensor ausgestattet, der in 15 cm Tiefe installiert wurde, einen Regenmesser und eine Datenfernübertragungseinheit. Nach der Installation der Sensornetzwerke wurden in-situ-Feldkalibrierungen durchgeführt, um Pedotransfer- und standortspezifische Kalibrierungen für die TDT Bodenfeuchtesensoren abzuleiten. Die chemische und physikalische Analyse der Bodenproben, die an jeder Station entnommen wurden, zeigte, dass in beiden Regionen die Lagerungsdichte das TDT-Messsignal beeinflusst. Darüber hinaus beinhalteten die Pedotransferkalibrierungen die elektrische Leitfähigkeit im KR und die Schluff-Fraktion und den organischen Stickstoffgehalt auf der SA. Diese Variablen sind relativ einfach zu messen. Damit stellen die Pedotransferkalibrierungen, die im Rahmen dieser Arbeit abgeleitet wurden, eine schnelle Möglichkeit dar, TDT-Sensoren in Gebieten zu kalibrieren, die ähnliche Bodeneigenschaften aufweisen wie im KR und SA. Allerdings erzielten die standortspezifischen

Kalibrierungen die besseren Ergebnisse und wurden aus diesem Grund in der weiteren Datenanalyse verwendet.

In der zweiten Studie wurden dreijährige Bodenwassergehalts- und Niederschlagsdaten ausgewertet. Die Reaktion des regionalen mittleren Bodenwassergehalts ($\langle\theta\rangle$) auf Niederschlagsereignisse wurde durch die saisonale Wasserbilanz (SWB) beeinflusst. Die Beziehung war im KR ausgeprägter für positive SWB und weniger stark für neutrale und negative SWB. Auf der SA, wo die SWB in allen drei Jahren positiv war, war die Reaktion von $\langle\theta\rangle$ auf Niederschlagsereignisse immer deutlich ausgeprägt. Auf der saisonalen Skala wurde die Beziehung zwischen der regionalen Standardabweichung des Bodenwassergehalts (σ_θ) und $\langle\theta\rangle$ über σ_θ-$\langle\theta\rangle$ Phasenraumdiagramme untersucht. Es wurde beobachtet, dass bei abnehmendem Wassergehalt die σ_θ-$\langle\theta\rangle$ Datenpunkte sich dem σ_θ beim permanenten Welkepunkt (σ_θ-$\langle\theta_{wp}\rangle$) nähern. Bei steigenden Wassergehalten hingegen bewegen sich die σ_θ-$\langle\theta\rangle$ Datenpunkte in Richtung der σ_θ bei Sättigung (σ_θ-$\langle\theta_s\rangle$). Diese beiden charakteristischen Punkte wurden als Ankerpunkte definiert. Die σ_θ-$\langle\theta\rangle$ Beziehungen bildeten Kombinationen aus konkaven und konvexen Hyperbeln und spiegelten damit die Variabilität der Bodentextur wider und waren abhängig von σ_θ in Relation zu den Ankerpunkten. Auf der Ereignisskala zeigten die σ_θ-$\langle\theta\rangle$ Beziehungen Hysterese. Die meisten hysteretischen σ_θ-$\langle\theta\rangle$ Beziehungen verliefen im Uhrzeigersinn und traten im intermediären sowie intermediären/nassen Bodenwassserzustand auf. Als Faktoren, die hystererische σ_θ-$\langle\theta\rangle$ Verläufe auslösen, wurden Niederschlagsereignisse mit räumlich stark variabler Intensität (die Schwelle der Niederschlagsintensität war 1.1 ± 0.6 für KR und 2.9 ± 2.8 für SA), präferentieller Fluss und hysteretische Bodenwasserretentionskurven identifiziert. Basierend auf den Ergebnissen wurde die folgende Hypothese aufgestellt: σ_θ-$\langle\theta\rangle$ Phasendiagramme sind nützlich, um zu testen, ob hydrologische Modelle oder LSMs die räumliche Variabilität der Bodenfeuchte realistisch widergeben.

Das Konzept wurde für das Noah-MP LSM getestet. Messungen aus dem KR und der SA aus den Jahren 2010 bis 2012 wurden zum Erstellen der σ_θ-$\langle\theta\rangle$ Phasenraumdiagramme verwendet. Im Rahmen der Studie wurden zwei Ansätze zur Berechnung der hydraulischen Leitfähigkeit und Diffusivität getestet: 1) der Standardansatz: die Clapp und Hornberger Funktionen und 2) die van Genuchten-Mualem-Funktionen. Die standardmäßige Modellparametrisierung wurde schrittweise durch stationsspezifische Niederschlags-,

Bodentextur, und Blattflächenindexdaten sowie den grünen Vegetationsanteil (GFV) substituiert. Der atmosphärische Antrieb erfolgte über meteorologischen Daten von Eddy-Kovarianz-Stationen, die sich in den Regionen befanden. Obwohl das Modell gut die beobachtete zeitliche Dynamik von $\langle\theta\rangle$ in den Lössböden des KRs trifft, zeigte das Modell im Fall der flachgründigen, tonigen und steinigen Böden der SA Schwächen. Die beste Übereinstimmung wurde mit der van Genuchten-Mualem-Funktion und standortsspezifischen Niederschlags-, Bodentextur-, GVF- und LAI-Daten erreicht. Allerdings konnte Noah-MP LSM die räumlichen Variabilität des Bodenwassergehalts nur ungenügend darstellen. In den meisten Fällen befanden sich die simulierten σ_θ-$\langle\theta\rangle$ Datenpunkte unterhalb des σ_θ-$\langle\theta\rangle$ Phasendiagramms, was darauf hinweist, dass das Modell die räumliche Variabilität der Bodenfeuchte glättet. Dieses Glätten der räumlichen Variabilität ist vor allem auf die fehlende Topographie- und Geländeinformation, die unzureichende Darstellung der räumlichen Variabilität von Bodentextur und hydraulischen Parametern, sowie der Modellannahme einer uniformen Wurzelverteilung zurückzuführen.

3. General Introduction

3.1. The role of soil moisture in land-atmosphere interactions

Land surface exchange processes are critical in influencing planetary boundary layer. Soil water content (SWC) is a key biophysical and hydrologic state variable, used in a range of practical applications including irrigation scheduling, water availability monitoring, quantitative rainfall forecasting, climate simulation and weather prediction (e.g. Morari and Giardini, 2002; Leib et al., 2003; Wraith et al., 2005). Sustainable irrigation management depends on reliable soil water monitoring. Next to sea surface temperature, anomalies in soil moisture may contribute to extreme weather events such as droughts, floods and summer heat waves (e.g. Fischer et al., 2007). Soil moisture also influences surface albedo and energy partitioning into sensible and latent heat flux (Seneviratne et al., 2010; Heathman et al., 2012), and is a strong predictor for future air temperatures (Georgakakos et al., 1995; Huang et al., 1996).

An enormous research effort has been devoted to the feedback between the state of SWC and cloud and precipitation formation over land. In the literature, both positive and negative feedbacks are reported (Eltahir, 1998; Hohenegger et al., 2009). Some studies state that the feedback depends on the relative humidity and the state of the air above the atmospheric boundary layer (Ek and Holtslag, 2004; Barthlott and Kalthoff, 2011). According to Koster et al. (2004), the coupling strength between soil moisture and rainfall anomalies varies regionally. Based on the results of the Global Land-Atmosphere Coupling Experiment (GLACE) multimodel run, areas with high sensitivity are located in the central Great Plains of North America, the Sahel, equatorial Africa and India. Areas of lower land-atmosphere coupling strength, but still sensitive, are located in South America, central Asia and China.

3.2. Spatial variability of soil moisture and its impact on the atmosphere

Spatial SWC variability is often expressed through the relationship between the spatial mean SWC ($\langle\theta\rangle$) and its standard deviation (σ_θ). The σ_θ-$\langle\theta\rangle$ usually trace out a convex top-closed curve (Vereecken et al., 2007; Famiglietti et al., 2008; Pan and Peters-Lidard, 2008; Brocca et al., 2012; Rosenbaum et al., 2012). The σ_θ has a maximum value in the middle range of $\langle\theta\rangle$ and descends to the wet and dry $\langle\theta\rangle$ regions. Grayson et al. (1997) defined two groups of factors that impact SWC variability, based on initial soil moisture conditions and the particular time of a season. According to their study and others (Famiglietti et al., 1998; Vereecken et al., 2007, Pan and

Peters-Lidard, 2008; Vivoni et al., 2010), local controls (soil texture, vegetation) dictate SWC variability under dry conditions, while non-local controls (topography, runoff) are the main drivers under wet conditions. In the intermediate state of SWC, σ_θ-$\langle\theta\rangle$ is mostly controlled by a combination of non-local and local controls. All of the factors are usually interrelated non-linearly and depend on the sampling scale. At scales exceeding 100 km^2, factors such as rainfall distribution in space gain significance in influencing SWC variability (Albertson and Montaldo, 2003).

Modelling studies (Avissar and Liu, 1996; Patton et al., 2005; Gantner and Kalthoff, 2010; Huang and Margulis, 2013) and observational case studies (Taylor et al., 2007) have shown that spatial SWC variability and its horizontal gradients lead to the occurrence of thermally induced mesoscale circulations (MSC). Gantner and Kalthoff (2010) underline that the physics of this feedback may change during the genesis of a convective cell. In their weather simulation of a MSC in the Sahel zone, they found that during the initiation phase, the triggering of convection was favored by drier surfaces. In contrast, matured convective cells were weakened in the vicinity of drier surfaces. Simulated convective cells preferably developed in the transition zone from a wetter to a drier surface, while the centers of the precipitating cells were positioned over the drier surface. Huang and Margulis (2013) concluded that the impact of soil moisture variability on turbulence structure in the atmospheric boundary layer increases with increasing soil moisture variability length scale (spatial extent of dry and wet patterns) within the 10 km × 10 km domain in the sequence 1.25, 2.5 and 5 km.

Numerous studies on SWC temporal dynamics and its spatial variability have been conducted at different spatial scales. They range from field measurements (representing a few hundreds of square meters; Famiglietti et al., 2008), small catchments (<10 km^2; Rosenbaum et al., 2012), region-wide (captured by soil moisture networks within an area of 10 to 1000 km^2; Brocca et al., 2012), and, finally, to coarse grid measurements performed with remote sensing (Zreda et al., 2008). Land-atmosphere interactions control cloud formation and the location of rainfall, thereby affecting weather, climate and hydrology foremost on the regional scale (Dirmeyer and Brubaker, 1999; Weaver and Avissar, 2001; Robock et al., 2003). The long-term observations are of a special interest, particularly for cropland because it is the most intensively managed (in terms of cropping and soil tillage), dynamic (in terms of mass and energy interactions in soil-plant-atmosphere system) and vital (in terms of food production) area.

Moreover, these data can serve to ground-truth remotely sensed SWC and to validate and develop land surface models (LSM) (Robinson et al., 2008).

3.3. Modelling spatial variability of soil moisture

Current individual hydrological models and LSMs harbor uncertainties and biases in simulated SWC (Chen and Dudhia, 2001; Niu et al., 2011; Ingwersen et al., 2011; Yang et al., 2011). Hauck et al. (2011) showed that underestimating SWC significantly influences simulated precipitation. Few studies have quantified the goodness of representation of soil moisture variability in space by LSMs. Koch et al. (2016) report that three state-of-the-art hydrological models systematically underestimated the spatial SWC variability at the Wüstebach catchment site in Germany. They observed improved model performance when heterogeneous porosity was introduced. Researchers suggest testing the sensitivity of modelling to the inhomogeneity of other soil hydraulic parameters, arguing that porosity is simply a scaling factor for SWC dynamics. Kishne et al. (2017) conducted an extensive study to determine differences between the default hydraulic parameters of the Noah LSM and those estimated based on measured soil data in Texas. The authors suggested replacing most of the default parameters in the Noah lookup table with those derived from the soil samples. The model may unrealistically represent total available water for plants, precipitation partitioning into runoff and infiltration, and, consequently, the amount of moisture in the soil profile. This is due to biases in hydraulic functions. Another issue was related to considering the spatial variability of soil texture rather than using one value for a given textural class.

3.4. The scope of the thesis

My thesis started with field work on establishing two regional soil moisture networks in Kraichgau (KR) and Swabian Alb (SA). The International Soil Moisture Network (Dorigo et al., 2011) lists only few networks that are constantly operated on arable land. Maintaining a regional soil moisture network on cropland is laborious due to tillage and other field activities that must be performed by growers. Nonetheless, long-term observations of topsoil water content dynamics and distribution in space on arable land at the scale of 10 to 1000 km^2 are necessary to validate remote sensing data and LSMs (Robinson et al., 2008). My thesis encompasses the following steps:

In the first study (Chapter 4), site-specific field calibrations of the Aquaflex TDT (Time Domain Transmission) soil moisture sensors were established. Since the site-specific calibration of a large number of sensors is labour-intensive and time consuming, an alternative approach was developed based on the measured physico-chemical properties of KR and SA topsoils. The comprehensive description of the study regions, soil moisture networks and installation procedure is also given in Chapter 4.

In the second study (Chapter 5), factors controlling the dynamics of $\langle\theta\rangle$ and σ_θ at the event and seasonal time scales were evaluated. The seasonal variability of SWC was characterized by the σ_θ-$\langle\theta\rangle$ phase-space diagram. This is the set of all possible σ_θ-$\langle\theta\rangle$ states, stretched upon the three-year σ_θ-$\langle\theta\rangle$ observational data cloud and two anchor points – σ_θ at the permanent wilting point (σ_θ-$\langle\theta_{wp}\rangle$) and σ_θ at saturation (σ_θ-$\langle\theta_s\rangle$). The hypothesis was drawn that a reasonably performing model should simulate σ_θ-$\langle\theta\rangle$ data pairs falling into the observed envelope.

The aforementioned concept was validated in the final study (Chapter 6). The Noah-MP LSM was tested against the observations obtained from KR and SA soil moisture networks over a three-year period from 2010 to 2012. The study set-up included two modifications of the hydrology scheme: the Clapp and Hornberger approach (CH; Cosby et al., 1984), used to compute the hydraulic conductivity and the diffusivity by the default, was compared with the van Genuchten-Mualem function (VG; van Genuchten, 1980). The parameterization included a stepwise introduction of observed rainfall, station-specific soil texture, LAI and GVF data into the model input files and subsequent replacement of the default data layout.

4. Calibration and application of Aquaflex TDT soil water probes to measure the soil water dynamics of agricultural topsoil in Southwest Germany

Chapter 4 is published with kind permission from the American Society of Civil Engineers

The original publication "Poltoradnev, M., Ingwersen, J., and T. Streck. 2015. Calibration and application of Aquaflex TDT soil water probes to measure the soil water dynamics of agricultural topsoil in Southwest Germany. *Irrigation and Drainage Engineering*, 141(6), 04014072" can be found via the following link: http://ascelibrary.org/doi/abs/10.1061/(ASCE)IR.1943-4774.0000838

Calibration and Application of Aquaflex TDT Soil Water Probes to Measure the Soil Water Dynamics of Agricultural Topsoil in Southwest Germany

Maxim Poltoradnev[1]; Joachim Ingwersen[2]; and Thilo Streck[3]

Abstract: Soil water plays a key role in crop growth and yield formation. A sustainable irrigation management depends on a reliable soil water monitoring. The present study was conducted to derive site-specific and pedotransfer calibrations for Aquaflex time domain transmission (TDT) soil water sensors and to test their performance under field conditions. In spring 2009, two soil moisture networks were installed in the Kraichgau region and in the Swabian Alb, southwest Germany. Each network consists of 21 stations, each equipped among others with an Aquaflex TDT sensor installed 15-cm-deep in the soil. At each station, soil samples were taken and analyzed for the gravimetric soil water content, bulk density, soil texture, electrical conductivity, pH, and organic nitrogen and carbon content. The factory calibration delivered highly biased soil water contents [~ -8.0 Volume (Vol.) %]. The root mean square errors (RMSEs) were high, reaching on average 8.3 and 12.6 Vol.% in Kraichgau and Swabian Alb, respectively. The RMSEs of pedotransfer calibrations declined to 3.7 Vol.% in Kraichgau and to 3.4 Vol.% in Swabian Alb. In both regions, the slope of the calibration curve was affected by soil bulk density. High-leverage independent variables affecting the intercept were electrical conductivity in Kraichgau and silt fraction in Swabian Alb. Site-specific calibrations performed best. On average, the RMSE in Kraichgau was 3.0 Vol.%, in Swabian Alb 1.9 Vol.%. The pedotransfer-based approach proposed in the present study is a good compromise between labour effort and accuracy for soil landscapes with similar texture and properties. **DOI: 10.1061/(ASCE)IR.1943-4774.0000838.**

Author keywords: Time domain transmission technique; Kraichgau; Swabian Alb; Regional scale; Soil moisture network.

Introduction

Since the introduction of an electromagnetic (EM) methods of soil water content (SWC) determination, many studies have shown its usefulness in various applications, such as precision agriculture, irrigation scheduling, or environment monitoring (Wraith et al. 2005; Leib et al. 2003; Baker and Spaans 1994). The plant available soil water plays a key role in crop growth and yield formation, and a sustainable irrigation management depends on a reliable soil water monitoring. Amount and frequencies of irrigation events should be adjusted to the water demand of the standing crop. Moreover, soil water is an important driver with regard to atmosphere-land surface feedbacks, cloud formation and rainfall distribution. SWC is a key to the partitioning of net radiation at the land surface into latent, sensible, and soil heat flux (Zhu and Liang 2005), and it also effects the partitioning between soil evaporation and transpiration (Gutmann and Small 2007).

EM techniques are nondestructive and suited for continuous in situ real-time soil water measurements (Robinson et al. 2008). Measurement of SWC using EM sensors is based on measuring the real part of the dielectric permittivity (ε) of soil, which directly relates to volumetric SWC (θ_v) because of the ε-contrast of soil constituents: $\varepsilon_a \sim 1$, $\varepsilon_s \sim 2$–9 and $\varepsilon_w \sim 80$ where the subscripts a, s, and w represent air, solids, and water, respectively (Topp et al. 1980). One such EM method is the time domain transmission (TDT) technique (Harlow et al. 2003; Hook et al. 2004). The TDT method is similar to the time domain reflectometry (TDR) method (Topp et al. 1980) in that the travel time of an electromagnetic wave is measured. The difference is that with TDT the pulse is not reflected at the end of the rod but travels in a loop along a transmission line that terminates within the measurement circuit.

A number of scientists have tested and applied different types of commercially available TDT soil moisture sensors, mostly with the purpose of irrigation scheduling. Morari and Giardini (2002) used 15 Gro-Point TDT moisture sensors (Environmental Sensors, Canada) to monitor SWC in a 2-ha area in a botanical garden. McCready et al. (2009) used seven Acclima Digital TDT RS500 (Acclima, Idaho) and seven LawnLogic LL1004 (Alpine Automation, Colorado) in their research (study area: 0.13 ha). They tested the performance of their irrigation system with programmed SWC thresholds as the need-for-irrigation indicator. They concluded that the irrigation conducted under the medium threshold of SWC [10 Volume (Vol.) %], measured by the TDT sensor, produced water savings of 11–53% and good turfgrass quality compared with the conventional (without TDT sensors control) irrigation method. Hedley and Yule (2009) installed three Aquaflex TDT (Streat Moisture Solutions, North Carolina) soil moisture sensors over an area of 35.2 ha to measure SWC within three management zones

[1]Researcher, Institute of Soil Science and Land Evaluation, Biogeophysics, Universität Hohenheim, Emil-Wolff-Str. 27, 70599 Stuttgart, Baden-Württemberg, Germany (corresponding author). E-mail: M.Poltoradnev@uni-hohenheim.de

[2]Researcher, Institute of Soil Science and Land Evaluation, Biogeophysics, Universität Hohenheim, Emil-Wolff-Str. 27, 70599 Stuttgart, Baden-Württemberg, Germany. E-mail: joachim.ingwersen@uni-hohenheim.de

[3]Researcher, Institute of Soil Science and Land Evaluation, Biogeophysics, Universität Hohenheim, Emil-Wolff-Str. 27, 70599 Stuttgart, Baden-Württemberg, Germany. E-mail: tstreck@uni-hohenheim.de

Note. This manuscript was submitted on May 16, 2014; approved on October 1, 2014; published online on November 11, 2014. Discussion period open until April 11, 2015; separate discussions must be submitted for individual papers. This paper is part of the ***Journal of Irrigation and Drainage Engineering***, © ASCE, ISSN 0733-9437/04014072(11)/$25.00.

defined by electrical conductivity (σ) properties. The Aquaflex TDT sensor has numerous advantages: fast response, long measuring line (3 m), large measuring volume (approximately 6 L), good accuracy (±2 Vol.%), and a connection cable length between data logger and sensor of up to 50 m (Streat Instruments Ltd 2003). Among its disadvantages is great disturbance of a soil while installing and the need of calibration. Hedley and Yule (2009) found, that the accuracy of measurements was limited by significant spatial variability of soil moisture because of the low number of applied sensors. It is important to stress at this point that none of the aforementioned studies dealt with a field calibration issues of TDT soil moisture sensors. All used a default factory calibration, and it remained unsettled whether the sensors accurately measured the absolute water content.

Attempts are made to monitor SWC with EM methods on a regional scale (a regional scale is considered to include areas from 10^1 to 10^3 km^2 (Harter and Hopmans 2004), because land-atmosphere interactions control cloud formation and rainfall distribution, thereby affecting regional climate (Dirmeyer and Brubaker 1999; Weaver and Avissar 2001; Robock et al. 2003). Studies conducted to collect regional soil water data are rare. Several such networks are currently operating in the United States in the states of Iowa and Illinois (Hollinger and Isard 1994; Robock et al. 2000), Oklahoma (Illstone et al. 2008), and Wyoming (Engda et al., unpublished data, 2011), along with the United States nationwide Soil Climate Analysis Network (SCAN, http://www.wcc.nrcs.usda.gov/scan/). The Illinois Climate Network (ICN) was founded by the Illinois State Water Survey in 1981. ICN consists of 19 stations providing measurements of solar radiation, soil temperature, and moisture since 1986 under turfgrass sites. A neutron probe system has been used to measure SWC at each ICN site at regular intervals throughout the year, twice a month during the growing season (March to October) and once a month during the rest of the year. The Oklahoma Mesonetwork was set up in 1991. Today it has over 100 stations with CSI 299-L heat-dissipation soil moisture sensors (Campbell Scientific, Utah) installed under turfgrass. The Wyoming automated soil water sensing network has conducted measurements on 18 turfgrass sites since 2010. The SCAN was initiated in 1991. It currently has over 150 soil moisture stations around the United States. They use Vitel HYDRA (Stevens Water Monitoring Systems, Oregon) soil water probes [frequency domain reflectometry (FDR) technique] to sense volumetric soil water content. In Switzerland, a soil moisture network was established in 2008 (Mittelbach et al. 2011). The Swiss Soil Moisture Experiment project (SwissSMEX) consists of 19 sites, at which soil moisture is measured continuously with TRIME-EZ and TRIME-IT sensors (IMKO, Germany) based on a quasi-TDR (Time Domain Reflectometry) technique (Evett et al. 2006). Fourteen sites were set up on turfgrass sites, four in forest and one on arable land. In Germany, wireless soil moisture sensor networks were recently established at the hill slope scale in the frame of the Terrestrial Environmental Observatories (TERENO) (Bogena et al. 2010; Zacharias et al. 2011).

The present study was designed: (1) to derive site-specific and pedotransfer-based calibrations of Aquaflex TDT sensors, and (2) to test their performance for monitoring the soil water dynamics in agricultural topsoil in two regions of southwest Germany (Kraichgau and Swabian Alb). Our results are intended to provide Aquaflex TDT sensor users (e.g., farmers, irrigation engineers, consulting services, and researchers) with information on the accuracy of the sensor and guidelines for a quick and reliable sensor calibration and application.

Materials and Methods

Research Project

The soil moisture networks were set up and tested in the frame of the Integrated German Research Foundation Project *Structure and functions of agricultural landscapes under climate change—processes and projections on a regional scale* (PAK 346). The follow-up research project is the research unit *Regional climate change* (FOR 1695). The research projects PAK 346/FOR 1695 aim at helping determine the effects of global climate change on the structure and functions of the agricultural landscape in southwest Germany. High-resolution climate projections from today until 2030 will be performed. The project will integrate regional climate, land surface, and crop models and multiagent systems into a land system model. To improve various model components and to validate the coupled model, system field measurements and controlled exposure experiments have been conducted (Biernath et al. 2011; Ingwersen et al. 2011). For further details see https://klimawandel.uni-hohenheim.de/.

Study Regions

Fig. 1 shows the two model regions of PAK 346/FOR 1695 in southwest Germany. The Kraichgau region is hilly and agriculturally intensively used. It is largely covered with loess, approximately 1,600 km^2 in size and on average 218 m above the sea level (asl). Kraichgau has a mild climate with an annual temperature of approximately 9°C. Mean annual precipitation ranges between 720 and 830 mm. Here, soils developed predominantly to Regosols [World Resources Reports (WRB 2006)] and Luvisols (WRB 2006). Forests cover approximately 29% of the total area. The agriculturally used land has a share of 53%. Crop rotation typically consists of winter wheat, summer barley, maize, winter rape, and sugar beet.

Another study area lies in the middle part of Swabian Alb region—the Middle Swabian Alb. It covers approximately 1,300 km^2 and will be named Swabian Alb in the rest of this paper (Fig. 1). Jurassic limestone forms a hilly plateau at an altitude between 800 and 850 m above the sea level (asl). The mean annual temperature is approximately 6–7°C, i.e., 2–3°C less than in Kraichgau. In Swabian Alb, annual precipitation ranges between 800 and 1,000 mm. Rainfall is more evenly distributed than in Kraichgau. The characteristic soil of the Swabian Alb is a shallow and stony Leptosol (WRB 2006). It has a clayey loam texture. Thirty-eight percent of the total area is forested. Arable land covers 52%. Agriculture is generally less intensive than in Kraichgau. Summer barley, maize, winter wheat, and winter barley are the predominant crops. The crop rotation in Swabian Alb is more diverse than that in Kraichgau. Spelt, triticale, perennial grass, and clover are often parts of crop rotation.

More details on physical and chemical properties of study sites are given in the "Results and Discussion" section and listed in Table 1.

Soil Moisture Networks

From April to June 2009, one soil moisture network was set up in each model region. Each soil moisture network consists of 21 stations. All stations were installed on cropped agricultural sites and were distributed across three spatial domains: an inner domain 3 × 3 km (five stations), a middle 9 × 9 km (eight stations), and an outer domain 27 × 27 km (eight stations) (Fig. 2). Each station has a TDT sensor (SI.99 Aquaflex Soil Moisture Sensor, Streat Instruments, New Zealand), which sensed both SWC and soil temperature; a rain gauge with a resolution of 0.2 mm per tip; a remote transfer unit (RTU, datalogger + GSM modem), which

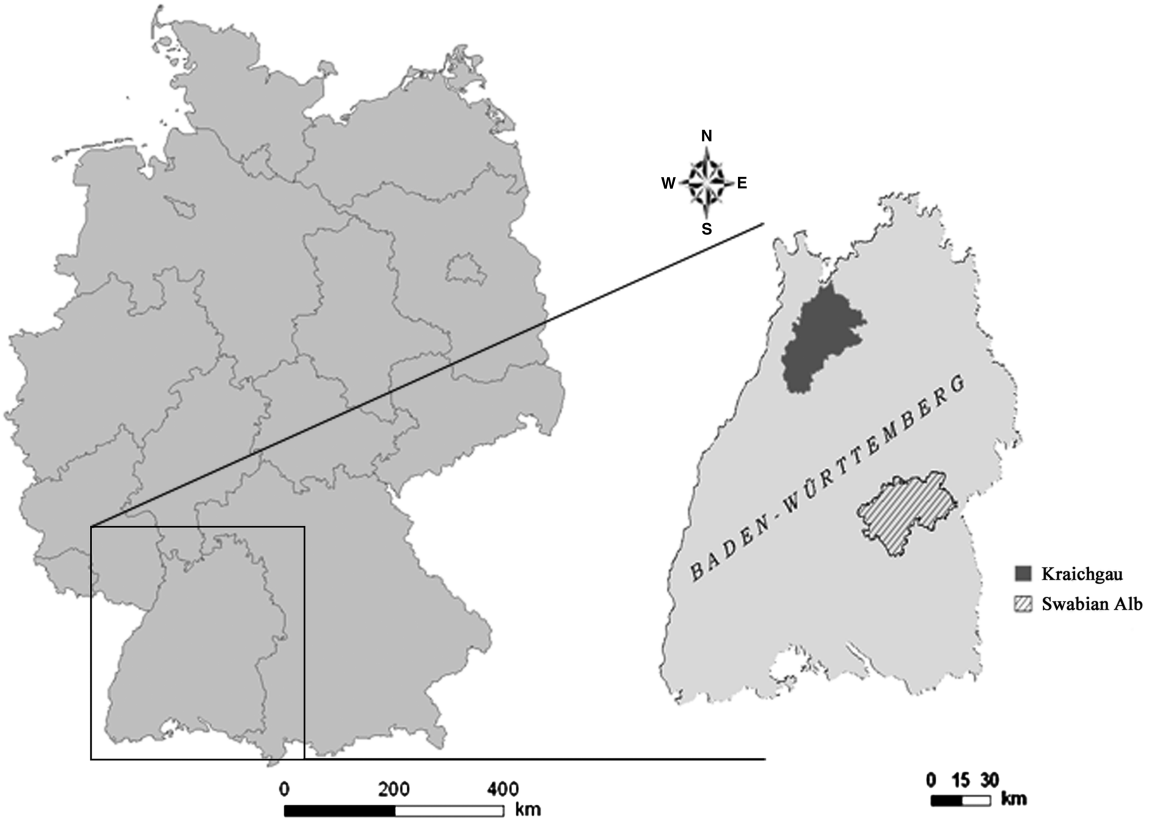

Fig. 1. Map of Baden-Württemberg state (Germany) and the two model regions of the integrated research project "structure and function of agricultural landscapes under global climate change—processes and projections on a regional scale" (PAK 346) (data from BKG 2014)

stored and transferred data using GPRS modem to the central data server (Adcon Telemetry, Austria) located at the University of Hohenheim; and a solar panel for power supply. The rain gauge, the RTU and the solar panel were mounted to an aluminum pole. The rain gauge was installed 1.8 m above ground. In the case of maize cropping, the installation height was increased to approximately 2.8 m when the canopy height exceeded 1.5 m to avoid its shadowing with plants. The TDT sensor was installed at 0.15 m depth. For installation, an approximately 0.17 m deep trench was dug using a motorized trencher (Laski TR-60 H, Laski spol. s r.o., Czech Republic). The sensor consists of a 3-m-long and 3-cm-wide flat transmission line. The start point of the transmission line was installed 5 m away from the pole. To avoid water logging above the 3-cm-wide transmission line, the line was installed in a vertical orientation. Data were collected every 15 min.

Every station was installed in the middle between two farming machine tracks, so that the farmer could easily pass the station when applying fertilizer or pesticides. To avoid damage to the sensor, the sensor area was not ploughed or grubbed by the farmer. Instead, these two tillage operations were performed manually using a bar spade. Tillage operations such as rotary harrowing and drilling were performed across the sensor area by the farmers with their usual machinery.

Calibration of TDT Sensors

The manufacturer provides a factory calibration for converting the TDT sensor signal into SWC (Streat Instruments Ltd 2003). The sensor output ranges between 0.5 and 2.5 V. For soils with clay contents below 40% the manufacturer recommends a simple linear equation to convert the sensor voltage V (V) into volumetric water content θ_v (Vol.%):

$$\theta_v(V) = aV + b \tag{1}$$

Here $a = 30$ Vol.% V^{-1} and $b = -15$ Vol.%. For clay and clay loam soils (clay content $> 40\%$) the default factory calibration uses a cubic equation

$$\theta_v(V) = a_1 V + a_2 V^2 + a_3 V^3 + b \tag{2}$$

where $a_1 = 23$ Vol.% V^{-1}; $a_2 = 13.7$ Vol.% V^{-2}; $a_3 = -4.4$ Vol.% V^{-3}; and $b = -14$ Vol.%.

In an alternative approach, each TDT sensor was calibrated individually. For this, soil samples were regularly taken at all

Table 1. Physical and Chemical Properties of the Topsoils of the Two Soil Moisture Networks in Kraichgau and Swabian Alb

Property	σ (μS cm^{-1})	ρ (g cm^{-3})	pH	C_t (%)	N_t (%)	$CaCO_3$ (%)	Sand (%)	Silt (%)	Clay (%)
Kraichgau									
$\bar{x}$	175.2	1.51	6.7	1.4	0.13	3.3	4.1	73.8	22.1
s	89.5	0.10	0.8	0.5	0.03	3.3	2.7	5.8	4.9
Minimum	33.5	1.32	5.4	0.8	0.06	0.0	1.7	59.4	13.7
Maximum	327.0	1.65	7.5	2.6	0.19	10.5	12.1	82.3	29.9
Swabian Alb									
$\bar{x}$	138.3	1.15	6.7	3.8	0.34	6.8	3.5	46.5	50.0
s	56.1	0.18	0.8	1.7	0.11	10.3	3.0	11.8	12.8
Minimum	63.0	0.78	4.7	1.8	0.17	0.0	1.5	29.1	24.9
Maximum	295.5	1.56	7.5	7.5	0.56	35.5	11.8	77.2	76.1

Note: Percentages are given as percentage by mass; C_t and N_t = total organic carbon and total nitrogen content of soil, respectively; $\bar{x}$, s, min, and max = mean, standard deviation, minimum and maximum values of a reference variable, respectively; σ = electrical conductivity; ρ = soil bulk density.

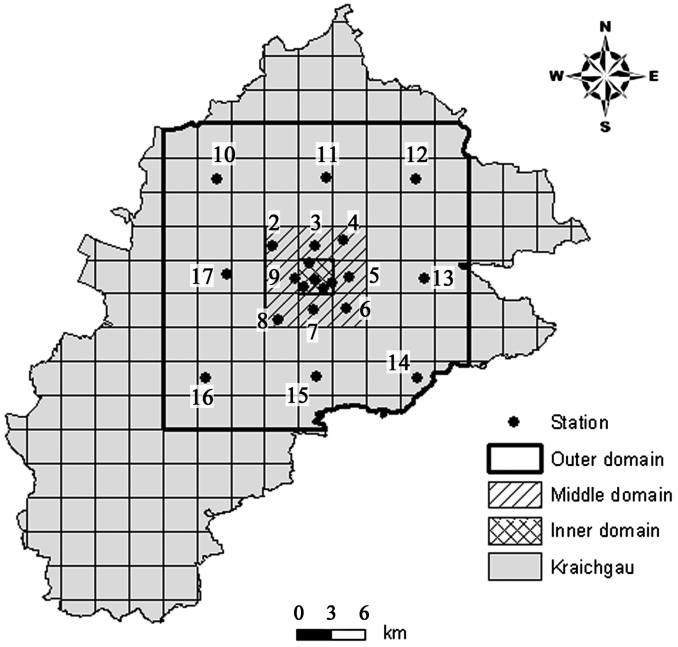

Fig. 2. Position of soil moisture stations of the soil moisture sensor network in Kraichgau; the area of the network has been divided in an inner (3×3 km^2), middle (9×9 km^2), and outer (27×27 km^2) domain; in the inner domain the five stations were labeled from 1-1 to 1-5 in the numerical order

stations. Each station was sampled in total 6–12 times during entire study period (2009–2012). At each sampling date, soil samples were taken from three positions along and close (<0.05 m) to the transmission line using a 0.30-m-long auger (Ø0.05 m wide). We did not take volume-proportional samples because that method requires digging small pits along the transmission line. Such sampling technique would have had destroyed the canopy and disturbed soil close to the sensor and thus the ongoing TDT soil water measurements. Soil material was collected with an auger from the 0.135 to 0.165 m depth. In 2009, water content was determined for all subsamples individually. After 2009, the three subsamples were mixed to one composite sample. Samples were stored in plastic bags and transported in a cooling box from the field to the lab. In the lab, water content was determined with a standard gravimetrical method. The gravimetric water content was converted to θ_v using bulk density (ρ). Soil cores (N = 5, each 100 cm^3) were taken at the day of installation close to the sensor from the same depth. Additionally, at each station, soil texture, total organic carbon (C_t), as a measure for the organic matter (OM) content (OM ~ $1.72C_t$), total organic nitrogen (N_t) content, carbonate content, pH and σ of topsoil were measured. Texture was measured with a standard pipette method (Scheffer and Schachtschabel 2008). C_t and N_t were measured with the C/N Analyzer Vario MACRO (Elementar Analysensysteme GmbH, Germany). Carbonate content was determined by the gas-volumetric Scheibler method (Schlichting et al. 1995). Soil pH was determined as follows: four grams of soil were suspended in 10 ml 0.01 M $CaCl_2$ solution. After two hours, soil pH was measured using a glass electrode pH meter (InLab Routine Pro ISM, Mettler Toledo Intl., Germany). To determine σ, 50 ml of distilled water were added to 10 g of air-dried soil. The soil suspension was left standing overnight. The next day, the samples were shaken for one hour. Afterwards, the samples were centrifuged (DJB Labcare, U.K.) for 5 min at 3,000 rpm (~1,510 g). Then, σ of a soil suspension was measured with a handheld electrical conductivity meter (LF90, WTW, Germany).

For each station a site-specific calibration was performed by a linear regression between sensor output voltage and measured θ_v [Eq. (1)]. Besides this simple linear regression, data were evaluated with a pedotransfer function approach. The slope and intercept in Eq. (1) were assumed to be a linear function of soil properties (X_i), yielding

$$\theta_v(V, X_i) = \left(\sum_{i=1}^{n} a_i X_i\right) V + \sum_{i=1}^{m} b_i X_i + C \tag{3}$$

Here a_i = coefficient of the slope; b_i = coefficient of the intercept; C = intrinsic intercept; X_i = soil properties; and n and m = number of soil properties considered. Soil properties considered in the regression were σ, ρ, pH, C_t, N_t, carbonate content, and the fractions of sand, silt and clay. The importance of these properties influencing the coefficients a_i, b_i and C was determined by a stepwise multiple linear regression.

We compared several regression approaches. Firstly, we analyzed all data in a single data set and consequently derived one regression (calibration) valid in both regions. Secondly, we derived a separate calibration for each soil moisture network. While building up a regression, we considered only results that did not show multicollinearity problems between chosen parameters. For data evaluation we used the statistical software package *PASW SPSS Version 18*.

For quantifying the performance of regressions, we used root mean square error (RMSE), bias and model efficiency (EF) (Nash and Sutcliffe 1970; Moriasi et al. 2007). RMSE was calculated as

$$\text{RMSE} = \sqrt{\frac{1}{n}\sum_{i=1}^{n}(P_i - O_i)^2} \tag{4}$$

where P_i = SWC determined with the TDT sensor; and O_i = gravimetrically determined θ_v.

Bias and EF were computed using Eqs. (5) and (6), respectively:

$$\text{bias} = \frac{1}{n}\sum_{i=1}^{n}(P_i - O_i) \tag{5}$$

$$\text{EF} = 1 - \sum_{i=1}^{n}(P_i - O_i)^2 \Big/ \sum_{i=1}^{n}(O_i - \bar{O})^2 \tag{6}$$

where $\bar{O}$ denotes the mean of O_i.

Results and Discussion

Table 1 summarizes chemical and physical properties of the topsoils of the two soil moisture networks. Topsoils of Kraichgau stations had, on average, higher ρ and σ than those of Swabian Alb. In both regions, average soil pH was close to neutral, and its variability was similar. Swabian Alb topsoils had distinctly higher C_t and N_t than Kraichgau soils. Also the carbonate content of Swabian Alb soils was, on average, approximately twice as high as that of Kraichgau soils. The loess soils of Kraichgau were dominated by the silt fraction, whereas the Swabian Alb soils had considerably higher clay contents.

Fig. 3 shows, by way of example, scatterplots and regressions between sensor output voltage and gravimetrically determined SWC at four selected Kraichgau stations for two different time windows. Measurements were made from June to September 2009, shortly after installation in April 2009, and five to ten months

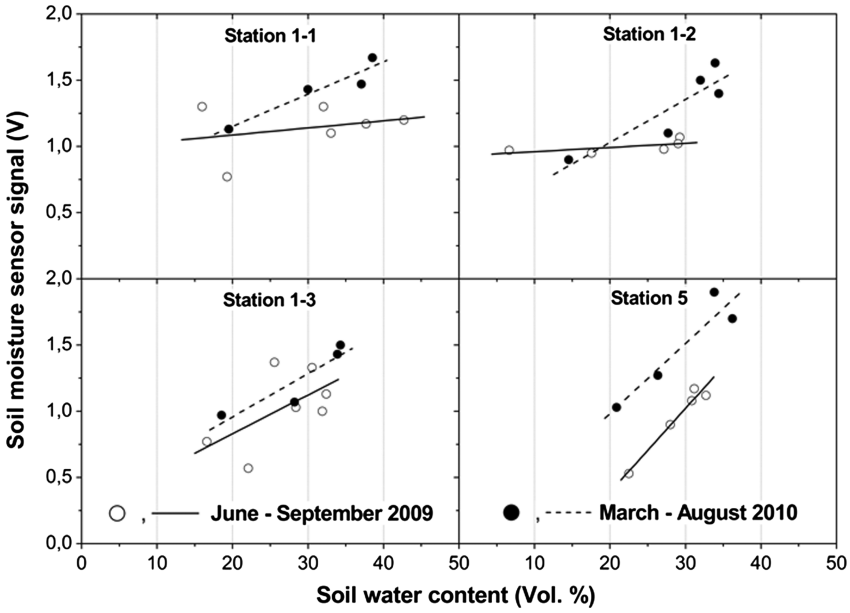

Fig. 3. Effect of recompaction on the regression between sensor output signal and gravimetrically determined soil water content

later, between March and August 2010. In the regressions for stations 1-3 and 5, essentially only the intercept changed between the two sampling periods. In contrast, at stations 1-1 and 1-2 also the slope of the two regressions changed. Moreover, the data collected in 2009, shortly after installation, showed a much greater scattering than the data of 2010. The reason for this is the disturbance of soil structure during installation and an ongoing soil recompaction. Its consequences on the time series of measured SWC is demonstrated on the Fig. 4. Directly after installation the sensor at Station 5 delivered unrealistically low soil water contents (<5 Vol.%). The sensor quickly responded to rain events, but after the event the water content dropped back to readings below five Vol.%, pointing to air voids between sensor cable and soil, shortly after installation [Plauborg et al. (2005) observed the similar behavior when using the standard factory calibration]. After approximately six months, sensor readings stabilized and no longer fell below 20 Vol.%. After nine months, the SWC after rainfall fell back to a range fluctuating around 35 Vol.%, indicating the recompaction

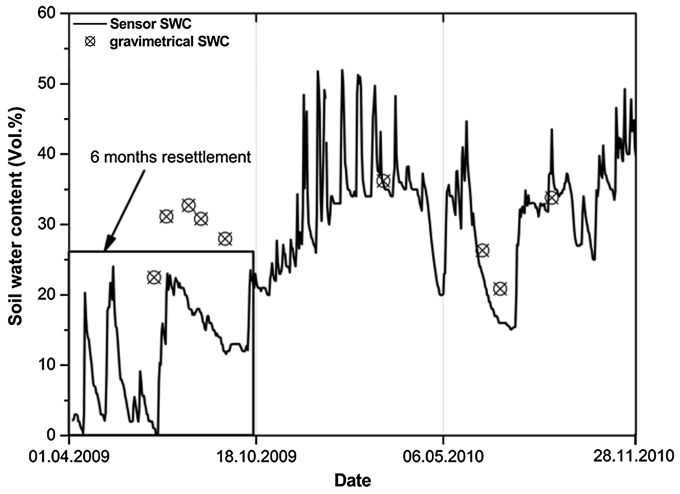

Fig. 4. Time series resettlement at Station 5 (Kraichgau network); volumetric water content is delivered by factory calibration

period was completed. The position of gravimetrically determined SWC data points on the figure also indicates a resettlement stage of the sensor. With regard to the continuous increase of the soil water content six to nine months after installation, it is difficult to judge whether this reflects ongoing recompaction or a refilling of soil water stock during autumn. The length of the recompaction period differed among stations, ranging from several weeks to several months. Compaction depends on the soil properties, soil tillage and moisture conditions (Ball et al. 1997). With a silty clay loam soil, Alletto and Coquet (2009) observed an increase of ρ during the first five months after tillage. After that period, ρ remained nearly constant. Based on our data we come to the estimate that the recompaction phase is completed after six or, at the latest, nine months. The period of time required for the resettlement could be most probably reduced by adding an excess amount of water along the sensor transmission line right after the installation. Because we wanted to avoid a disturbance of the soil water status we refrained from this approach. Because of the ongoing recompaction phase after installation, the soil water data of 2009 were not considered in the statistical analysis.

Because of events such as equipment defects, animal browsing or mechanical damaging of the sensor the number of running stations was not constant over the time. For instance, in 2010 in the Kraichgau network only 14 out of 21 stations could be continuously operated (without shut downs). To perform the site-specific calibration for all stations additional soil sampling campaigns were conducted in the year 2012.

Thus, because the data of the season 2009 were discarded, the total number of soil samples entered the data set was 85 in Kraichgau and 79 in Swabian Alb. It consisted of the data delivered by sampling campaigns of 2010 and 2012. On average, we used four data points to estimate site-specific and pedotransfer-based parameters in Kraichgau and five data points in Swabian Alb. The results are given in Table 2.

The factory calibration led to a strong bias in SWC (Table 3). The recorded SWCs were on average approximately 8–9 Vol.% less than the SWCs determined gravimetrically. The RMSE were also relatively high. In Swabian Alb, with its clay-rich and humus-rich soils, the RMSE reached the highest value among all tested approaches (12.6 Vol.%). Pedotransfer calibrations performed much

Table 2. Results of Site-Specific Linear Calibrations of TDT Sensors

	Kraichgau			Swabian Alb		
Variable	$\bar{x}$	s	Range	$\bar{x}$	s	Range
a	22.81	6.74	14–37	14.38	7.48	2–30
b	1.62	9.69	−22–13	21.82	12.08	−0.3–45
R^2	0.86	—	0.75–0.98	0.93	—	0.80–0.99
RMSE	2.16	—	0.85–5.34	1.36	—	0.31–2.45

Note: a = slope; b = intercept; R^2 = coefficient of determination; RMSE = root mean square error; s = standard deviation values of a reference variable; $\bar{x}$ = mean values of a reference variable.

better (Table 3). There was almost no bias, and EF was 0.77 in the case of the combined data set. When data were pooled over both regions, N_t and ρ affected the slope of the regression, whereas the intercept was a function of the silt and clay fractions. If applied separately for each region, however, this calibration led to biased estimates. The stepwise regression was therefore performed separately for the two regions. The separated data sets have a relatively narrow distribution with regard to texture and humus content. In Kraichgau, N_t and soil texture were replaced by σ as regression variables. The increment in R^2 coefficient made from 0.61, when only ρ was entered by the model, to 0.64 when both ρ and σ were entered. In Swabian Alb, clay was removed from the computation of the intercept. The R^2 was improved by the following steps: when N_t entered, R^2 made 0.66, ρ and silt fraction content inclusion improved the R^2 to 0.71 and 0.74, respectively. These region-specific pedotransfer functions slightly improved EF and RMSE and removed the bias. The wide range of slope and intercept values (Table 2) underlines the need for a site-specific calibration.

Graphically the performance of three calibrations (factory, pedotransfer-based, and site-specific) against gravimetrically

Table 3. Results of the Pedotransfer-Based Calibration of the TDT Sensors

Database	Applied to	Regression	R^2	RMSE (Volume %)	Bias (Volume %)	EF
Factory calibration						
—	Kraichgau	$\theta = 30V - 15$	0.57	8.3	−8.14	−1.54
—	Swabian Alb	$\theta = 23V + 13.7V^2 - 4.4V^3 - 14$	0.53	12.6	−8.81	−2.42
Pedotransfer-based calibration						
Both regions	Both regions	$\theta = 14.81N_tV + 8.61\rho V + 0.71\,\text{Silt}$	0.77	4.0	−0.02	0.77
Both regions	Kraichgau	$+ 0.15\,\text{Clay} + 2.89$	0.59	4.0	0.29	0.57
Both regions	Swabian Alb		0.71	3.9	−0.43	0.67
Kraichgau	Kraichgau	$\theta = 12.18\rho V + 0.02\sigma + 4.6$	0.64	3.7	−0.04	0.64
Swabian Alb	Swabian Alb	$\theta = 14.06N_tV + 5.86\rho V - 0.14\,\text{Silt} + 31.28$	0.74	3.4	−0.09	0.74

Note: C_t and N_t = total organic carbon and nitrogen content of soil, respectively; EF = modelling efficiency; R^2 = coefficient of determination; RMSE = root mean square error; V = sensor signal in volt; σ = electrical conductivity; ρ = soil bulk density.

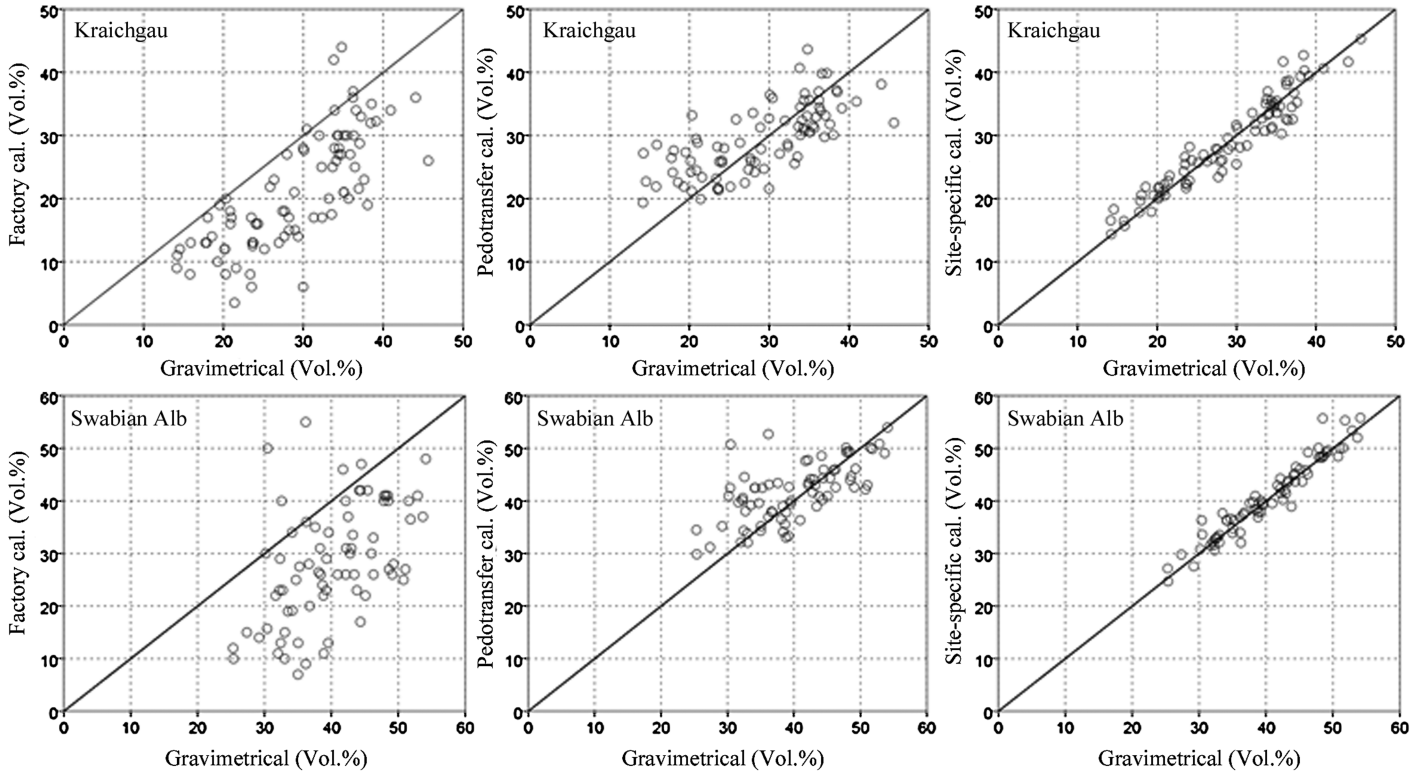

Fig. 5. Factory, pedotransfer, and site-specific calibrations against gravimetrical SWC for Kraichgau and SwabianAlb soil moisture network's stations, delivered by the sampling campaigns of 2010 and 2012

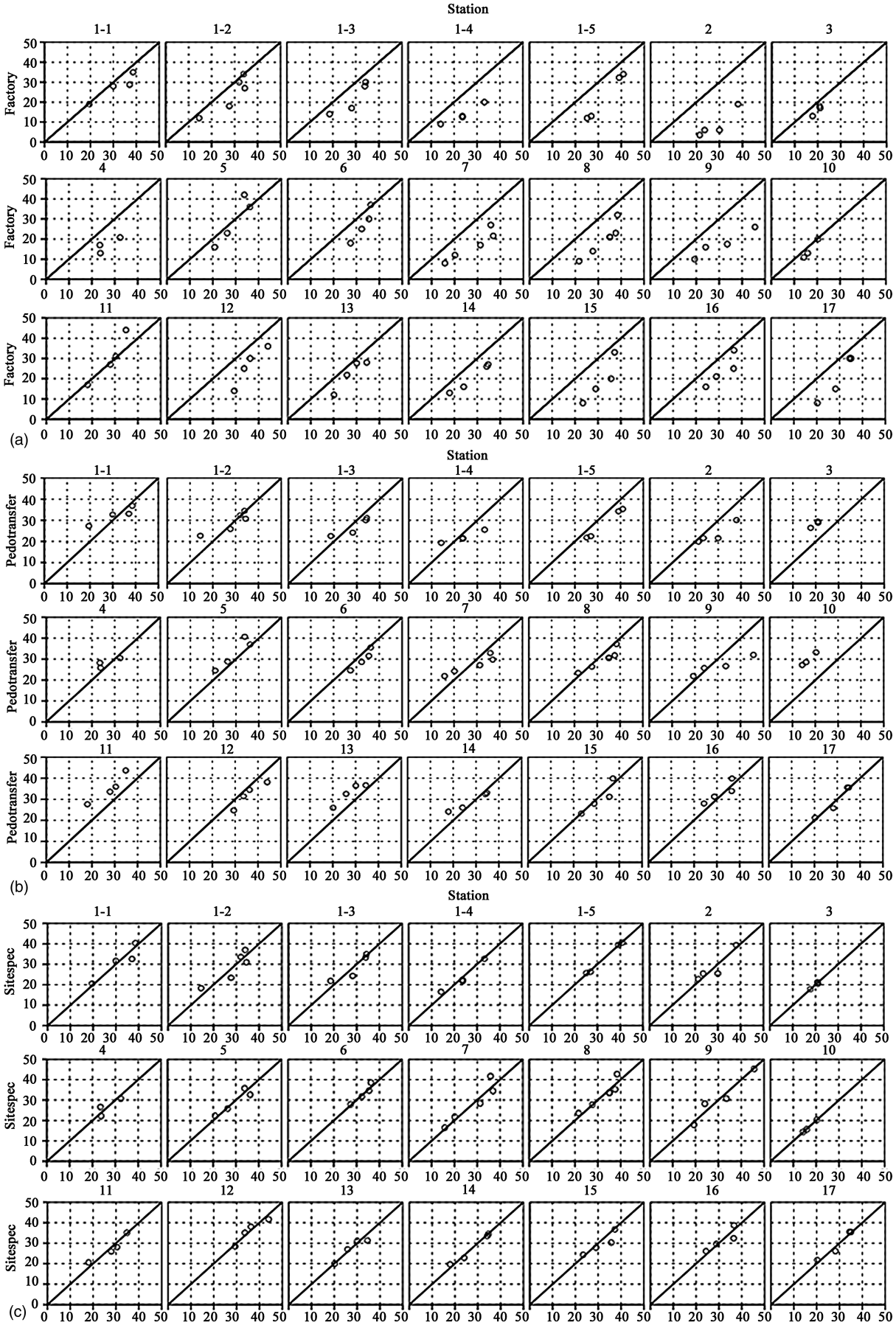

Fig. 6. Calibrations (Vol.%, axis *Y*) against gravimetrically determined SWC (Vol.%, axis *X*) for Kraichgau soil moisture network's stations: (a) factory; (b) pedotransfer; (c) site-specific

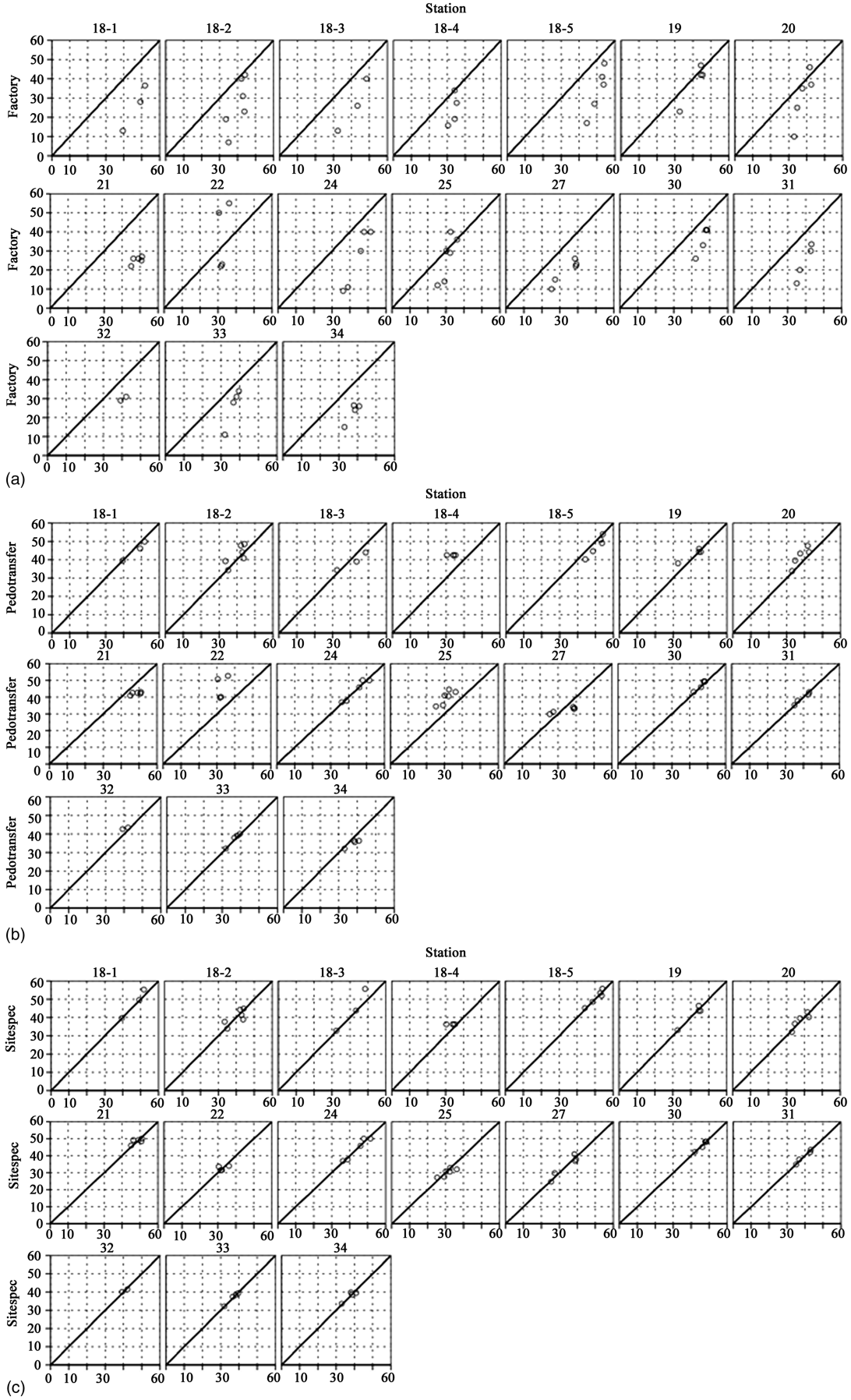

Fig. 7. Calibrations (Vol.%, axis *Y*) against gravimetrically determined SWC (Vol.%, axis *X*) for Swabian Alb soil moisture network's stations: (a) factory; (b) pedotransfer; (c) site-specific

obtained SWC for both regions is introduced on the Fig. 5 (data pooled over all stations) and on the Figs. 6 and 7 (station-wise). The highest scattering was observed for factory calibration, the lowest—for site specific. For the Kraichgau region the underestimation and overestimation of SWC, delivered by pedotransfer-based calibration [Fig. 6(b)], was greatly expressed at the stations, where soil properties differed drastically from the mean value. For example, σ at stations 3, 10, and 11 was higher compared with the mean, making difference of 136, 152, and 77 μS cm^{-1}, respectively, while σ at stations 1-4 and 1-5 was correspondingly 99 and 131 μS cm^{-1} lower.

Fig. 8 shows the soil water dynamics at Station 15 (Sulzfeld) in the Kraichgau region over a vegetation period in 2010. During this period, summer barley was grown. The factory calibration yields SWCs that are substantially lower than the reference data determined by the gravimetrical method. In high and middle SWC range pedotransfer-based approach tends to overestimate SWC, whereas in dry conditions the situation changes, and the pedotransfer-based calibration shows a better match.

We took soil samples with an auger, determined the gravimetric water content and converted the gravimetric into volumetric water content based on bulk density. This conversion entails a certain error. The standard error of the mean bulk density of the five samples taken at the day of installation averaged 0.03 g cm^{-3} (CV = 2.0%) and 0.04 (CV = 3.5%) g cm^{-3} in the Kraichgau and Swabian Alb, respectively. That means, for example, that at a gravimetric water content of 20% by weight, the error associated with bulk density conversion is in the range of ±0.6 Vol.% in Kraichgau and ±0.9 Vol.% in Swabian Alb. In Kraichgau the CV of ρ over all 21 stations (i.e., the overall spatial variability of bulk density) was 7%. In the Alb, this value was 16%. To determine whether bulk density varies from year to year, we remeasured bulk density at six stations in Kraichgau in 2011. At none of the six stations did the 2011 value differ significantly ($a = 0.05$) from that determined in 2009.

A further error is associated with sample size. At each sampling day, we sampled at three positions along the transmission line. In 2009, we did not pool the three samples to one composite sample, but we determined the gravimetric water content for each sample individually. The average standard error of the mean water content (N = 3) was 1.2 Vol.% in Kraichgau and 1.6 Vol.% in Swabian Alb. Hence, the overall error (conversion and sampling error) of the gravimetrically determined volumetric soil water contents is in the range of ±1.8 Vol.% in Kraichgau and ±2.5 Vol.% in Swabian Alb.

The physical and chemical state of the soil is known to effect TDR and TDT measurements. This has been discussed by other authors as influencing variables during calibration (Robinson et al. 2003; Gong et al. 2003; Schwartz et al. 2008; Stangl et al. 2009; Rosenbaum et al. 2011; Qu et al. 2013). The increase of σ gains the apparent dielectric permittivity (K_a), which is related to SWC (Gong et al. 2003). In the Qu et al. (2013) study on SPADE ring oscillator sensor calibration, which is an analogue to TDT technique, researchers reported that sensor output voltages nonlinearly elevate with increasing K_a. Payero et al. (2006) indicated a positive linear relation between the nitrogen concentration in the soil solution and TDR σ readings for non saline soils. This might be a reason why the model has chosen the N_t parameter influencing the slope of Swabian Alb regression in present study. In contrast, the N_t and silt content might be a better proxy for the long-term average field σ, than the one measured in the lab in a soil suspension with artificial soil:solution ratio. The greater the concentration of the solute, the more pronounced the effect of temperature on σ (Payero et al. 2006). Qu et al. (2013) found that the effect of temperature on sensor output is the largest at high rates of K_a. Based on manufacturer information, the Aquaflex TDT sensor has a temperature compensation implemented in the internal electronics of the measurement circuitry. Therefore, there is no need for an external temperature correction. Unfortunately, the manufacturer does not provide any details about the implemented temperature correction referring it as proprietary information.

Miyamoto et al. (2001) and Gong et al. (2003) stated that soil ρ directly proportionally influences the time delay of the TDR sensor signal. This effect is associated with greater dielectric constant of solid particles compared with that of air. In contrast, Whalley et al. (2004) reported that ρ has little or no influence on TDR readings. Schwartz et al. (2008) included soil ρ in their TDR calibration equation because of its statistical significance and ease of measurement. In contrast to our study, however, in their equation ρ influenced the intercept of regression and not the slope.

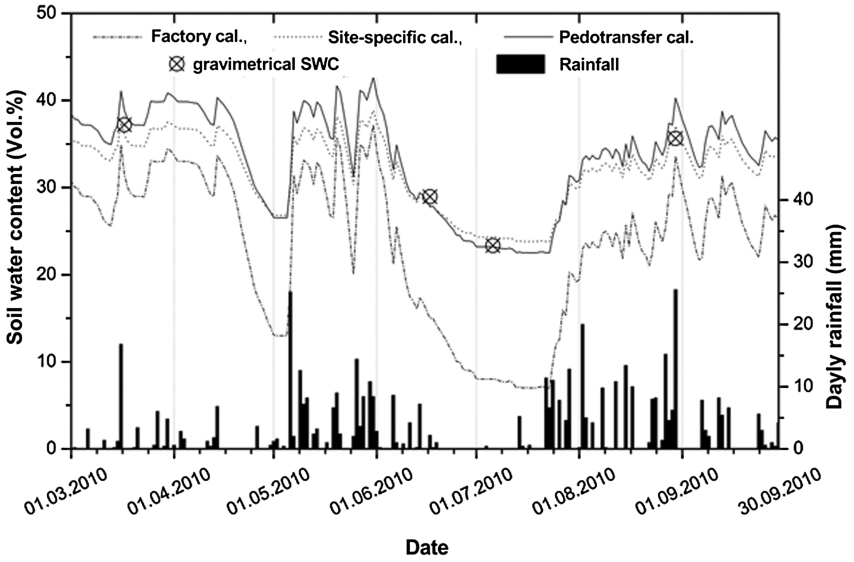

Fig. 8. Time series of soil water content at Station 15 (Sulzbach, Kraichgau network) delivered by factory, site-specific, and pedotransfer-based calibrations during summer 2010

Schwartz et al. (2008) reported that additional chemical properties (pH and organic matter) improved the calibration in small, but statistically significant increments. They concluded that inclusion of these properties was not justified because of the small increase in R^2 and cross-correlation problems. This is in line with our findings in that we found collinearity between pH, clay content and parameters, chosen by the regression (N_t, ρ, and silt content).

Our pedotransfer-based calibrations use physical and chemical properties, which are relatively easy to measure. We are convinced that these calibrations can be easily used in other regions with similar soils. We echo the recommendations of Schwartz et al. (2008) and Stangl et al. (2009) in that site-specific calibration should be used over default calibration because site-specific calibration delivered the highest R^2 values and lowest biases and RMSEs. Nonetheless, a site-specific calibrations are time consuming and labour intensive.

Conclusions

It is unavoidable that the soil around the Aquaflex TDT sensor becomes heavily disturbed and loosened during sensor installation. This calls for a resettlement phase before the sensor readings can be used. When it is not possible to mud in the sensor after its installation, we recommend taking the first readings at the earliest approximately six months after installation. Under west European conditions, it is therefore advisable to install the sensor in early autumn, enabling the soil around the sensor to settle down over winter. Then, first readings can be taken in spring.

The best agreement between TDT soil water data and gravimetrically determined SWCs was achieved based on a site-specific calibration. A site-specific calibration, however, is laborious and time-consuming. The pedotransfer-based approach we propose here is a good compromise between labour effort and accuracy. We identified for the silty soils of the Kraichgau region ρ and σ as soil variables affecting the calibration curve. For the soils of the Swabian Alb, slope and intercept of the calibration curve were a function of the total nitrogen content, ρ, and silt fraction. This approach can be applied to a large number of sensors when soils have similar textures and properties, as in our study areas, without the need to continuously collect soil samples for site-specific calibration. Our study demonstrates the importance of calibrating the Aquaflex TDT sensor for quantitative purposes. Based on the factory calibration the sensor might deliver highly biased SWCs.

Acknowledgments

We gratefully acknowledge the funding of the project by the German Research Foundation (DFG) in the frame of PAK 346 *Structure and functions of agricultural landscapes under climate change—processes and projections on a regional scale* and the research unit FOR 1695 *Regional climate change*. Moreover, we are thankful to 41 local farmers of Kraichgau and Swabian Alb for their willingness to support our research.

References

Alletto, L., and Coquet, Y. (2009). "Temporal and spatial variability of soil bulk density and near-saturated hydraulic conductivity under two contrasted tillage management systems." *Geoderma*, 152(1–2), 85–94.

Baker, J. M., and Spaans, E. J. A. (1994). "Measuring water exchange between soil and atmosphere with TDR-microlysimetry." *Soil Sci.*, 158(1), 22–30.

Ball, B. C., Campbell, D. J., Douglas, J. T., Henshall, J. K., and O'Sullivan, M. F. (1997). "Soil structural quality, compaction and land management." *Eur. J. Soil Sci.*, 48(4), 593–601.

Biernath, C., et al. (2011). "Evaluating the ability of four crop models to predict different environmental impacts on spring wheat grown in open-top chambers." *Eur. J. Agron.*, 35(2), 71–82.

Bogena, H. R., Herbst, M., Huisman, J. A., Rosenbaum, U., Weuthen, A., and Vereecken, H. (2010). "Potential of wireless sensor networks for measuring soil water content variability." *Vadose Zone J.*, 9(4), 1002–1013.

Bundesamt für Kartographie und Geodäsie (BKG). (2014). ⟨http://www.geodatenzentrum.de/geodaten/gdz_rahmen.gdz_div⟩.

Dirmeyer, P. A., and Brubaker, K. L. (1999). "Contrasting evaporative moisture sources during the drought of 1988 and the flood of 1993." *J. Geophys. Res.*, 104(D16), 19383–19397.

Evett, S. R., Tolk, J. A., and Howell, T. A. (2006). "Soil profile water content determination: Sensor accuracy, axial response, calibration, temperature dependence, and precision." *Vadose Zone J.*, 5(3), 894–907.

Gong, Y., Cao, Q., and Sun, Z. (2003). "The effects of soil bulk density, clay content and temperature on soil water content measurement using time-domain reflectometry." *Hydrol. Processes*, 17(18), 3601–3614.

Gutmann, E. D., and Small, E. E. (2007). "A comparison of land surface model soil hydraulic properties estimated by inverse modeling and pedotransfer functions." *Water Resour. Res.*, 43(5), W05418.

Harlow, R. C., Burke, E. J., and Ferre, T. P. A. (2003). "Measuring water content in saline sands using impulse time domain transmission techniques." *Vadose Zone J.*, 2(3), 433–439.

Harter, T., and Hopmans, J. W. (2004). "Role of vadose zone flow processes in regional scale hydrology: Review, opportunities and challenges." *Unsaturated zone modeling: Progress, challenges and applications*, R. A. Feddes, G. H. De Rooij, and J. C. van Dam, eds., Kluwer Academic, Dordrect, Netherlands, 179–210.

Hedley, C. B., and Yule, I. J. (2009). "A method for spatial prediction of daily soil water status for precise irrigation scheduling." *Agric. Water Manage.*, 96(12), 1737–1745.

Hollinger, S. E., and Isard, S. A. (1994). "A soil moisture climatology of Illinois." *J. Climatol.*, 7(5), 822–833.

Hook, W. R., Ferre, T. P. A., and Livingston, N. J. (2004). "The effects of salinity on the accuracy and uncertainty of water content measurement." *Soil Sci. Soc. Am. J.*, 69(3), 47–56.

Ilstone, B. G., Basara, J. B., Fiebrich, C. A., Crawford, K. C., and Hunt, E. (2008). "Mesoscale monitoring of soil moisture across a statewide network." *Am. Meteorolog. Soc.*, 25(2), 167–182.

Ingwersen, J., et al. (2011). "Comparison of Noah simulations with eddy covariance and soil water measurements at a winter wheat stand." *Agric. For. Meteorol.*, 151(3), 345–355.

Leib, B. G., Jabro, J. D., and Matthews, G. R. (2003). "Field evaluation and performance comparison of soil moisture sensors." *Soil Sci.*, 168(6), 396–408.

McCready, M. S., Dukes, M. D., and Miller, G. L. (2009). "Water conservation potential of smart irrigation controllers on St. Augustinegrass." *Agric. Water Manage.*, 96(11), 1623–1632.

Mittelbach, H., Casini, F., Lehner, I., Teuling, A. J., and Seneviratne, S. I. (2011). "Soil moisture monitoring for climate research: Evaluation of a low-cost sensor in the framework of the Swiss soil moisture experiment (SwissSMEX) campaign." *J. Geophys. Res. Atmos.*, 116(D5), D05111.

Miyamoto, T., Kobayashi, R., Annaka, T., and Chikushi, J. (2001). "Applicability of multiple length TDR probes to measure water distributions in an Andisol under different tillage systems in Japan." *Soil Tillage Res.*, 60(1–2), 91–99.

Morari, F., and Giardini, L. (2002). "Irrigation automation with heterogeneous vegetation: The case of the Padova botanical garden." *Agric. Water Manage.*, 55(3), 183–201.

Moriasi, D. N., Arnold, J. G., Van Liew, M. W., Bingner, R. L., Harmel, R. D., and Veith, T. L. (2007). "Model evaluation guidelines for systematic quantification of accuracy in watershed simulations." *Trans. ASABE*, 50(3), 885–900.

Nash, J. E., and Sutcliffe, J. V. (1970). "River flow forecasting through conceptual models. Part I. A discussion of principles." *J. Hydrol.*, 10(3), 282–290.

PASW SPSS Version 18 [Computer software]. Armonk, NY, IBM Corporation.

Payero, J. O., Tarkalson, D. D., and Irmak, S. (2006). "Use of time domain reflectometry for continuous monitoring of nitrate-nitrogen in soil and water." *Appl. Eng. Agric.*, 22(5), 689–700.

Plauborg, F., Iversen, B. V., and Lærke, P. E. (2005). "In situ comparison of three dielectric soil moisture sensors in drip irrigated sandy soils." *Vadose Zone J.*, 4(4), 1037–1047.

Qu, W., Bogena, H. R., Huisman, J. A., and Vereecken, H. (2013). "Calibration of a novel low-cost soil water content sensor based on a ring oscillator." *Vadose Zone J.*, 12(2), 0139–0149.

Robinson, D. A., et al. (2008). "Soil moisture measurement for ecological and hydrological watershed-scale observatories: A review." *Vadose Zone J.*, 7(1), 358–389.

Robinson, D. A., Jones, S. B., Wraith, J. M., Or, D., and Friedman, S. P. (2003). "A review of advances in dielectric and electrical conductivity measurement in soils using time domain reflectometry." *Vadose Zone J.*, 2(4), 444–475.

Robock, A., et al. (2000). "The global soil moisture data bank." *Bull. Am. Meteorol. Soc.*, 81(6), 1281–1299.

Robock, A., et al. (2003). "Evaluation of the North American land data assimilation system over the southern great plains during the warm season." *J. Geophys. Res. Atmos.*, 108(D22), GCP 7–GCP 21.

Rosenbaum, U., Huisman, J. A., Vrba, J., Vereecken, H., and Bogena, H. R. (2011). "Correction of temperature and electrical conductivity effects on dielectric permittivity measurements with ECH2O sensors." *Vadose Zone J.*, 10(2), 582–593.

Scheffer, F., and Schachtschabel, P. (2008). *Soil science handbook*, 15. Auflage. Spektrum Akademischer, Heidelberg.

Schlichting, E., Blume, H. P., and Stahr, K. (1995). *Soil science practical cource—Implementation to pedology for ecology, land and geology scientists*, Blackwell Wiss, Berlin.

Schwartz, B. F., Schreiber, M. E., Pooler, P. S., and Rimstidt, J. D. (2008). "Calibrating access-tube time domain reflectometry soil water measurements in deep heterogeneous soils." *Soil Sci. Soc. Am. J.*, 72(4), 917–930.

Stangl, R., Buchan, G. D., and Loiskandl, W. (2009). "Field use and calibration of a TDR-based probe for monitoring water content in a high-clay landslide soil in Austria." *Geoderma*, 150(1–2), 23–31.

Streat Instruments Ltd. (2003). "Aquaflex sensor part # SI.99." *Instruction manual*, ⟨http://www.streatsahead.com/Pages/Aquaflex%20level2/Product%20Notes/SI_99productnote.pdf⟩ (Apr. 16, 2003).

Topp, G. C., Davis, J. L., and Annan, A. P. (1980). "Electromagnetic determination of soil water content: Measurements in coaxial transmission lines." *Water Resour. Res.*, 16(3), 574–582.

Weaver, C. P., and Avissar, R. (2001). "Atmospheric disturbances caused by human modification of the landscape." *Bull. Am. Meteorolog. Soc.*, 82(2), 269–281.

Whalley, W. R., Cope, R. E., Nicholl, C. J., and Whitmore, A. P. (2004). "In-field calibration of a dielectric soil moisture meter designed for use in an access tube." *Soil Use Manage.*, 20(2), 203–206.

World Resources Reports (WRB). (2006). "WRB and food and agricultural organization of the united nations. World reference base for soil resources." *World Resources Rep. 103*, Rome.

Wraith, J. M., Robinson, D. A., Jones, S. B., and Long, D. S. (2005). "Spatially characterizing apparent electrical conductivity and water content of surface soils with time domain reflectometry." *Comp. Electron. Agric.*, 46(1–3), 239–261.

Zacharias, S., et al. (2011). "A network of terrestrial environmental observatories in Germany." *Vadose Zone J.*, 10(3), 955–973.

Zhu, J., and Liang, X. (2005). "Regional climate model simulation of U.S. soil temperature and moisture during 1982–2002." *J. Geophys. Res. Atmos.*, 110(D24), 1–12.

5. Spatial and temporal variability of soil water content in two regions of southwest Germany over a three-year observation period

The original publication “Poltoradnev, M., Ingwersen, J., and T. Streck. 2016. Spatial and Temporal Variability of Soil Water Content in Two Regions of Southwest Germany during a Three-Year Observation Period. *Vadose Zone Journal*, 15(6)” can be found via the following link: http://vzj.geoscienceworld.org/content/15/6/vzj2015.11.0143

Original Research

Core Ideas

- The variability of soil physical properties determines the anchor points of the mean spatial soil water content versus standard deviation of soil water content (sigmatheta-theta) phase space.
- The lower bound of the sigmatheta-theta envelope reflects the regional variability of soil water retention curves.
- The sigmatheta generation or dissipation depends on its momentary location in relation to the anchor points and envelope bounds.
- The initiation of clockwise hysteretic loops is triggered by rainstorms with spatially highly variable intensities.
- The sigmatheta-theta envelopes are useful to test the performance of distributed hydrological or land surface models.

M. Poltoradnev, Institute of Soil Science and Land Evaluation, Biogeophysics, Universität Hohenheim, Emil-Wolff-Str. 27, 70599 Stuttgart, Germany; J. Ingwersen, Institute of Soil Science and Land Evaluation, Biogeophysics, Universität Hohenheim, Emil-Wolff-Str. 27, 70599 Stuttgart, Germany; and T. Streck, Institute of Soil Science and Land Evaluation, Biogeophysics, Universität Hohenheim, Emil-Wolff-Str. 27, 70599 Stuttgart, Germany. Received 3 Nov. 2015. Accepted 17 March 2016. *Corresponding author (m.poltoradnev@uni-hohenheim.de).

Vadose Zone J.
doi:10.2136/vzj2015.11.0143
Received 3 Nov. 2015.
Accepted 17 Mar. 2016.

Spatial and Temporal Variability of Soil Water Content in Two Regions of Southwest Germany during a Three-Year Observation Period

Maxim Poltoradnev,* Joachim Ingwersen, and Thilo Streck

The topsoil water content (SWC) plays a key role in partitioning energy and water fluxes at the land surface. Knowledge about its spatial and temporal variability is crucial for improving climate and hydrology modeling. We investigated SWC variability, its relation to the mean spatial soil water content ($\langle\theta\rangle$), and the variability of rainfall on the regional spatial and event temporal scales. We used a 3-yr data set, obtained at 15-min resolution from two soil moisture sensor networks (spatial extent: 25 by 25 km), set up at croplands in the Kraichgau and Swabian Alb regions in southwest Germany. The relationship of SWC standard deviation (σ_θ) versus $\langle\theta\rangle$ was studied (σ_θ–$\langle\theta\rangle$). The closer σ_θ is located to the edge of the envelope, the σ_θ at the permanent wilting point (σ_θ–$\langle\theta_{wp}\rangle$), and the σ_θ at saturation (σ_θ–$\langle\theta_s\rangle$)—the anchor points—the easier it is to apprehend whether σ_θ will increase or decrease on a change in $\langle\theta\rangle$. The σ_θ–$\langle\theta\rangle$ relationship forms combinations of concave and convex hyperbolas reflecting the variability of soil texture and depending on σ_θ in relation to the anchor points. Most σ_θ–$\langle\theta\rangle$ clockwise hysteresis cases occurred in an intermediate and intermediate-wet state of SWC. The initiation of a clockwise hysteretic loop is initiated by preferential flow. The σ_θ phase space can be used to test whether hydrological or land surface models capture a realistic range of soil water heterogeneity.

Abbreviations: DWD, drying-wetting-drying cycles; EC, eddy covariance; ET_C, crop evapotranspiration; SWB, seasonal water balance; SWC, soil water content; TDT, time-domain transmission; WDP, wetting-drying periods.

Research on the dynamics of the soil water content (SWC) is essential to understand land surface–atmosphere feedbacks. The SWC directly influences cloud formation and precipitation (Goodrich et al., 1994; Famiglietti et al., 1998; Heathman et al., 2009; López-Vicente et al., 2009; Heathman et al., 2012). It plays a key role in partitioning precipitation into infiltration and runoff. The SWC is spatially variable because of variable rainfall and the heterogeneity of soil, vegetation, and topography (Yoo et al., 1998; Albertson and Montaldo, 2003; Vereecken et al., 2007; López-Vicente et al., 2009; Bogena et al., 2010). The impact of these factors, however, varies depending on the time of season and initial conditions (Grayson et al., 1997). There is a growing interest in different research fields, such as hydrology, meteorology, plant physiology, and soil physics among others, in long-term data sets on the dynamics of topsoil water content. A better knowledge of the mechanisms governing the spatiotemporal variability of SWC is key to improving atmospheric and hydrological process modeling on scales from field to global.

The spatial variability of SWC is often evaluated by exploring the relationship between the spatial mean ($\langle\theta\rangle$) of SWC and its standard deviation (σ_θ). In the following, this relationship will be denoted σ_θ–$\langle\theta\rangle$. It is typically visualized in a scatterplot. Patterns are often evaluated with regard to three SWC states: dry, intermediate, and wet. To identify factors affecting the σ_θ–$\langle\theta\rangle$ relationship, numerous authors performed numerical simulation experiments on the dynamics of spatial SWC distribution and tested the results against field and remote sensing data (Albertson and Montaldo, 2003; Vereecken

et al., 2007; Pan and Peters-Lidard, 2008; Vivoni et al., 2010). Some authors also used geostatistical methods for data analysis (Grayson et al., 1997; Western et al., 2004).

As expected, different factors affect the spatial and temporal patterns of SWC to a varying degree, depending on sampling scale and hydrological conditions. In small catchments (<10 km^2), under wet conditions nonlocal controls dictate SWC variability (Grayson et al., 1997; Western et al., 2004; Vereecken et al., 2007; Vivoni et al., 2010). In contrast, under dry conditions local controls (evapotranspiration, vegetation, and microrelief) are the main drivers (Grayson et al., 1997; Pan and Peters-Lidard, 2008; Vivoni et al., 2010). In the intermediate state of SWC, σ_θ–$\langle\theta\rangle$ is mostly controlled by variations in hydraulic properties and vegetation, that is, a combination of nonlocal and local controls (Famiglietti et al., 1998; Vereecken et al., 2007, Pan and Peters-Lidard, 2008; Vivoni et al., 2010). At larger scales (>100 km^2), additional factors such as rainfall distribution influence SWC variability (Albertson and Montaldo, 2003). All of the above-mentioned factors are usually interrelated in a nonlinear way. Some are more important than others during limited periods of time and environmental conditions. Moreover, controls may change seasonally (Grayson et al., 1997; Western et al., 2004).

Most studies report that σ_θ decreases as $\langle\theta\rangle$ increases (Grayson et al., 1997; Brocca et al., 2007; De Lannoy et al., 2006; Choi et al., 2007; Hu et al., 2008; López-Vicente et al., 2009; Bogena et al., 2010; Mittelbach and Seneviratne, 2012). A few authors, however, have also observed the opposite: σ_θ increased with increasing $\langle\theta\rangle$ (Famiglietti et al., 1998; Hu et al., 2011). Some studies showed that during drying periods σ_θ–$\langle\theta\rangle$ increased and then decreased after peaking at some critical $\langle\theta\rangle$ (Vereecken et al., 2007; Famiglietti et al., 2008; Pan and Peters-Lidard, 2008; Brocca et al., 2012; Rosenbaum et. al., 2012).

Most of the studies mentioned above were conducted at the catchment scale and/or the data were collected over a short period of time (a few months in summer), or were based on simulations. In contrast, Famiglietti et al. (2008) analyzed measurements at different scales (from several square meters to 50 by 100 km). Sampling campaigns were performed using impedance probes on cropland (winter wheat, corn, soybean, cotton, and forested area), and the sampling period covered 3 wk in summer. The authors observed a convex upward σ_θ–$\langle\theta\rangle$ relationship, with the highest σ_θ values at an intermediate SWC state. Brocca et al. (2012) took weekly SWC measurements using time-domain reflectometry (TDR) networks over a 1-yr period. The networks covered an arable land (grassland and bare soil sites) area of 178 and 242 km^2, but no measurements were taken in summer. The patterns observed were similar to those of Famiglietti et al. (2008), but the variability of SWC was lower. Rosenbaum et al. (2012) also reported a convex upward shape of σ_θ–$\langle\theta\rangle$ peaking in the intermediate state of SWC. Their measurements were taken over a period of 1 yr in a small, forested catchment of 0.27 km^2. They used a wireless soil moisture sensor network consisting of 150 measurement locations equipped with capacitance probes. Mittelbach and Seneviratne (2012) conducted continuous measurements over a period of 15 mo at 14 grassland sites of the SwissSMEX soil moisture network, covering an area of 150 by 210 km. They used TDR and capacitance probe sensors and observed that σ_θ increased with decreasing $\langle\theta\rangle$.

In numerical simulation experiments, several researchers reported a hysteresis in the σ_θ–$\langle\theta\rangle$ plot (Teuling et al., 2007; Ivanov et al., 2010; Vivoni et al., 2010). This is in line with field observations (Rosenbaum et al., 2012). Hysteresis was found in sequential wetting-drying periods (WDP) in different ranges of SWC and was named event-scale clockwise (primarily in the wet and intermediate SWC state) or contraclockwise hysteresis (in the dry SWC state). All studies agree in that hysteretic loops occur after rainfalls above a threshold value and are particularly distinct when the rainfall is high. Vivoni et al. (2010) and Rosenbaum et al. (2012) concluded that precipitation is a main factor controlling the ascending (wetting) branch of the hysteretic loop. Topography and evapotranspiration are essential for establishing a descending (drying) branch that converges to the initial point (Ivanov et al., 2010; Vivoni et al., 2010). It was hypothesized that distinctiveness of drying and wetting branches strongly depends on the spatial variation of these factors.

For cropland, we lack long-term, multiple-year, continuous ground-based measurements of SWC at scales from 10 to 1000 km^2 (i.e., regional scale). Among 48 soil moisture networks of the International Soil Moisture Network (Dorigo et al., 2011), only three were fully or partially established and continuously operated on arable lands: OzNet (Smith et al., 2012), HOBE (Bircher et al., 2012), and REMEDHUS (Sánchez et al., 2012). On cropland, the operation and maintenance of a soil sensor network is quite labor intensive because of tillage and other field activities. The rapid changes in the vegetation cover, however, make such data very important for validating and further developing land surface models. They may further serve as ground truth of remotely sensed SWC.

The main objective of the present study was twofold: first, to quantify and evaluate the dynamics of $\langle\theta\rangle$ and σ_θ and their controls on cropland on the regional and seasonal scale, and, second, to elucidate what triggers hysteresis loops on the event scale. For this, we installed two networks of 21 time-domain transmission (TDT) sensors, each in topsoils of two arable landscapes in southwest Germany with distinctly different climates. All 42 stations were equipped with rainfall and temperature sensors. Measurements were taken over a 3-yr period.

Materials and Methods

Study Sites

In brief, the Kraichgau region has a mild climate with a mean temperature of about 9°C. Annual precipitation ranges between 720 and 830 mm. Predominant soil types are Regosols (World Reference Base [WRB], 2006) and Luvisols (WRB, 2006) from Loess. Agricultural land has a share of 53%. The mean temperature on Swabian Alb is 6 to 7°C. Annual precipitation ranges between 800 and 1000 mm. The main soil type is an A-C soil: a Leptosol (WRB, 2006) with a shallow solum, and thickness is usually less than 0.3 m. Agricultural land covers 52%. Topsoils in Kraichgau show, on average, higher bulk density and higher electrical conductivity than on Swabian Alb (Table 1). In Kraichgau, soil texture is dominated by the silt fraction, whereas the soils of Swabian Alb have considerably higher clay content.

In Kraichgau, the vegetation period starts typically about 2 to 3 wk earlier than on Swabian Alb. Primary soil tillage is different in both regions. Because the silty soils of the Kraichgau region are prone to water erosion, farmers are advised to grub instead of plow. Grubbing depth ranges between 0.15 and 0.20 m. On Swabian Alb, soils are commonly plowed. Because the soils are shallow, plowing depth is typically only about 0.10 m. The crop rotation is different in both regions. In Kraichgau it typically consists of winter wheat, summer barley, maize, winter rape, and sugar beet. On Swabian Alb spelled, triticale, perennial grass, and clover are often parts of crop rotation.

Regional Soil Moisture Sensor Networks

In each model region, a soil moisture sensor network was installed from April to June 2009. Each sensor network consisted of 21 stations. All stations were located on cropland and were distributed across three spatial domains: an inner domain 3 by 3 km (5 stations), a middle 9 by 9 km (8 stations), and an outer domain 27 by 27 km (8 stations) (Fig. 1). The sizes of the three domains correspond to typical grid sizes used in coupled atmosphere-land surface models. Each station consisted of a TDT soil moisture sensor (SI.99 Aquaflex Soil Moisture Sensor, Streat Moisture Solutions, USA), a rain gauge, a solar panel, and a remote transfer unit (RTU, datalogger + global system for mobile modem), which stores and transfers the data via the GSM modem to the central data server (Adcon Telemetry, Austria) located at the University of Hohenheim. Rain gauge (1.80 m above ground), RTU, and solar panel were mounted to an aluminum mast. The TDT sensor was buried in 0.15 m of soil depth. Data were collected at 15-min resolution.

Every station was set up in the middle between two machine tracks, so that the farmer could easily pass the station when applying fertilizer or pesticides. To avoid damage to the sensor, the sensor area was not plowed or grubbed by the farmer, but manually tilled with a bar spade. Other tillage operations, such as rotary harrowing and drilling, were performed by the farmers with their usual machinery.

Table 1. Topsoil properties of the two soil moisture networks in Kraichgau and on Swabian Alb.†

	σ	ρ	Sand	Silt	Clay
	μS cm^{-1}	g cm^{-3}	% by mass		
Kraichgau					
$\bar{x}$	175.2	1.51	4.1	73.8	22.1
S	89.5	0.10	2.7	5.8	4.9
Min	33.5	1.32	1.7	59.4	13.7
Max	327.0	1.65	12.1	82.3	29.9
Swabian Alb					
$\bar{x}$	138.3	1.15	3.5	46.5	50.0
S	56.1	0.18	3.0	11.8	12.8
Min.	63.0	0.78	1.5	29.1	24.9
Max.	295.5	1.56	11.8	77.2	76.1

† σ, electrical conductivity; ρ, soil bulk density.

More information on study sites and sensor networks is given elsewhere (Poltoradnev et al., 2015; website of PAK 346/FOR 1695: https://klimawandel.uni-hohenheim.de/).

Data Analysis

All TDT sensors were calibrated site specifically based on a linear regression between the volumetric water content (θ_v) and the output signal of the sensor (Poltoradnev et al., 2015):

$$\theta_v(V) = aV + b \quad [1]$$

Here, a and b are the site-specific slope [% (v/v) V^{-1}] and intercept [% (v/v)] of a sensor, respectively, and V denotes the TDT output voltage (V). Calibration RMSE (root mean square error) was on average 2.2 and 1.4 for the Kraichgau and the Swabian Alb sensor network, respectively.

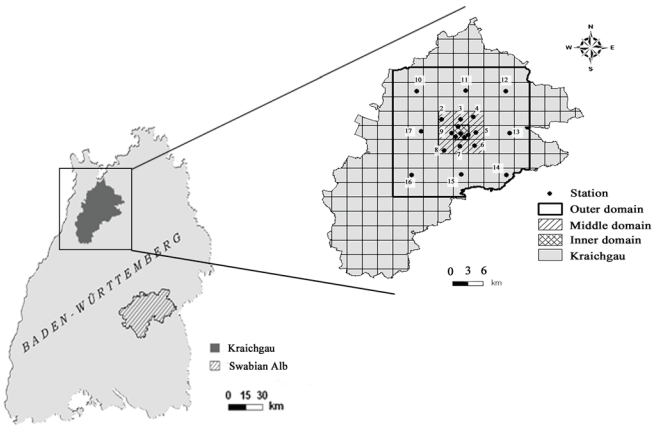

Fig. 1. Map of Baden-Württemberg state (Germany) with two model regions (on the left) and position of soil moisture sensor network stations in Kraichgau region (on the right). Network was divided into inner (3 by 3 km^2), middle (9 by 9 km^2), and outer (27 by 27 km^2) domains. In the inner domain the five stations were labeled from 1-1 to 1-5 in the numerical order. Map source: www.geodatenzentrum.de.

We analyzed three vegetation periods, each lasting from 1 April to 31 October 2010, 2011, and 2012. The original SWC data were taken at 15-min resolution. On the basis of these data, aggregated daily means were also analyzed. Before the analysis, data were inspected and inconsistent measurements discarded. Data failure originated from incomplete settlement of TDT sensors (because of installation <6 mo before a data collection period) and various other reasons. Every action taken at each station was documented in a field book. The SWC time series were visually evaluated by plotting them separately for each sensor. We obtained complete SWC time series of 17 stations in 2010 and 2011 as well as of 16 stations in 2012 from Kraichgau and of 15 stations in 2010, 14 stations in 2011, and 10 stations in 2012 from Swabian Alb.

Spatial mean ($\langle\theta\rangle$) and standard deviation of SWC (σ_θ) were estimated by the standard formulas available in the Excel software (Version 2010, Microsoft). Student's *t*-test was performed to test the statistical significance of differences between selected parameters using the Excel data analysis package.

To indicate the contingent phase space of σ_θ and $\langle\theta\rangle$, that is, the set of possible σ_θ–$\langle\theta\rangle$ states, we used the PlotRegionHighlighter package (Noma, 2013) available in R (version 3.1.1, Lucent Technologies Bell Labs Innovations, France). This software routine computes the envelope surrounding a data cloud. For each region, the three observation periods were pooled. Additionally, two characteristic points of the phase space, that is, σ_θ at the permanent wilting point (σ_θ–$\langle\theta_{wp}\rangle$) and σ_θ at saturation (σ_θ–$\langle\theta_s\rangle$), were included in computing the envelope. In the following, these points will be called anchor points. For each region the PlotRegionHighlighter routine created a polygon with a continuous boundary, leaning on the outermost points of the resulting data cloud, consisting of a pooled data set and anchor points, as a belt leans under tension on pulleys.

The SWC at wilting point (θ_{wp}) was determined in the lab. Soil samples, collected on the day of installation along the sensor area at each station, were placed on a porous ceramic plate at −1.5 MPa pressure. After equilibration, θ_{wp} was determined gravimetrically after drying at 105°C. The SWC at saturation (θ_s) was estimated from bulk density (ρ_s, g cm^{-3})

$$\theta_s = 1 - \rho_s / \rho_f \qquad [2]$$

where the coefficient ρ_f indicates the average particle density (2.65 g cm^{-3}). To determine the soil bulk density, five 100 cm^3 soil cores were taken on the day of installation close to the sensor from 0.15 m of soil depth.

To indicate the relative contribution of soil and rainfall and other factors into the σ_θ–$\langle\theta\rangle$ phase space, we computed the $\langle\theta\rangle$ and σ_θ over spatially homogeneous matric potentials with 10-hPa lag beginning from 0 and terminating at −1600 hPa. The van Genuchten parameters (van Genuchten, 1980) were calculated with the Rosetta Lite v.1.1 module (Schaap et al., 2001) from measured bulk density, sand, silt, and clay content obtained from in situ samples collected in immediate proximity to each measuring location.

To facilitate the interpretation of the results, similarly to Rosenbaum et al. (2012), we grouped observations into three SWC states: for the Kraichgau data we selected a dry, intermediate, and wet state to be $\langle\theta\rangle$ < 25 % (v/v), 25 % (v/v) < $\langle\theta\rangle$ < 35 % (v/v), and $\langle\theta\rangle$ > 35 % (v/v), while for the Swabian Alb the corresponding values were $\langle\theta\rangle$ < 35 % (v/v), 35 % (v/v) < $\langle\theta\rangle$ < 45 % (v/v), and $\langle\theta\rangle$ > 45 % (v/v).

For each vegetation period, total rainfall, mean rainfall intensity, and rainfall frequency were calculated. Mean rainfall intensity (mm d^{-1}) was computed as total rainfall divided by the number of rainy days per season. A rainy day was defined as a day on which rainfall was recorded at least at one of the 21 sensor stations.

Crop evapotranspiration (ET_c, mm d^{-1}) was calculated using the FAO Penman–Monteith approach (Allen and Pereira, 1998). For each station ET_c was calculated by

$$ET_c = K_c ET_0 \qquad [3]$$

where ET_0 is the reference crop evapotranspiration (mm d^{-1}) and K_c is a crop-specific coefficient (K_c factor) taken from Allen and Pereira (1998, Table 12) and adjusted to the weather and crop conditions of the study areas. From the difference between total rainfall and ET_c, we computed the seasonal water balance (SWB). The ET_0 was calculated as:

$$ET_0 = \frac{0.408\Delta(R_n - G) + \gamma\frac{900}{T+273}u_2(e_s - e_a)}{\Delta + \gamma(1 + 0.34u_2)} \qquad [4]$$

where R_n is net radiation (MJ m^{-2} d^{-1}), G is a soil heat flux (MJ m^{-2} d^{-1}), T is a daily mean air temperature at 2 m height (°C), u_2 is wind speed at 2 m height (m s^{-1}), e_s is saturation vapor pressure (kPa), e_a is actual vapor pressure (kPa), Δ is the slope of the vapor pressure curve (kPa °C^{-1}), and γ is the psychrometric constant (kPa °C^{-1}). Data were taken from an eddy covariance (EC) station operated about 30 km south of the network center in the case of Kraichgau and about 28 km in the case of Swabian Alb (Ingwersen et al., 2011; Wizemann et al., 2014).

To analyze the soil water data on the event scale (Rosenbaum et al., 2012), each seasonal data set was split into drying-wetting-drying (DWD) cycles. Each DWD cycle was selected in such a way that it consisted of an initial continuous drying period (decreasing $\langle\theta\rangle$), followed by a rewetting event due to rainfall, and a second drying period. Some DWD cycles selected occurred in the transition

phases between dry and intermediate or intermediate and wet SWC states. For the sake of simplicity and to avoid having DWD cycles spreading over two SWC states, we introduced dry-intermediate and intermediate-wet transition states.

A DWD cycle was characterized by the following properties: total rainfall (mm), length of the wetting period (h), rainfall intensity (as the ratio of the former two quantities), and change in $\langle\theta\rangle$. The wetting period length was defined as the period of time between first increase and maximum of $\langle\theta\rangle$. The change of $\langle\theta\rangle$ was defined as the difference in $\langle\theta\rangle$ observed at the beginning and the end of a wetting period. To determine whether DWD was hysteretic or nonhysteretic, we visually inspected each DWD and estimated the absolute difference in σ_θ between drying and wetting branches. We set the threshold value at 0.2. When the difference was greater than the threshold value, DWD was attributed to hysteretic.

To facilitate the description and interpretation of the time series and the interrelation between $\sigma_\theta(t)$, $\langle\theta\rangle(t)$, $\sigma_\theta - \langle\theta\rangle$, and σ_θ – (rainfall intensity), we pinpointed 7 to 12 characteristic points for every DWD. The first and the last point indicate the start and the end of the DWD. The third or fourth point usually pinpoint the onset of the rewetting period, and the following points indicate the rewetting period.

Results

Table 2 gives the temporal statistics of the spatial mean and the spatial variation of the SWC. The mean topsoil water content, $\langle\theta\rangle$, of Swabian Alb was between 11 and 16 % (v/v) higher than in Kraichgau (Table 2). The 2010 observation period showed the broadest range of $\langle\theta\rangle$, occurring in Kraichgau. The mean of σ_θ was higher on Swabian Alb than in Kraichgau, while its range was lower in the former.

The mean topsoil water content at the permanent wilting point, $\langle\theta_{wp}\rangle$, was 19.5 % (v/v) in Kraichgau and 29.6 % (v/v) on Swabian Alb. These values were reached closest only in 2010. The $\langle\theta_s\rangle$ was 42.8 % (v/v) in Kraichgau and 55.8 % (v/v) on Swabian Alb. As expected, topsoils were, on average, never saturated, neither in Kraichgau nor on Swabian Alb.

Table 2. Statistics of the spatially averaged soil water content ($\langle\theta\rangle$) in Kraichgau and on Swabian Alb in the April–October measuring periods in 2010, 2011, and 2012. The temporal variation is indicated by the coefficient of variation (CV).

	Kraichgau				Swabian Alb			
	Mean	CV	Max.	Min.	Mean	CV	Max.	Min.
	% (v/v)							
	2010							
$\langle\theta\rangle$	30.2	13.8	38.1	21.9	41.1	8.5	46.0	31.9
σ_θ	4.0	18.6	6.3	2.3	6.3	11.7	8.1	4.8
	2011							
$\langle\theta\rangle$	28.0	8.2	34.8	23.9	41.0	8.1	47.1	34.7
σ_θ	5.9	15.2	7.5	3.9	6.5	10.5	8.0	4.7
	2012							
$\langle\theta\rangle$	27.9	7.5	33.8	24.2	44.0	6.4	48.7	36.8
σ_θ	5.3	16.7	7.3	3.6	6.1	14.8	7.8	4.3

Rainfall Variability and Distribution in Kraichgau and Swabian Alb Networks

The 2010 observation period was the wettest (Table 3) and showed the highest rainfall intensities of the three study years. In Kraichgau, rains were less frequent and intensive than on Swabian Alb, where total annual rainfall was higher by about 200 mm. Cumulative ET_c was similar in both regions. Cumulative ET_c was the lowest in the wettest year (2010). The average difference between mean spatial ET_c, calculated with the Penman–Monteith method, and actual ET_c, measured at EC stations, did not exceed 6.2% in Kraichgau and 6.1% in Swabian Alb. On Swabian Alb, the SWB was highly positive in all 3 years. In Kraichgau the situation was very different. While in 2010 SWB was highly positive, in 2011 it was nearly balanced, and in 2012 it was even negative. The CV of SWB was lowest when the SWB was even, and highest when SWB was highly positive or negative (Tables 2 and 3).

Temporal Variability of $\langle\theta\rangle$ and σ_θ

Figure 2 shows daily $\langle\theta\rangle$ and σ_θ in the observation periods. In Kraichgau, the relation between rainfall and the SWC dynamics was the strongest during the period with the highest positive

Table 3. Weather data in Kraichgau and on Swabian Alb in the April–October measuring periods in 2010, 2011, and 2012.

	Kraichgau			Swabian Alb		
Parameter	2010	2011	2012	2010	2011	2012
Total rainfall (R) ± SD, mm	509 ± 181	386 ± 157	415 ± 164	710 ± 250	615 ± 244	615 ± 224
Rainfall frequency, %	64	60	64	72	70	70
Rainfall intensity ± SD, mm/d	3.7 ± 0.9	3.0 ± 0.7	3.0 ± 0.8	4.6 ± 1.2	4.1 ± 1.1	4.1 ± 1.1
Potential ET_c ± SD, mm†	356 ± 73	383 ± 85	465 ± 63	343 ± 74	395 ± 94	388 ± 77
Seasonal water balance (R-ET_c) ± SD, mm	153 ± 108	3 ± 72	−50 ± 111	367 ± 176	220 ± 150	227 ± 147

† ET_c, cumulative crop evapotranspiration.

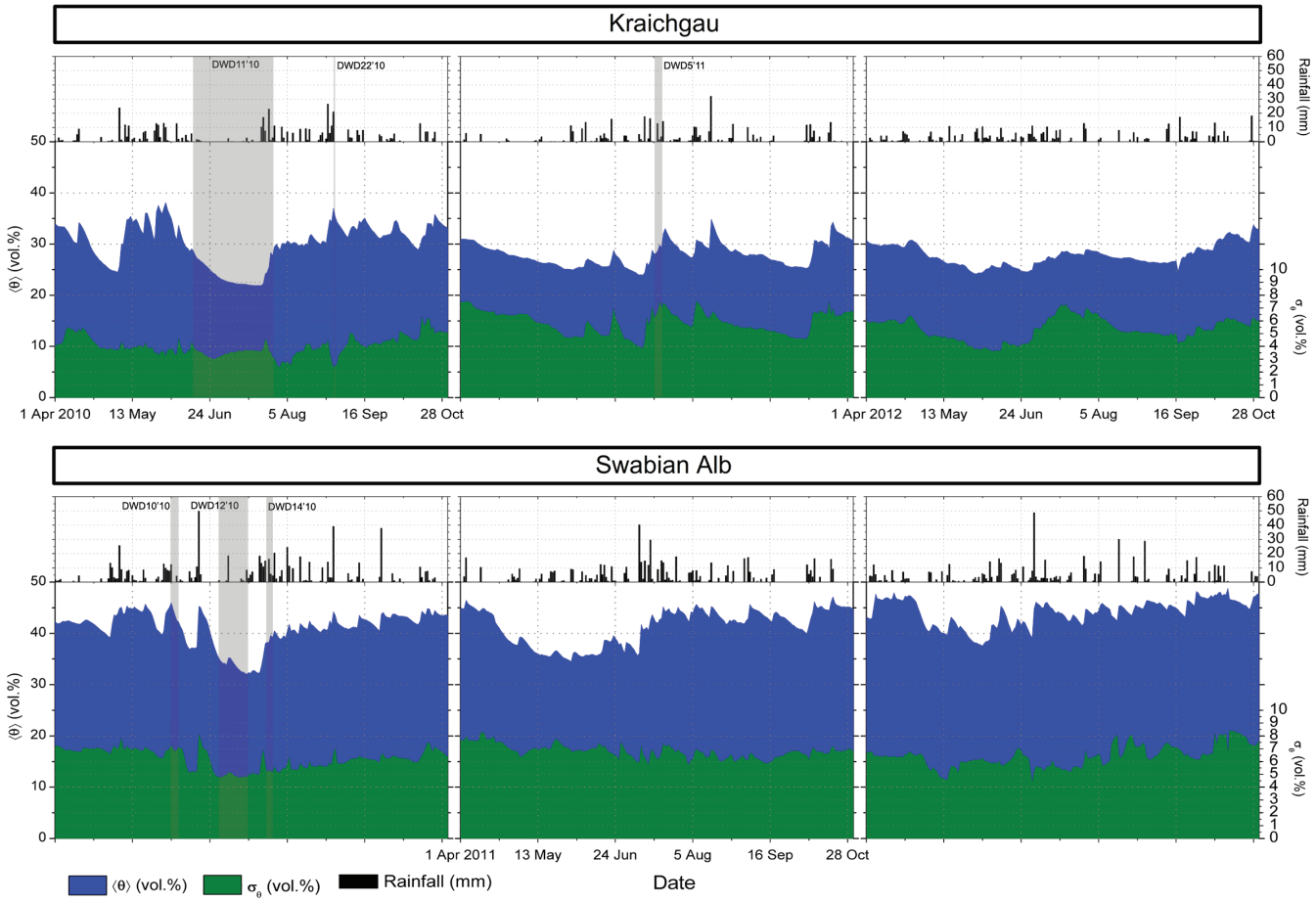

Fig. 2. Time series of spatial average soil water content ($\langle\theta\rangle$), its standard deviation (σ_θ), and daily rainfall at Kraichgau and Swabian Alb sensor networks during the April–October (214 days) measuring time period in 2010, 2011, and 2012. Light gray bands indicate the time frames of the selected drying-wetting-drying cycles (DWDs).

SWB (2010). In 2011, when SWB was nearly balanced, the relation was weaker, and in 2012, when SWB was negative, a rainfall event often did not result in a response of SWC in 0.15-m depth. On Swabian Alb, where SWB was highly positive in all 3 years, the response of SWC to rainfall was always strong.

In every observation period and in both regions, several distinct drying-out phases occurred. The highest $\langle\theta\rangle$ values were recorded in spring and autumn as well as after heavy rains in summer. Peaks were usually followed by rapid decays.

The longest and the most distinct drying-out phase, without any interposing rewetting events, took place in Kraichgau in June–July 2010 (Fig. 2). The drying-out phases during 2011 and 2012 were less extreme. In these years, $\langle\theta\rangle$ never fell below 23.9 % (v/v) in Kraichgau or below 34.7 % (v/v) on Swabian Alb (Table 2). On the other hand, because of lower rainfall in 2011 and 2012, soils of the Kraichgau region were on average about 2% (v/v) drier than in 2010. In contrast, though the mean seasonal $\langle\theta\rangle$ on Swabian Alb in 2011 was the same as in 2010, minimum and maximum $\langle\theta\rangle$ was higher. The year 2012 was the wettest on Swabian Alb. Nevertheless, $\langle\theta\rangle$ never approached the wet state in both networks.

In both regions, σ_θ tended to decrease during drying periods, to increase during rewetting, and to peak after rainfall (Fig. 2). This observation is, however, not universal. In Kraichgau, for instance, σ_θ slightly reincreased at the final stage of the drying-out period in June and July 2010.

Autocorrelation lengths of daily $\langle\theta\rangle$, defined as the time lag at which the autocorrelation becomes less than $1/e$ (where e is Euler's number), ranged between 8 and 23 d (Fig. 3). In Kraichgau, correlation lengths were shorter than on Swabian Alb. In Kraichgau the shortest correlation length was in the year with positive SWB (2010) and the longest in the year with negative SWB (2012).

The σ_θ–$\langle\theta\rangle$ Relationship

The standard deviation plotted against the spatial mean of SWC is given in Fig. 4 (video clips showing the seasonal evolution of daily σ_θ–$\langle\theta\rangle$ are available in the supplemental material for this paper at https://dl.sciencesocieties.org/publications/vzj). The σ_θ–$\langle\theta\rangle$ envelopes are the widest in the intermediate SWC state, that is, at medium $\langle\theta\rangle$ σ_θ varies the most. At drier and wetter $\langle\theta\rangle$, σ_θ is limited by the anchor points ($\langle\theta_{wp}\rangle$, $\langle\theta_s\rangle$), where the upper and the lower edges of the envelopes must converge. In Kraichgau, σ_θ

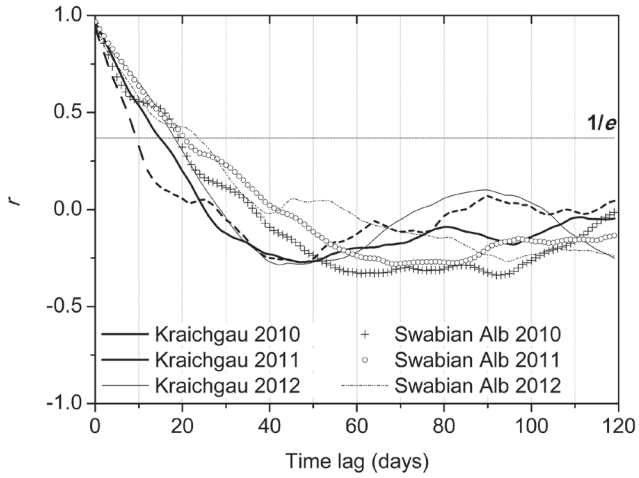

Fig. 3. Temporal autocorrelation of spatial average soil water content for Kraichgau and Swabian Alb sensor networks.

took similar values at the two anchor points [3.9 % (v/v) at $\langle\theta_{wp}\rangle$ and 3.6 % (v/v) at $\langle\theta_s\rangle$]. On Swabian Alb, it was about 2 % (v/v) higher at the wet compared with the dry anchor point [4.6 % (v/v) at $\langle\theta_{wp}\rangle$ and 6.3 % (v/v) at $\langle\theta_s\rangle$]. The lower bounds of the σ_θ–$\langle\theta\rangle$ envelopes are close to the lines computed for the hypothetical case of a spatially homogeneous matric potential (Fig. 4). It has a concave shape with minimum σ_θ corresponding to the lowest heterogeneity of soil water retention curves in intermediate state of SWC (Fig. 5). The ensemble of retention curves shows the highest variability toward the anchor points in both regions.

Figure 6 shows how σ_θ developed in drying and wetting phases. Arrows demonstrate the direction and typical trajectory of σ_θ with $\langle\theta\rangle$ decrease (drying) or increase (wetting). In 2010, σ_θ–$\langle\theta\rangle$ formed combinations of convex and concave hyperbolas in both regions. Because $\langle\theta\rangle$ never came close to the anchor points in 2011, σ_θ–$\langle\theta\rangle$ tended to move along the top closed hyperbolic shape paths or had a downward trend when drying.

Hysteresis Loops at the Event Scale

The data sets were split into DWD cycles, yielding a total number of 31 in Kraichgau and 43 on Swabian Alb. The characteristics of the DWD cycles are given in Table 4. Their time frames are indicated in Fig. 2, and their characteristics are presented in Table 5.

In Kraichgau, 76% of the DWDs showed a hysteretic loop. On Swabian Alb, the percentage was lower (60%). Most of the DWD cycles (45 in total, both networks) were observed at intermediate SWC. Twenty-one DWDs were detected in the transition from intermediate to wet SWC state. Thus, more than a half of the

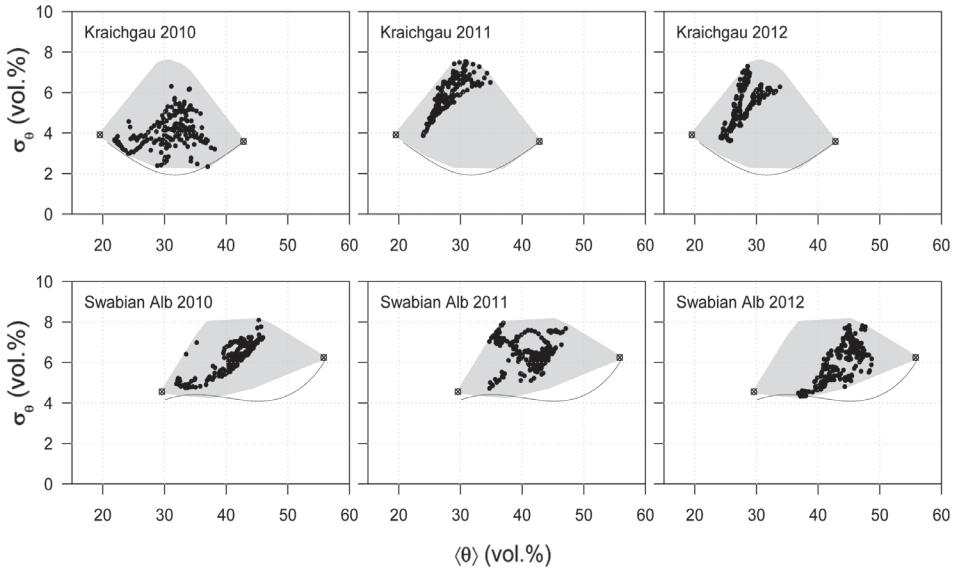

Fig. 4. Standard deviation of spatial average soil water content (σ_θ) versus spatial average soil water content ($\langle\theta\rangle$) for Kraichgau and Swabian Alb sensor networks. Grey area indicates the contingent phase space of σ_θ and $\langle\theta\rangle$; solid line is the σ_θ–$\langle\theta\rangle$ over constant matric potentials.

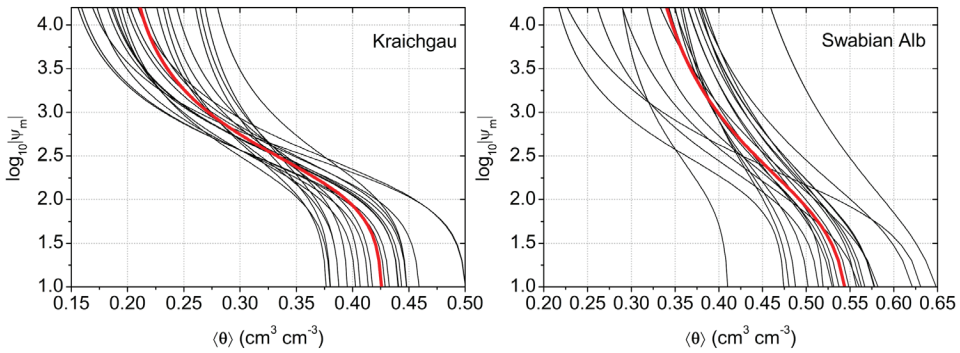

Fig. 5. Soil water retention curves for 21 stations of the Kraichgau soil moisture network and 21 stations of the Swabian Alb sensor network (black solid lines). Red solid lines indicate mean retention curves.

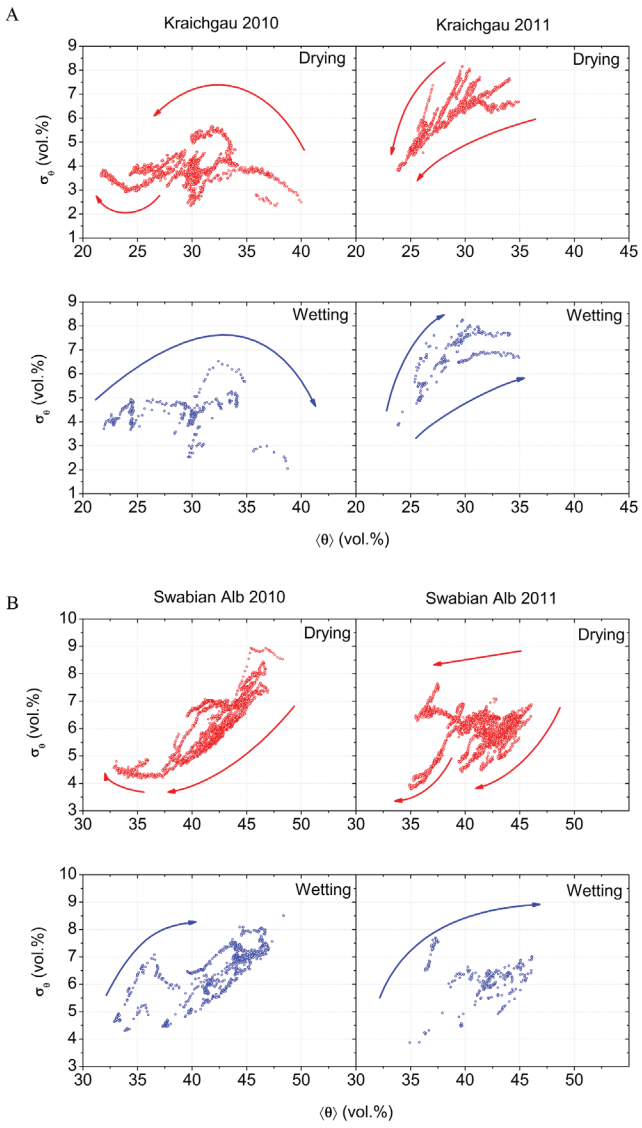

Fig. 6. Standard deviation of spatial average soil water content (σ_θ) versus spatial average soil water content ($\langle\theta\rangle$) for Kraichgau (a) and Swabian Alb (b) sensor networks during wetting and drying processes. Only data of hysteretic DWDs are plotted.

observed DWD cycles occurred under intermediate and intermediate-wet conditions.

Rain intensities triggering hysteretic DWD cycles were, on average, about twice as high as those not resulting in hysteretic behavior (Table 4). As confirmed by Student's *t*-test the difference between these two groups of rainfall intensities was significant at $\alpha = 0.05$. The average spatial variability of rainfall intensity resulting in hysteretic DWDs tended to be higher, while total rainfall was slightly lower and less variable in space, but these differences were not statistically significant. Also, the wetting periods of hysteretic DWD cycles were shorter, but this finding could only be confirmed statistically in Kraichgau and, there, only at intermediate SWC.

Hysteretic DWD cycles were found in the entire range of $\langle\theta\rangle$. In overwhelming majority of cases, σ_θ–$\langle\theta\rangle$ showed a clockwise trend. Just one cycle with anticlockwise hysteresis was observed in the wet $\langle\theta\rangle$ state on Swabian Alb. In all other cases, when no σ_θ–$\langle\theta\rangle$ hysteresis loops were observed, the relation resembled those during the DWD12'10 in Kraichgau and DWD14'11 on Swabian Alb, depicted in Fig. 7.

Intermediate Topsoil Water Content State

All wetting periods in the intermediate SWC range resulted in a rapid increase of $\langle\theta\rangle$ (Tables 2 and 3, Fig. 8). In most cases, with hysteresis, σ_θ tended to follow a hysteretic loop as shown in Fig. 8b (Kraichgau) and Fig. 8d (Swabian Alb). During the drying phase, σ_θ steadily declined (from point 1 to 2 or 3), increased because of wetting-up thereafter, reached a new maximum at point 3 (Fig. 8d) or 6 (Fig. 8b), and continuously decreased when the soil started to dry again. During the DWD5'11 the first 3.5 h after the rewetting process initiation resulted in a σ_θ change of 0.2 % (v/v). High intensity rainfall at point 4 (6.3 mm/h) increased the variability of SWC, and σ_θ increased drastically within the next 2.75 h [$\Delta\sigma_\theta$ = 1.7 % (v/v)]. In the case of DWD14'10, the change in σ_θ within the first 2 h after the wetting phase started was 0.2 % (v/v). Highly intensive rainfalls, reaching 9.5 mm/h and 16.9 mm/h, occurred 30 and 15 min before peak in σ_θ at point 3, correspondingly. $\Delta\sigma_\theta$ within 30 min made 1.6 % (v/v).

Dry-Intermediate Topsoil Water Content State

Both DWDs (DWD11'10, Kraichgau, and DWD 12'10, Swabian Alb), presented in Fig. 9, demonstrate that σ_θ tended to decrease with decreasing $\langle\theta\rangle$ during the beginning of the first drying period. The minimum σ_θ was reached at point 2 (Fig. 9a–9d). At $\langle\theta\rangle$ below this minimum, the trajectory turns into the opposite: σ_θ increases with decreasing $\langle\theta\rangle$. The drying phase was stopped by a subsequent rewetting phase. Thus, σ_θ–$\langle\theta\rangle$ branches resulted in smooth concave hyperbolas along the dry patterns.

Two peaks in σ_θ (points 6 and 9) occurred during rewetting in DWD11'10 (Fig. 9b). The change in σ_θ was 0.2 % (v/v), and the average rainfall intensity was 1.1 mm/h in the first 12 h of the rewetting phase. After 4.2 mm/h intensive rainfall at point 5, σ_θ increased by 1.1 % (v/v) in 13.75 h until its first peak at point 6. Then, wetting was shortly abrupt, but proceeded again after intensive rainfall at points 8 and 9 (8.3 and 17.8 mm/h, respectively), yielding the second peak in σ_θ (Fig. 9b, point 9). The change in σ_θ was 0.7 % (v/v) within 15 min.

During the first 4.5 h of DWD12'10 rewetting, SWC heterogeneity increased very smoothly, but after the rains at points 4 and 5 (8.0 and 15.3 mm/h, respectively) the process accelerated. The change of σ_θ amounted to 0.9 % (v/v) within the next 3.25 h (point 4–6). After initiating SWC redistribution, rainfall grew less intensive, which led to σ_θ dissipation (points 6–8).

Table 4. Characteristics of the drying-wetting-drying cycles in Kraichgau and on Swabian Alb.

Parameter name	Region	Hysteresis	Topsoil water content state				
			Dry	Dry-intermediate	Intermediate	Intermediate-wet	Wet
Number of cases	Kraichgau	no	0	0	5	6	1
		yes	1	1	16	0	1
		total	1	1	21	6	2
	Swabian Alb	no	0	0	10	7	0
		yes	0	2	15	8	1
		total	0	2	25	15	1
Percentage of hysteretic events	Kraichgau	no	0	0	24	100	50
		yes	100	100	76	0	50
	Swabian Alb	no	0	0	40	47	0
		yes	0	100	60	53	100
Average rainfall ± SD, mm	Kraichgau	no			12.7 ± 4.0	19.2 ± 11.1	21.2
		yes	47.0	17.6	11.5 ± 5.6		10.4
	Swabian Alb	no			18.1 ± 11.8	16.4 ± 15.4	
		yes		48.5 ± 28.6	16.9 ± 11.1	26.1 ± 20.4	13.9
Average rainfall SD ± SD, mm	Kraichgau	no			13.0 ± 6.8	21.3 ± 11.5	13.7
		yes	52.0	22.9	10.5 ± 5.8		8.1
	Swabian Alb	no			18.4 ± 16.6	14.3 ± 13.1	
		yes		50.0 ± 23.9	16.1 ± 11.4	15.5 ± 11.5	7.8
Average wetting period length ± SD, h	Kraichgau	no			26.1 ± 6.4	20.5 ± 14.2	27.5
		yes	84.3	11.8	16.0 ± 10.0		2.5
	Swabian Alb	no			42.0 ± 77.8	29.7 ± 30.2	
		yes		118.4 ± 108.1	24.7 ± 45.5	29.8 ± 34.4	21.0
Average rainfall intensity ± SD, mm/h	Kraichgau	no			0.4 ± 0.1	1.7 ± 1.3	0.8
		yes	0.6	1.5	1.1 ± 0.6		4.2
	Swabian Alb	no			1.1 ± 0.9	0.9 ± 0.6	
		yes		1.1 ± 0.8	2.9 ± 2.8	1.3 ± 0.7	0.7
Average rainfall intensity SD ± SD, mm/h	Kraichgau	no			0.6 ± 0.2	1.9 ± 1.6	0.5
		yes	0.6	2.0	0.9 ± 0.8		3.2
	Swabian Alb	no			1.0 ± 0.9	0.8 ± 0.7	
		yes		1.4 ± 1.1	2.9 ± 3.8	0.9 ± 0.4	0.4
Average change of $\langle\theta\rangle$ ± SD, % (v/v)	Kraichgau	no			4.0 ± 2.0	5.4 ± 2.9	5.1
		yes	7.4	3.3	2.8 ± 1.6		3.1
	Swabian Alb	no			3.0 ± 1.0	2.8 ± 2.1	
		yes		4.1 ± 1.9	3.2 ± 1.5	4.4 ± 2.5	2.2

Table 5. Characteristics of the drying-wetting-drying cycles plotted in Fig. 8–10.†

SWC region	Study region	DWD N°	Total rainfall ± SD	Wetting period length	Rainfall intensity ± SD	SWC change
			mm	h	mm/h	% (v/v)
Intermediate	Kraichgau	DWD 5'11	11.0 ± 4.8	6.8	1.6 ± 0.7	2.6
Intermediate	Swabian Alb	DWD 14'10	14.8 ± 15.0	5.0	3.0 ± 3.0	2.9
Dry	Kraichgau	DWD 11'10	47.0 ± 52.0	84.3	0.6 ± 0.6	7.4
Dry-intermediate	Swabian Alb	DWD 12'10	19.9 ± 26.1	10.3	1.9 ± 2.5	2.2
Wet	Kraichgau	DWD 22'10	10.4 ± 8.1	2.5	4.2 ± 3.2	3.1
Wet	Swabian Alb	DWD 10'10	13.9 ± 7.8	21.0	0.7 ± 0.4	2.2

† SWC, topsoil water content; DWD, drying-wetting-drying.

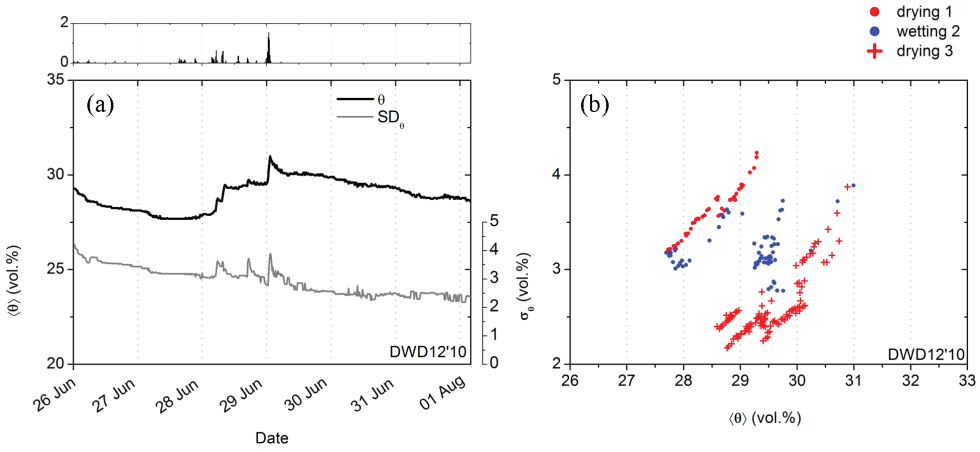

Fig. 7. Example of nonhysteretic DWDs in the intermediate state of topsoil water content (SWC) in Kraichgau (DWD12'10) and Swabian Alb (DWD14'11) networks.

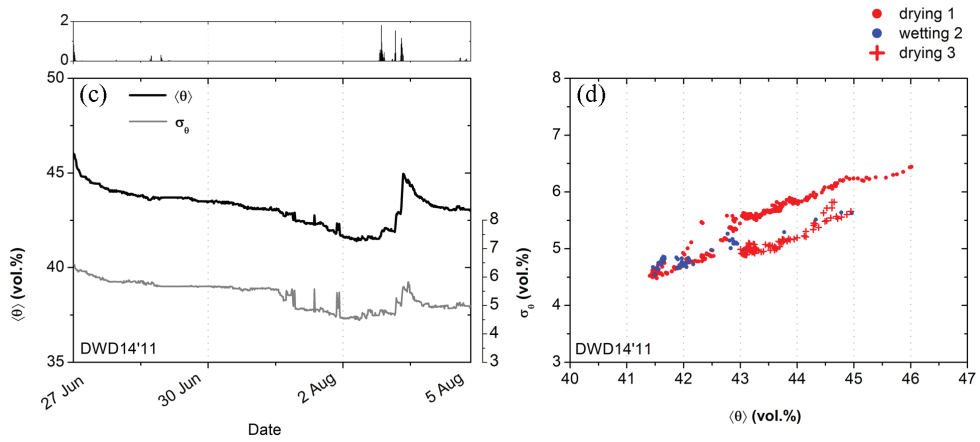

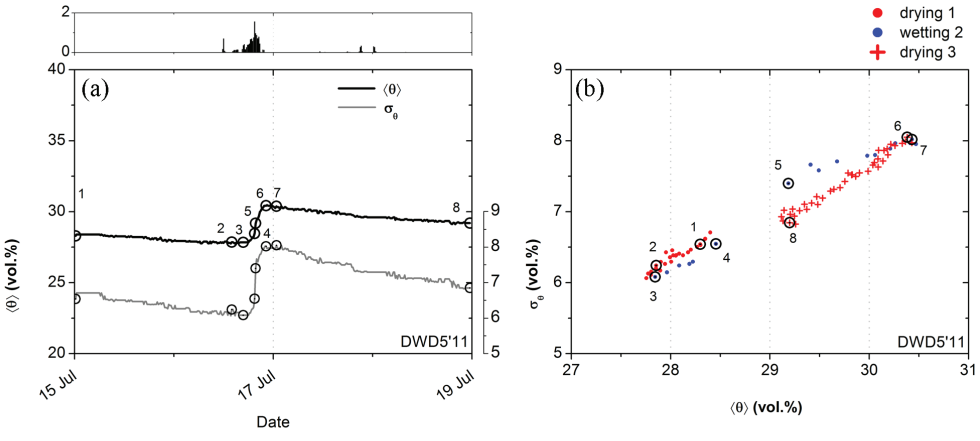

Fig. 8. Hysteretic DWDs in the intermediate state of SWC in Kraichgau and Swabian Alb networks. Time frames of the DWD5'11 (Kraichgau) and the DWD14'10 (Swabian Alb) are indicated in Fig. 3 by name as light gray bands.

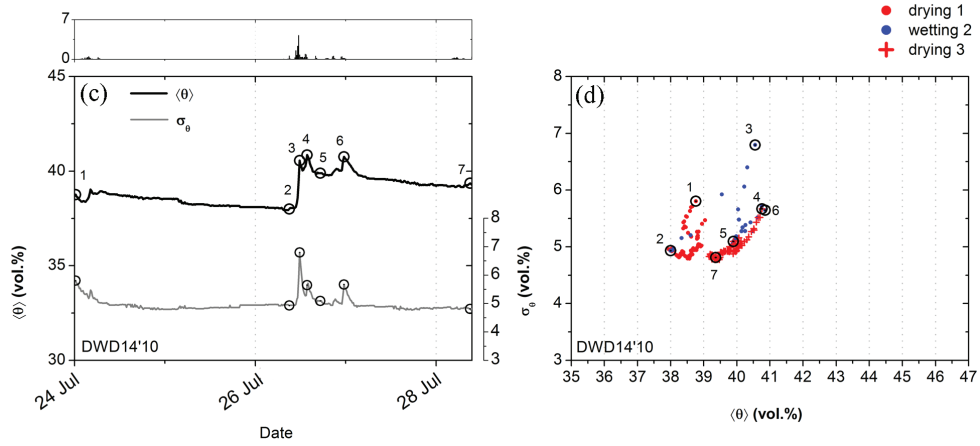

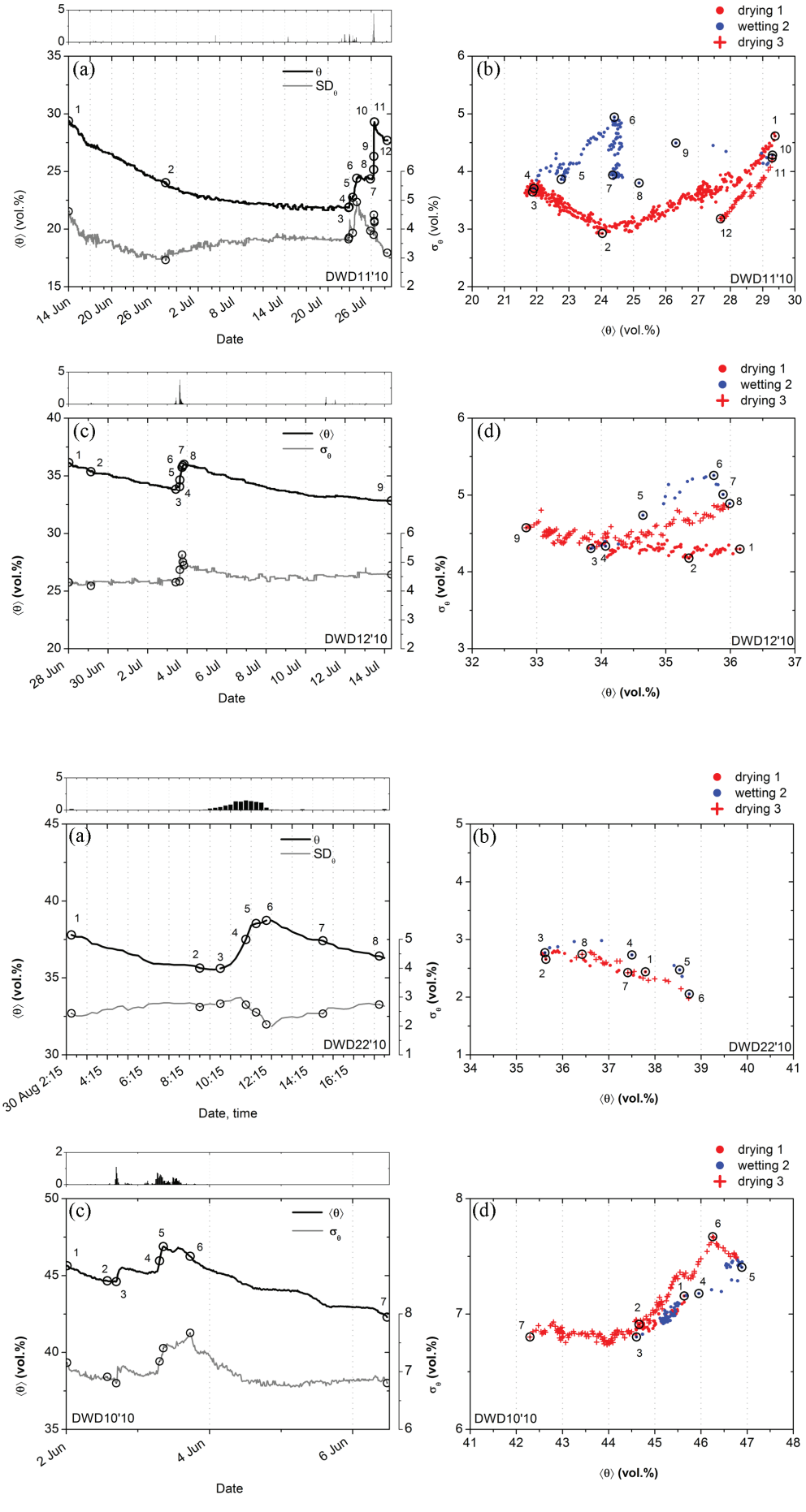

Fig. 9. Hysteretic DWDs in the dry-intermediate state of SWC in Kraichgau and Swabian Alb networks. Time frames of the DWD11'10 (Kraichgau) and the DWD12'10 (Swabian Alb) are indicated in Fig. 3 by name as light gray bands.

Fig. 10. Hysteretic DWDs in the wet and the intermediate-wet states of SWC in Kraichgau and Swabian Alb networks. Time frames of the DWD22'10 (Kraichgau) and the DWD10'10 (Swabian Alb) are indicated in Fig. 3 by name as light gray bands.

Wet Topsoil Water Content State

DWD22'10 (Kraichgau) took place at wet SWC state (Fig. 10a and 10b). The σ_θ tended to increase with decreasing $\langle\theta\rangle$ (points 1–3). High rainfall intensities at points 4 and 5 (6.0 and 5.0 mm/h, respectively) reduced the variability of $\langle\theta\rangle$ by 0.7 % (v/v) within 1 h.

During DWD10'10 (Swabian Alb), σ_θ decreased in a dry-out sequence (Fig. 10c, points 1–3). After rewetting, when $\langle\theta\rangle$ reached 46.9 % (v/v) (point 5) and began to dry out, σ_θ increased until a peak at point 6, and decreased thereafter. Although $\langle\theta\rangle$ started to diminish, it was still raining. Average rainfall intensity was 0.3 mm/h during the following 3.5 h (points 5–6), which led to an additional increase of σ_θ by 0.3 % (v/v). The σ_θ–$\langle\theta\rangle$ hysteresis loop took a contraclockwise direction. The drying arm formed a smooth concave curve of a σ_θ–$\langle\theta\rangle$ relationship.

Discussion

Various authors reported that the response time of $\langle\theta\rangle$ and σ_θ to a rainfall event depends on precipitation amount, antecedent SWC, and rainfall intensity among other factors (Famiglietti et al., 1998; Albertson and Montaldo, 2003; De Lannoy et al., 2006; Rosenbaum et al., 2012; Mittelbach and Seneviratne, 2012). The magnitudes of $\langle\theta\rangle$ and σ_θ time series were greater with high precipitation, wet SWC conditions, and high rainfall intensities. The pace of dissipation of SWC variability, in contrast, is impacted by the evapotranspiration rate among other factors, as observed in the present study. Thus, the response and attenuation of $\langle\theta\rangle$ and σ_θ to rain events is controlled by the balance between rainfall and evapotranspiration as well as the state of SWC among other factors. We used crop evapotranspiration ET_c, estimated with the Penman–Monteith approach. Since it fits quite well with actual ET observed at EC stations, we assume that spatial mean of calculated ET_c fairly represent differences among networks and seasons.

We characterized the seasonal variability of σ_θ by σ_θ–$\langle\theta\rangle$ phase-space diagrams. The upper and lower bounds of the σ_θ–$\langle\theta\rangle$ envelope reflect the variability of rainfall and evapotranspiration among other factors. The lower bound coincides with the σ_θ–$\langle\theta\rangle$ of a hypothetical case of spatially homogeneous matric potentials during constant drying out. It represents the within-variability of the water retention curve ensemble or the variability caused by soil texture and structure. The left anchor point of the phase space is determined by the variability of soil texture. The right anchor point mirrors the variability of bulk density, assuming minor effects of the variability of mineral density and organic matter content.

The closer σ_θ is located to the edge of the envelope and the anchor point, the easier it is to apprehend whether σ_θ will increase or decrease. The shape of the envelope indicates that, under very wet conditions, rainfall may even reduce the spatial variability of SWC, if σ_θ approaches the right anchor point from a starting point above σ_θ–$\langle\theta_s\rangle$. Under dry conditions, evapotranspiration may generate spatial variability of SWC, if initial position of σ_θ is at starting point below σ_θ–$\langle\theta_{wp}\rangle$. For example, in Kraichgau at the latest stage of the long drying-out period in 2010, σ_θ increased with the further decrease of SWC. This increase is related to the fact that in Kraichgau the lower bound of the σ_θ–$\langle\theta\rangle$ envelope has a lower σ_θ value than the left anchor point. Mittelbach and Seneviratne (2012) also observed a notable reincrease of σ_θ during a long period without rainfall in July 2010 and April–May 2011. They attributed this to the meteorological conditions, noting potential additional factors such as variations in soil properties. Rosenbaum et al. (2012) argued that the increase of σ_θ during long periods without rainfall may be due to the limited water availability for root water uptake and evapotranspiration. Since our networks were located on arable land, differences in vegetation senescence might have increased spatial heterogeneity of SWC. For instance, wheat and rape start ripening at the beginning of July, while maize and sugar beet are still at the vegetative growth stage. In a numerical simulation study it was demonstrated that SWC spatial heterogeneity might to a great extent be controlled by biotic factors in dry soil moisture conditions (Fatichi et al., 2015). Qu et al. (2015) derived a closed form expression which describes the σ_θ–$\langle\theta\rangle$ relationship based on the mean and variability of soil hydraulic parameters of the van Genuchten–Mualem model. They found that σ_θ–$\langle\theta\rangle$ to a large extent can be explained by the variability in hydraulic conductivity (K_s), θ_s, and parameters α and n. Our results suggest that the lower edge of the σ_θ–$\langle\theta\rangle$ envelope is constrained by the variability of soil water retention curves. Therefore, observed reincrease of σ_θ can be explained by the variability of θ_s, θ_r, α, and n. Certainly, the year 2010 was very special compared with the other 2 years. It was characterized by a very dry summer and a wet spring and fall. On the other hand, it delivered the broadest range of $\langle\theta\rangle$. Our study clearly demonstrates that multiple-year observations are needed to reliably identify the characteristics of σ_θ–$\langle\theta_s\rangle$ in a particular area. A single observation period would not have enabled constructing the complete envelope of σ_θ–$\langle\theta\rangle$. The σ_θ–$\langle\theta\rangle$ envelope, moreover, has the potential to be used to assess hydrological or land surface models with regard to their performance to represent the spatial variability of SWC. A reasonably performing model should deliver σ_θ–$\langle\theta\rangle$ data pairs that are located within the σ_θ–$\langle\theta\rangle$ envelope. The more simulated σ_θ–$\langle\theta\rangle$ data points, for example, are located below the lower bound of the σ_θ–$\langle\theta\rangle$ envelope the more pronounced the model systematically underestimates the spatial variability of SWC.

In the present study we described DWD periods, though it is alike to WDP reported by Rosenbaum et al. (2012), with DWD displaying one step before the rewetting process. Hysteretic σ_θ–$\langle\theta\rangle$ loops were triggered when rainfall intensities exceeded a threshold value (1.1 ± 0.6 and 2.9 ± 2.8 for Kraichgau and Swabian Alb, respectively), being twofold higher than the mean intensity of

nonhysteretic σ_θ–$\langle\theta\rangle$ events. Results of our DWD analysis indicate that initiation of hysteresis depends on whether rainfall is convective (rainstorm, intensity highly variable in space) or advective (steady rain, intensity less variable in space). Also, Rosenbaum et al. (2012) argued that rain characteristics (advective vs. convective) determine hysteretic behavior. On our sites, rainfall resulting in hysteretic DWD cycles was typically insufficient to uniformly saturate the upper 15-cm soil layer everywhere. This suggests that clockwise hysteretic cycles involve preferential flow phenomena initiating a nonequilibrium state and the formation of additional SWC variability. Our last idea is supported by the findings of Wiekenkamp et al. (2016). Their analysis of field observations revealed that spatial occurrence of preferential flow depends on antecedent SWC, precipitation amount, and intensity. Finally, a hysteretic loop in σ_θ–$\langle\theta\rangle$ might also be related to the hysteresis of the water retention curve. Because we did not measure pF hysteresis, in the present study we are not able to quantify the role of hysteretic water retention curves on the hysteresis of σ_θ–$\langle\theta\rangle$.

Conclusions

Based on the data from two regional soil moisture networks, we presented a 3-yr data set of topsoil SWC and its variability at the event and seasonal scale. Moreover, we evaluated the effect of rainfall intensity and its variability on SWC variability. The anchor points in the σ_θ–$\langle\theta\rangle$ phase space are determined by the regional variability of soil texture and soil structure. The lower bound of the envelope reflects the regional variability of soil water retention curves. The σ_θ–$\langle\theta\rangle$ envelope is broadest in the intermediate SWC state and narrows toward the two anchor points. At the edges of the envelope the momentary location of σ_θ in relation to the anchor points and the upper and lower bounds of the σ_θ–$\langle\theta\rangle$ envelope determines whether SWC variability increases or decreases on a change in $\langle\theta\rangle$. At the event scale, most hysteretic σ_θ–$\langle\theta\rangle$ loops occurred in the intermediate and intermediate-wet state. The initiation of clockwise hysteretic loops was triggered by rainstorms with spatially highly variable intensities.

Our data demonstrate that $\langle\theta\rangle$ alone is not a good predictor for SWC variability. The σ_θ–$\langle\theta\rangle$ relation is a combined response to a variety of processes and soil properties. Therefore it is not possible to estimate σ_θ when knowing $\langle\theta\rangle$. Hence, the power of σ_θ–$\langle\theta\rangle$ to forecast σ_θ based on $\langle\theta\rangle$ is limited at our study site. Nevertheless, the σ_θ–$\langle\theta\rangle$ envelopes are useful to test the performance of distributed hydrological or land surface models. A reasonably performing model must be able, as a minimum requirement, to produce $\langle\theta\rangle$–σ_θ data pairs falling into the observed σ_θ–$\langle\theta\rangle$ envelopes.

Acknowledgments

The authors thank three anonymous reviewers for their valuable and constructive comments.

References

Albertson, J.D., and N. Montaldo. 2003. Temporal dynamics of soil moisture variability: 1. Theoretical basis. Water Resour. Res. 39(10):1275.

Allen, R.G., and L.S. Pereira. 1998. Crop evapotranspiration—Guidelines for computing crop water requirement, FAO Papers No. 56. FAO, Rome.

Bircher, S., N. Skou, K.H. Jensen, J.P. Walker, and L. Rasmussen. 2012. A soil moisture and temperature network for SMOS validation in western Denmark. Hydrol. Earth Syst. Sci. 16:1445–1463. doi:10.5194/hess-16-1445-2012

Bogena, H.R., M. Herbst, J.A. Huisman, U. Rosenbaum, A. Weuthen, and H. Vereecken. 2010. Potential of wireless sensor networks for measuring soil water content variability. Vadose Zone J. 9:1002–1013. doi:10.2136/vzj2009.0173

Brocca, L., R. Morbidelli, F. Melone, and T. Moramarco. 2007. Soil moisture spatial variability in experimental areas of central Italy. J. Hydrol. 333:356–373. doi:10.1016/j.jhydrol.2006.09.004

Brocca, L., T. Tullo, F. Melone, T. Moramarco, and R. Morbidelli. 2012. Catchment scale soil moisture spatial-temporal variability. J. Hydrol. 422–423:63–75. doi:10.1016/j.jhydrol.2011.12.039

Choi, M., J.M. Jacobs, and M.H. Cosh. 2007. Scaled spatial variability of soil moisture fields. Geophys. Res. Lett. 34:L01401. doi:10.1029/2006GL028247

De Lannoy, G.J.M., N.E.C. Verhoest, P.R. Houser, T.J. Gish, and M. Van Meirvenne. 2006. Spatial and temporal characteristics of soil moisture in an intensively monitored agricultural field (OPE3). J. Hydrol. 331:719–730. doi:10.1016/j.jhydrol.2006.06.016

Dorigo, W.A., W. Wagner, R. Hohensinn, S. Hahn, C. Paulik, A. Xaver, A. Gruber, M. Drusch, S. Mecklenburg, P. van Oevelen, A. Robock, and T. Jackson. 2011. The international soil moisture network: A data hosting facility for global in situ soil moisture measurements. Hydrol. Earth Syst. Sci. 15(5):1675–1698. doi:10.5194/hess-15-1675-2011

Famiglietti, J.S., J.W. Rudnicki, and M. Rodell. 1998. Variability in surface moisture content along a hillslope transect: Rattlesnake Hill, Texas. J. Hydrol. 210:259–281. doi:10.1016/S0022-1694(98)00187-5

Famiglietti, J.S., D. Ryu, A.A. Berg, M. Rodell, and T.J. Jackson. 2008. Field observations of soil moisture variability across scales. Water Resour. Res. 44:W01423.

Fatichi, S., G.G. Katul, V.Y. Ivanov, C. Pappas, A. Paschalis, A. Consolo, J. Kim, and P. Burlando. 2015. Abiotic and biotic controls of soil moisture spatiotemporal variability and the occurrence of hysteresis. Water Resour. Res. 51:3505–3524. doi:10.1002/2014WR016102

Goodrich, D.C., T.J. Schmugge, T.J. Jackson, C.L. Unkrich, T.O. Keefer, R. Parry, L.B. Bach, and S.A. Am. 1994. Runoff simulation sensitivity to remotely sensed initial soil water content. Water Resour. Res. 30(5):1393–1405. doi:10.1029/93WR03083

Grayson, R.B., A.W. Western, F.H.S. Chiew, and G. Bloschl. 1997. Preferred states in spatial soil moisture patterns: Local and nonlocal controls. Water Resour. Res. 33(12):2897–2908. doi:10.1029/97WR02174

Heathman, G.C., M.H. Cosh, V. Merwade, and E. Han. 2012. Multi-scale temporal stability analysis of surface and subsurface soil moisture within the upper Cedar Creek watershed, Indiana. Catena 95:91–103. doi:10.1016/j.catena.2012.03.008

Heathman, G.C., M. Larose, M.H. Cosh, and R. Bindlish. 2009. Surface and profile soil moisture spatio-temporal analysis during an excessive rainfall period in the southern great plains, USA. Catena 78:159–169. doi:10.1016/j.catena.2009.04.002

Hu, W., A.S. Ming, J.W. Quan, and K. Reichardt. 2008. Soil water content temporal-spatial variability of the surface layer of a loess plateau hillside in China. Sci. Agric. 65:277–289.

Hu, W., M. Shao, F. Han, and K. Reichardt. 2011. Spatio-temporal variability behavior of land surface soil water content in shrub- and grass-land. Geoderma 162:260–272. doi:10.1016/j.geoderma.2011.02.008

Ingwersen, J., K. Steffens, P. Högy, K. Warrach-Sagi, D. Zhunusbayeva, M. Poltoradnev, R. Gäbler, H.-D. Wizemann, A. Fangmeier, V. Wulfmeyer, and T. Streck. 2011. Comparison of Noah simulations with eddy covariance and soil water measurements at a winter wheat stand. Agric. For. Meteorol. 151:345–355. doi:10.1016/j.agrformet.2010.11.010

Ivanov, V.Y., S. Fatichi, G.D. Jenerette, J.F. Espeleta, P.A. Troch, and T.E. Huxman. 2010. Hysteresis of soil moisture spatial heterogeneity and the "homogenizing" effect of vegetation. Water Resour. Res. 46:W09521.

López-Vicente, M., A. Navas, and J. MacHín. 2009. Effect of physiographic conditions on the spatial variation of seasonal topsoil moisture in Mediterranean soils. Aust. J. Soil Res. 47:498–507. doi:10.1071/SR08250

Mittelbach, H., and S.I. Seneviratne. 2012. A new perspective on the spatio-temporal variability of soil moisture: Temporal dynamics versus time-invariant contributions. Hydrol. Earth Syst. Sci. 16:2169–2179. doi:10.5194/hess-16-2169-2012

Noma, E. 2013. Package PlotRegionHighlighter. https://cran.r-project.org/web/packages/PlotRegionHighlighter/index.html (accessed 28 Apr. 2016).

Pan, F., and C.D. Peters-Lidard. 2008. On the relationship between mean and variance of soil moisture fields. J. Am. Water Resour. Assoc. 44(1):235–242. doi:10.1111/j.1752-1688.2007.00150.x

Poltoradnev, M., J. Ingwersen, and T. Streck. 2015. Calibration and Application of Aquaflex TDT Soil Water Probes to Measure the Soil Water Dynamics of Agricultural Topsoil in Southwest Germany. J. Irrig. Drain. Eng. 141(6). doi:10.1061/(ASCE)IR.1943-4774.0000838

Qu, W., H.R. Bogena, J.A. Huisman, J. Vanderborght, M. Schuh, E. Priesack, and H. Vereecken. 2015. Predicting subgrid variability of soil water content from basic soil information. Geophys. Res. Lett. 42:789–796. doi:10.1002/2014GL062496

Rosenbaum, U., H.R. Bogena, M. Herbst, J.A. Huisman, T.J. Peterson, A. Weuthen, A.W. Western, and H. Vereecken. 2012. Seasonal and event dynamics of spatial soil moisture patterns at the small catchment scale. Water Resour. Res. 48:10544–10566.

Sánchez, N., J. Martínez-Fernández, A. Scaini, and C. Pérez-Gutiérrez. 2012. Validation of the SMOS L2 Soil Moisture Data in the REMEDHUS Network (Spain). IEEE Trans. Geosci. Rem. Sens. 50:1602–1611. doi:10.1109/TGRS.2012.2186971

Schaap, M.G., F.J. Leij, and M.Th. van Genuchten. 2001. Rosetta: A computer program for estimating soil hydraulic parameters with hierarchical pedotransfer functions. J. Hydrol. 251:163–176. doi:10.1016/S0022-1694(01)00466-8

Smith, A.B., J.P. Walker, A.W. Western, R.I. Young, K.M. Ellett, R.C. Pipunic, R.B. Grayson, L. Siriwidena, F.H.S. Chiew, and H. Richter. 2012. The Murrumbidgee Soil Moisture Monitoring Network Data Set. Water Resour. Res. 48:W07701.

Teuling, A.J., F. Hupet, R. Uijlenhoet, and P.A. Troch. 2007. Climate variability effects on spatial soil moisture dynamics. Geophys. Res. Lett. 34:L06406.

van Genuchten, M.Th. 1980. A closed-form equation for predicting the hydraulic conductivity of unsaturated soils. Soil Sci. Soc. Am. J. 44:892–898. doi:10.2136/sssaj1980.03615995004400050002x

Vereecken, H., T. Kamai, T. Harter, R. Kasteel, J. Hopmans, and J. Vanderborght. 2007. Explaining soil moisture variability as a function of mean soil moisture: A stochastic unsaturated flow perspective. Geophys. Res. Lett. 34:L22402. doi:10.1029/2007GL031813

Vivoni, E.R., J.C. Rodr'guez, and C.J. Watts. 2010. On the spatiotemporal variability of soil moisture and evapotranspiration in a mountainous basin within the North American monsoon region. Water Resour. Res. 46:W02509.

Western, A.W., S.-L. Zhou, R.B. Grayson, T.A. McMahon, G. Bloschl, and D.J. Wilson. 2004. Spatial correlation of soil moisture in small catchments and its relationship to dominant spatial hydrological processes. J. Hydrol. 286:113–134. doi:10.1016/j.jhydrol.2003.09.014

Wiekenkamp, I., J.A. Huisman, H.R. Bogena, H.S. Lin, and H. Vereecken. 2016. Spatial and temporal occurrence of preferential flow in a forested headwater catchment. J. Hydrol. 534:139–149. doi:10.1016/j.jhydrol.2015.12.050

Wizemann, H.-D., J. Ingwersen, P. Högy, K. Warrach-Sagi, T. Streck, and V. Wulfmeyer. 2014. Three year observations of water vapor and energy fluxes over agricultural crops in two regional climates of Southwest Germany. Meteorol. Z. 24(1):39–59.

World Reference Base. 2006. World Reference Base and Food and Agricultural Organization of the United Nations. World Reference Base for Soil Resources. World Resour. Rep. 103. Rome, Italy.

Yoo, C., J.B. Valdés, and G.R. North. 1998. Evaluation of the impact of rainfall on soil moisture variability. Adv. Water Resour. 21:375–384. doi:10.1016/S0309-1708(97)00002-X

6. How well does Noah-MP simulate the regional mean and spatial variability of topsoil water content in two agricultural landscapes in Southwest Germany?

The original publication "Poltoradnev, M., J. Ingwersen, K. Imukova, P. Högy, H. Wizemann, and T. Streck, 2018: How Well Does Noah-MP Simulate the Regional Mean and Spatial Variability of Topsoil Water Content in Two Agricultural Landscapes in Southwest Germany? *Journal of Hydrometeorology*, 19, 555–573." can be found via the following link: https://journals.ametsoc.org/doi/10.1175/JHM-D-17-0169.1

How Well Does Noah-MP Simulate the Regional Mean and Spatial Variability of Topsoil Water Content in Two Agricultural Landscapes in Southwest Germany?

M. POLTORADNEV, J. INGWERSEN, AND K. IMUKOVA

Institute of Soil Science and Land Evaluation, Biogeophysics, Universität Hohenheim, Stuttgart, Germany

P. HÖGY

Institute of Landscape and Plant Ecology, Plant Ecology and Ecotoxicology, Universität Hohenheim, Stuttgart, Germany

H.-D. WIZEMANN

Institute of Physics and Meteorology, Physics and Meteorology, Stuttgart, Germany

T. STRECK

Institute of Soil Science and Land Evaluation, Biogeophysics, Universität Hohenheim, Stuttgart, Germany

(Manuscript received 6 September 2017, in final form 1 February 2018)

ABSTRACT

The spatial variability of topsoil water content (SWC) is often expressed through the relationship between its spatial mean $\langle\theta\rangle$ and standard deviation σ_θ. The present study tests the concept that a reasonably performing land surface model (LSM) should be able to produce σ_θ–$\langle\theta\rangle$ data pairs that fall into a polygon, spanned by the cloud of observed data and two anchor points: σ_θ at the permanent wilting point σ_θ–$\langle\theta_{wp}\rangle$ and σ_θ at saturation σ_θ –$\langle\theta_s\rangle$. A state-of-the-art LSM, Noah-MP, was driven by atmospheric forcing data obtained from eddy covariance field measurements in two regions of southwestern Germany, Kraichgau (KR) and Swabian Alb (SA). KR is characterized with deep loess soils, whereas the soils in SA are shallow, clayey, and stony. The simulations series were compared with SWC data from soil moisture networks operating in the two study regions. The results demonstrate that Noah-MP matches temporal $\langle\theta\rangle$ dynamics fairly well in KR, but performs poorly in SA. The best match is achieved with the van Genuchten–Mualem representation of soil hydraulic functions and site-specific rainfall, soil texture, green vegetation fraction (GVF) and leaf area index (LAI) input data. Nevertheless, most of the simulated σ_θ–$\langle\theta\rangle$ pairs are located outside the envelope of measurements and below the lower bound, which shows that the model smooths spatial SWC variability. This can be mainly attributed to missing topography and terrain information and inadequate representation of spatial variability of soil texture and hydraulic parameters, as well as the model assumption of a uniform root distribution.

1. Introduction

Soil moisture, next to sea surface temperature, is the second-most important factor determining the predictability of the atmosphere's state (Dirmeyer and Shukla 1994; Dirmeyer 1995). Soil water content (SWC), in particular that of the topsoil, interacts with atmospheric temperature, clouds, and precipitation formation over land. It also influences surface albedo, boundary layer evolution, and energy partitioning into sensible and latent heat fluxes (Yeh et al. 1984; Goodrich et al. 1994; Heathman et al. 2009; Seneviratne et al. 2010; Heathman et al. 2012). SWC is an important variable at the lower boundary of large-eddy simulation (LES) and numerical atmospheric models. Its realistic representation is essential, because it is a key biophysical and hydrologic state variable, used in a range of practical applications

Supplemental information related to this paper is available at the Journals Online website: https://doi.org/10.1175/JHM-D-17-0169.s1.

Corresponding author: Maxim Poltoradnev, m.poltoradnev@uni-hohenheim.de

DOI: 10.1175/JHM-D-17-0169.1

including irrigation scheduling, agriculture, turbulent flux simulations, quantitative rainfall forecasting, climate simulation, and weather prediction (e.g., Morari and Giardini 2002; Leib et al. 2003; Wraith et al. 2005).

Currently, individual atmospheric models provide uncertainties and biases in simulated SWC (Koster et al. 2004; Dirmeyer et al. 2006). Hauck et al. (2011) showed that biases in soil moisture significantly influence simulated precipitation. Gantner and Kalthoff (2010) found that spatial variability of the top 0.1-m SWC impacted the formation of precipitation in West African conditions—an area of strong land surface–atmosphere coupling (Koster et al. 2004). Simulations showed that inhomogeneous soil moisture conditions induced more intense rainfalls than homogeneous conditions. When a mature convective system moved over the study area, the precipitation pattern was significantly reduced over drier areas. This calls for further model improvements and validation against observations.

During the past five decades, land surface models (LSMs) have been continuously evolving according to the requirements of atmospheric and hydrological disciplines (Chen and Dudhia 2001; Seneviratne et al. 2010; Niu et al. 2011). Noah is one of the commonly used land surface models for hydrological processes (Chen and Dudhia 2001). Using the dataset of the First International Satellite Land Surface Climatology Project (ISLSCP) Field Experiment (FIFE; Betts and Ball 1998), the test of the Noah LSM with multiparameterization options (Noah-MP) showed that simulated daily soil water storage over 1 m matched observations well (Niu et al. 2011). The study period lasted 2 months during summer 1987. The data were averaged over 20 grassland sites within a domain area of 15 km × 15 km. Cai et al. (2014) reported fairly low root-mean-square errors (RMSEs) against monthly averaged observations of 60 Soil Climate Analysis Network (SCAN; Schaefer et al. 2007) stations during a 5-yr period. In the top 0.1-m soil layer, the RMSE was 0.016 $m^3 m^{-3}$. The research sites were located on cropland, grassland, and shrubland. In contrast, Yang et al. (2011) found, during a 10-yr simulation run, that Noah-MP either significantly overestimated monthly SWC or excessively depleted the top 1-m soil profile in summertime, particularly in dry seasons in Illinois (Illinois Climate Network; Hollinger and Isard 1994). On a winter wheat stand in southern Germany, Ingwersen et al. (2011) showed that the Noah LSM tends to uniformly deplete the soil profile; this overestimates SWC in the top (0.15 m) soil layer and underestimates it in deeper layers.

The Noah-MP LSM was built on the original Noah LSM (Niu et al. 2011). It has improved physics, including dynamic vegetation, introduction of a simple groundwater model, and a three-layer snowpack. The Noah-MP has a choice of parameterization options in leaf dynamics, canopy stomatal resistance, a soil moisture factor for stomatal resistance, runoff, and groundwater. Another reason to test the Noah-MP LSM in our study is its coupling with the Weather Research and Forecasting (WRF) Model (Skamarock et al. 2008), where Noah-MP LSM represents a land component.

Spatial variability of SWC is often evaluated by exploring the relationship between the spatial mean of SWC $\langle\theta\rangle$ and the corresponding standard deviation σ_θ (e.g., Famiglietti et al. 2008). In the following, this relationship will be denoted σ_θ–$\langle\theta\rangle$. The range of all possible σ_θ–$\langle\theta\rangle$ states forms a phase space. Poltoradnev et al. (2016) suggested creating a σ_θ–$\langle\theta\rangle$ phase space from a polygon that is stretched upon the cloud of observed data and two anchor points: σ_θ at the permanent wilting point σ_θ–$\langle\theta_{wp}\rangle$ and σ_θ at saturation σ_θ–$\langle\theta_s\rangle$. The lower edge of the σ_θ–$\langle\theta\rangle$ envelope reflects the regional variability associated with the variability of soil water retention curves.

The objective of the present study was to evaluate the performance of Noah-MP in simulating the soil water dynamics in plowing horizons of two agricultural landscapes in southwest Germany. In particular, we focused on the question of how well the model reproduces the spatial variability of SWC. In this context, we followed the concept that a reasonably performing model should be able to produce σ_θ–$\langle\theta\rangle$ data pairs falling into the observed σ_θ–$\langle\theta\rangle$ envelope. For this purpose, we performed Noah-MP simulations and tested the model performance against a dataset of regional SWC observations (spatial extent: 27 km × 27 km) from our previously published work (Poltoradnev et al. 2016).

2. Materials and methods

a. Study sites

The study area has already been described in detail in Poltoradnev et al. (2015) and Wizemann et al. (2015). The Kraichgau (KR) region is covered with loess soils (predominantly luvisols; WRB 2006). The mean temperature is about 9°C. Annual precipitation ranges between 720 and 830 mm. The dominant soil type of the Swabian Alb (SA) region is leptosol (WRB 2006) with shallow stony solum and prevailing clay fraction. The mean temperature is 6°–7°C, and annual precipitation ranges between 800 and 1000 mm.

b. Soil moisture networks and eddy covariance stations

In total, 42 soil moisture stations were installed in KR and SA during the summer of 2009. Per region, 21 stations were distributed across the three spatial domains

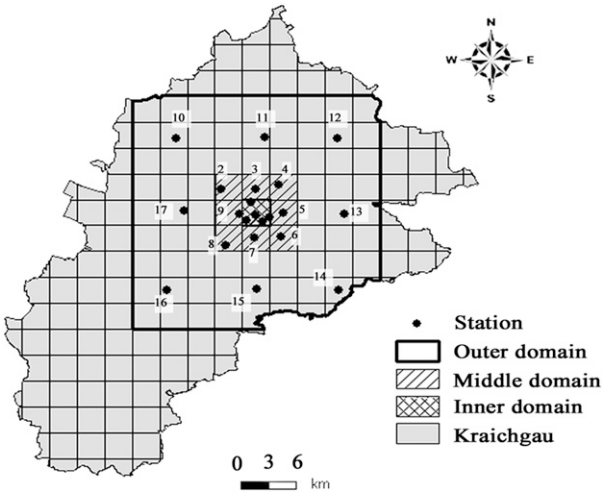

FIG. 1. Map of model region KR and the positions of the soil moisture sensor network stations. The region was divided into inner ($3 \times 3\,km^2$), middle ($9 \times 9\,km^2$) and outer ($27 \times 27\,km^2$) domains. In the inner domain the five stations were labeled from 1-1 to 1-5 in numerical order.

(inner, middle, and outer, with spatial extents of 3 km × 3 km, 9 km × 9 km, and 27 km × 27 km, respectively), as shown in Fig. 1. Soil moisture was measured on cropland with time domain transmission (TDT) soil moisture sensors (SI.99 Aquaflex Soil Moisture Sensor, Streat Moisture Solutions, United States) buried 0.15 m deep. Rainfall was recorded with a tipping-bucket rain gauge (resolution of 0.2 mm per tip) installed 1.8 m above ground.

Six eddy covariance (EC) stations were erected on arable land in 2009 (Ingwersen et al. 2011; Wizemann et al. 2015). In KR, three EC stations (hereafter EC1, EC2, and EC3) were set up near the city of Pforzheim close to the "Katharinentaler Hof" (48.9°N, 8.7°E), about 30 km south from the center of the KR soil moisture network. Another three EC stations (EC4, EC5, and EC6) were set up close to the village of Nellingen (48.5°N, 9.8°E) in SA, about 28 km from the SA soil moisture network center. More information on the soil moisture networks and EC measurements is given in Ingwersen et al. (2011), Poltoradnev et al. (2015), and Wizemann et al. (2015).

c. *Tillage and crops within the study sites*

Local soil properties determine different soil tillage strategies in KR and SA. Because of water erosion concerns, KR farmers grub instead of plow. Grubbing depth ranges between 0.15 and 0.20 m. In contrast, the common practice for SA soils is plowing. However, the typical depth is only about 0.10 m, because the soils are shallow. In KR, winter wheat is the most commonly cultivated crop, whereas in SA, the crop rotation is more diverse (Table 1).

TABLE 1. Number of fields within each soil moisture network occupied by a particular crop in the 2010, 2011, and 2012 seasons.

Region	Crop	2010	2011	2012
KR	Winter wheat	6	9	7
	Summer barley	4	0	7
	Sugar beet	4	1	1
	Corn	2	6	0
	Winter barley	1	0	1
	Winter rape	4	3	3
SA	Summer barley	6	4	9
	Corn	1	5	0
	Winter wheat	2	2	5
	Winter barley	3	1	1
	Winter rape	0	1	1
	Clover grass	2	2	1
	Triticale	2	3	4
	Spelt	2	1	0
	Pea	1	0	0
	Oat	2	0	0

d. *Field measurements*

The continuous SWC and rainfall observations were obtained from soil moisture networks over a 3-yr period from 2010 to 2012. Stations that contained gaps in the SWC series were excluded from the analysis. Thus, the KR data pool contained SWC measurements from 17 stations in 2010 and 2011 and 16 stations in 2012. The data pool of SA consisted of SWC records from 15 stations in 2010, 14 stations in 2011, and 10 stations in 2012. Further, seasonal datasets were extracted from the 3-yr data pools. These datasets covered the period from 1 April to 31 October, that is, 214 days, in 2010, 2011, and 2012. Then, the original 15-min resolution data were aggregated to 30-min, hourly, and daily averages. The spatial mean $\langle\theta\rangle$ and standard deviation of SWC σ_θ were estimated using the standard formulas.

On the day of installation at each station, soil samples were collected along the sensor area from the same depth. Particle size distribution and SWC at the wilting point θ_{wp} (pF = 4.2) were determined in the laboratory. Fractions of sand, silt, and clay were measured with the standard pipette method (Scheffer and Schachtschabel 2008). Soil texture was classified using the U.S. Department of Agriculture (USDA) scheme (Soil Survey Division Staff 1993). To determine θ_{wp}, soil samples were placed on a porous ceramic plate at −1.5 MPa pressure. After equilibration, θ_{wp} was determined gravimetrically by drying at 105°C. SWC at saturation θ_s was estimated from bulk density ρ_s ($g\,cm^{-3}$) as follows:

$$\theta_s = 1 - \rho_s/\rho_f, \tag{1}$$

where the coefficient ρ_f stands for particle density ($2.65\,g\,cm^{-3}$). Soil bulk density was determined on five

100-cm^3 soil cores taken close to the sensor from 0.15-m soil depth on the day of sensor installation.

Crop evapotranspiration (ET_c; mm day^{-1}) was calculated using the FAO Penman–Monteith approach (Allen et al. 1998). More details on calculation steps are given elsewhere (Poltoradnev et al. 2016). From the difference between total rainfall R and ET_c, we computed the seasonal water balance (SWB).

The weather data (wind speed, wind direction, air temperature, relative humidity, atmospheric pressure, radiation flux) as well as soil temperature and SWC that were used for model initialization were measured in 30-min time lags at EC stations under winter wheat cultivation.

Within the footprint of every EC station, the leaf area index (LAI) was measured biweekly. For that purpose, at the beginning of each season five subplots of 4 m^2 were randomly selected within the footprint. LAI was tracked at the central square meter of every subplot with an LAI-2000 Plant Canopy Analyzer (LI-COR Biosciences Inc., United States) throughout each season. The phenological development of 10 labeled plants (wheat, rape, or maize) per subplot was assessed using the Biologische Bundesanstalt, Bundessortenamt und CHemische Industrie (BBCH) growth stage code (Meier 2001). The green vegetation fraction (GVF) was measured at KR EC stations in 2012 and 2013. Color photos were taken weekly at 1-m height above the canopy with a digital camera at five permanently marked 1-m^2 plots within each field (Imukova et al. 2015). The GVF was not measured in SA, but was adapted by shifting corresponding KR GVF observation dates by 2 weeks. This is the typical time lag between vegetation periods and farmers' activity between SA and KR.

e. The σ_θ–$\langle\theta\rangle$ phase space

To indicate possible σ_θ–$\langle\theta\rangle$ states, we used the Plot RegionHighlighter package (Noma 2013) available as an R software routine (version 3.1.1, Lucent Technologies Bell Laboratories Innovations, France). To compute the σ_θ–$\langle\theta\rangle$ envelope for each region, we combined observations of three seasons and two anchor points (σ_θ–$\langle\theta_{wp}\rangle$, σ_θ–$\langle\theta_s\rangle$) to form a dataset. Then, we generated a polygon, stretched over the outermost data points, for each dataset using the PlotRegionHighlighter routine.

As discussed in our previous study (Poltoradnev et al. 2016), the lower boundary of a σ_θ–$\langle\theta\rangle$ phase space reflects the spatial variability of soil water retention (pF) curves. To build an ensemble of retention curves, we computed SWC at given matric potentials Ψ_m, denoted as SWC(Ψ_m), starting at 0 hPa and ending at −16 000 hPa with a 10-hPa lag, for the topsoil of each station. For this, we used two hydraulic functions: van Genuchten–Mualem (VG; van Genuchten 1980) and Clapp and Hornberger (CH; Cosby et al. 1984). The VG parameters were estimated using Rosetta Lite version 1.1 (USDA; Schaap et al. 2001) based on measured soil texture and bulk density. CH parameters were derived from fitting the CH function to the VG retention curve. Initial parameters of CH were taken from Cosby et al. (1984). To judge CH versus VG curves, the index of disagreement F (Nash and Sutcliffe 1970) was computed as

$$F = \sum_i (P_i - O_i)^2, \tag{2}$$

wherein P_i and O_i denote SWC(Ψ_m), computed with CH and VG, respectively. The F value was minimized by changing the CH parameters using the Solver Excel add-in (version 2010, Microsoft Ltd.). The outputted CH retention curves are hence as close as possible to the VG curves. In this way, we computed $\langle\theta\rangle$ and σ_θ as a function of Ψ_m for every soil moisture network (KR and SA).

To characterize the upper bound of the σ_θ–$\langle\theta\rangle$ envelope, we computed the greatest σ_θ–$\langle\theta\rangle$ value theoretically possible. To achieve this we assumed that one of the two utmost SWC states (θ_s or θ_{wp}) per station materializes at a given point in time. This results in 2^{21} (2 097 152) combinations of binary SWC states per soil moisture network. To compute σ_θ and $\langle\theta\rangle$ of all possible combinations, a Fortran computer code was written (Annex 1; see online supplemental material). After this, the entire dataset was grouped into $\langle\theta\rangle$ classes at 1 Vol.% intervals (i.e., $15 \le \langle\theta\rangle < 16$ Vol.%, $16 \le \langle\theta\rangle < 17$ Vol.%, etc.; Vol.% is the volumetric percentage). The maximum σ_θ and the corresponding $\langle\theta\rangle$ of each class were determined and assigned to an array giving the upper bound curve of σ_θ–$\langle\theta\rangle$ envelope.

f. The Noah-MP LSM (version 1.1)

1) SOIL WATER REGIME

In the Noah-MP LSM (version 1.1), SWC dynamics are simulated based on the Richards equation:

$$\frac{\partial\theta}{\partial t} = \frac{\partial}{\partial z}\left[D(\theta)\frac{\partial\theta}{\partial z}\right] + \frac{\partial K(\theta)}{\partial z} - F(\theta). \tag{3}$$

Here, θ (m^3 m^{-3}) stands for the volumetric soil water content, t (s) is time, z (m) denotes the vertical coordinate (positive upward), $D(\theta)$ (m^2 s^{-1}) is the soil water diffusivity, $K(\theta)$ (m s^{-1}) is the hydraulic conductivity, and $F(\theta)$ (s^{-1}) is a sink term for root water uptake. In the present study, we tested two functions to describe $K(\theta)$ and $D(\theta)$. The first is the CH approach by Cosby et al. (1984) used in Noah-MP by default:

$$K(\theta) = K_s\left(\frac{\theta}{\theta_s}\right)^{2b+3}, \tag{4}$$

$$D(\theta) = K(\theta)\left(\frac{\partial \Psi_m}{\partial \theta}\right), \quad \text{and} \tag{5}$$

$$\Psi_m = \Psi_s \left(\frac{\theta}{\theta_s}\right)^b, \tag{6}$$

where K_s denotes the saturated hydraulic conductivity; Ψ_m and Ψ_s stand for the matric potential and matric potential at the air entry point, respectively; and b determines the slope of the retention curve. The second function, the VG approach according to van Genuchten (1980), reads

$$K(\theta) = K_s S_e^{0.5}[1 - (1 - S_e^{1/m})^m]^2, \tag{7}$$

$$D(\theta) = \frac{(1-m)K_s}{\alpha m(\theta_s - \theta_r)} S_e^{0.5-1/m}[(1 - S_e^{1/m})^{-m} + (1 - S_e^{1/m})^m - 2], \quad \text{and} \tag{8}$$

$$S_e = \frac{\theta - \theta_r}{\theta_s - \theta_r}, \tag{9}$$

where S_e is the effective water content and θ_r represents the residual water content, while α and $m = (1 - n)/n$ are parameters.

2) MODEL PARAMETERIZATION

Simulations were run with a time step of 1800 s (30 min) point-by-point for each station of the two soil moisture networks left in the analysis (see section 2d) in order to get the same dataset of SWC as observed. The spinup time was set to 3 months prior to April of each year, that is, the first day of every simulation run was 1 January. The soil profile was divided into five layers (0.1, 0.1, 0.3, 0.5, and 1.0 m thick). Accordingly, the total thickness of the soil profile was set to 2 m. The initial temperatures and water contents of the soil layers were derived from EC field measurements. The soil temperature at 2-m depth was set to the mean temperature. A free drainage boundary condition was set at the bottom of the soil column. The vegetation parameters were based on the U.S. Geological Survey (USGS) "dryland cropland and pasture" land cover class. The main rooted zone was assumed to extend to the uppermost 0.3 m.

3) SIMULATION SETUP AND OUTPUT

To determine the contribution of different factors to the spatial variability of SWC, rainfall, soil texture, and vegetation were stepwise included as spatial variables. The modification process included a stepwise introduction of station-by-station observed rainfall, soil texture, LAI, and GVF data into the model input files and consequent replacement of the default data layout. These model runs were performed only for 2010. The 2011 and 2012 observations were investigated only with the full set of influencing factors. Each simulation produced a set of SWC data for the second soil layer (0.15-m soil depth). From these, we estimated $\langle\theta\rangle$ and σ_θ and compared them with the corresponding statistical parameters of the observed data.

(i) S1: Simulation with spatially variable rainfall

In the first set of simulations (S1), rainfall was introduced as the only factor varying among stations. Rainfall data were derived from the observations at the stations and aggregated to 30-min time spans. Soil texture was set to be uniform among all stations, defined as silty loam for KR and silty clay for SA. The soil parameters used in the CH equation were taken from Cosby et al. (1984). Class average VG parameters were estimated with Rosetta Lite version 1.1 (Schaap et al. 2001). The default monthly mean LAI and GVF were taken from the USGS dryland cropland and pasture category. Monthly LAI and GVF values from January to December were set to 0.0, 0.0, 0.0, 0.0, 1.0, 2.0, 3.0, 3.0, 1.5, 0.0, 0.0, 0.0 and 0.05, 0.05, 0.25, 0.32, 0.93, 0.96, 0.25, 0.05, 0.05, 0.05, 0.05, 0.05, respectively.

(ii) S2: Simulation with spatially variable rainfall and soil texture

The soil texture of measuring locations varied among the USDA texture classes as follows: in KR, silt loam ($N = 17$) and silty clay loam ($N = 4$); in SA clay ($N = 8$), silty clay ($N = 8$), silty clay loam ($N = 4$), and silt loam ($N = 1$) (Fig. 2). The S2 simulation was divided into two parts. In a first variation (S2a), hydraulic parameters specific for the respective soil texture class were used. Parameters of the CH function are provided in the Noah-MP lookup table by default, while VG parameters for the modified Noah-MP were taken from Table 3 of Cosby et al. (1984). In a second variation (S2b), VG parameters were estimated with Rosetta Lite version 1.1 based on soil texture and bulk density, measured at each station. Site-specific CH functions were fitted to the VG retention curve as described in section 2e. Monthly mean LAI and GVF were kept at the default values.

(iii) S3: Simulation with spatially variable rainfall, soil texture, and vegetation dynamics

In the S3 simulations, we additionally considered the heterogeneity of vegetation. Similar to Imukova et al. (2015), the croplands were divided into four groups: "early covering crops winter wheat like" (ECC1; winter wheat, summer barley, winter barley, triticale, spelt, pea, and oats), "early covering crops winter rape like" (ECC2; here only winter rape), "late covering crops silage maize like" (LCC; silage maize, corn, sugar beet, and sunflower) and "grassland." LAI and GVF data were compiled for crops and regions separately. LAI and GVF data for the ECC1, ECC2, and LCC groups

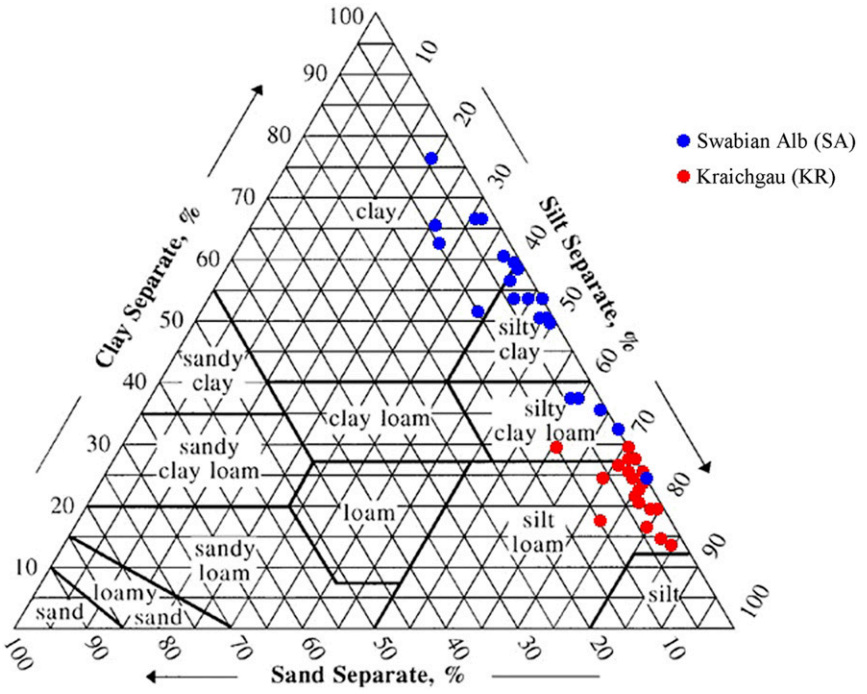

FIG. 2. Soil texture of the measuring locations in the KR and SA sensor networks according to the USDA soil texture classification.

were derived from winter wheat, winter rape, and silage maize data measured at the EC stations (Wizemann et al. 2015). The default LAI and GVF were used for "grassland." Values for the twenty-fourth day of every month of a year were derived by linear interpolation. LAI and GVF dynamics of the different crop groups are shown in Fig. 3.

(iv) S4: Monte Carlo–based sensitivity analysis

To determine the contribution of the spatial distribution of soil hydraulic properties and atmospheric forcing into the σ_θ–$\langle\theta\rangle$ relationship, two additional simulations were run for KR. The S4a set of simulations was performed in the same way as S2b (VG approach). Yet, instead of deriving K_s from Rosetta, K_s values were drawn from a lognormal distribution with the mean and standard deviation taken from Wang et al. (2013). These authors measured K_s in the surface layer of a loess soil. The S4b simulation was also set up like S2b (VG approach), but with variable atmospheric forcing. To model the variability of weather conditions, weather data were collected from the EC stations and five German Weather Service (DWD; Offenbach am Main, Germany) weather stations, located close to the soil moisture networks. Wind speed, wind direction, air temperature, relative humidity, atmospheric pressure, and radiation fluxes were randomly generated for each soil moisture station within the range of the mean standard deviation of each weather variable.

4) MODEL EVALUATION

For quantifying the performance of the model in simulating SWC dynamics, the RMSE, bias, and model efficiency (EF) were employed (Nash and Sutcliffe 1970; Moriasi et al. 2007). RMSE was calculated as

$$\mathrm{RMSE} = \sqrt{\frac{1}{n}\sum_{i=1}^{n}(P_i - O_i)^2}, \tag{10}$$

where P_i stands for the predicted value, O_i is the corresponding observed value, and n is the number of observations.

Bias and model efficiency were computed as

$$\mathrm{bias} = \frac{1}{n}\sum_{i=1}^{n}(P_i - O_i) \quad \text{and} \tag{11}$$

$$\mathrm{EF} = 1 - \sum_{i=1}^{n}(P_i - O_i)^2 \Big/ \sum_{i=1}^{n}(O_i - \overline{O})^2, \tag{12}$$

where $\overline{O}$ denotes the mean of O_i.

To verify the performance of a simulation in regard to the spatial variability of SWC, we computed the fraction of data points within the σ_θ–$\langle\theta\rangle$ envelope, the mean distance from simulated data points to the lower edge of the

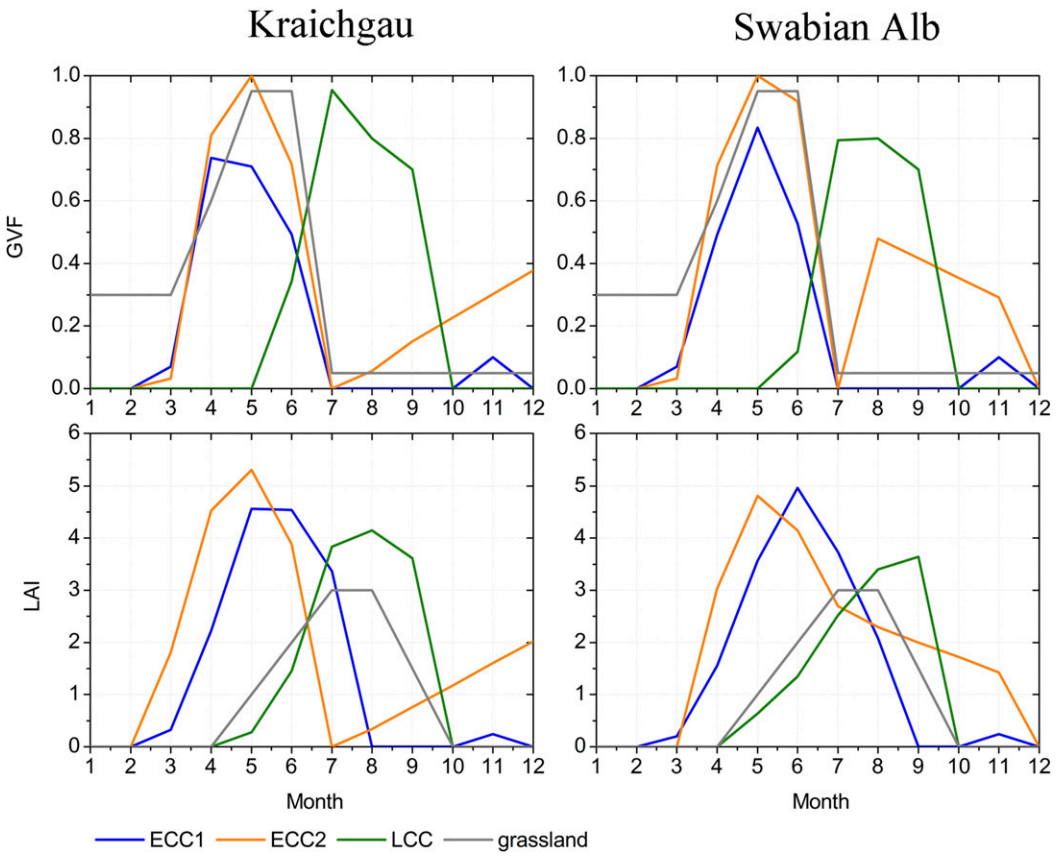

FIG. 3. GVF and LAI dynamics for different crop groups in the two study regions. Crops were grouped as ECC1, ECC2, LCC, and grassland.

envelope, and the distance between measured and simulated cluster centers. The R "sp" package (Pebesma and Bivand 2005; Roger et al. 2013) was used to calculate the number of data points falling into the σ_θ–$\langle\theta\rangle$ envelope.

3. Results

a. *Comparison of Noah-MP model runs with observations of the 2010 season*

1) $\langle\theta\rangle$ DYNAMICS

Figure 4 shows the observed and simulated $\langle\theta\rangle$ dynamics in KR and in SA during the 2010 season. For both networks, S3 performed best (Fig. 4, Table 2). In general, $\langle\theta\rangle$ dynamics was reproduced better for the loess soils of the KR region than for the shallow clayey soils of SA. In KR, when only spatially variable rainfall (S1) or both the rainfall and texture class (S2a) were considered, $\langle\theta\rangle$ was overestimated during April, early May, and the June–July time periods using the CH approach. Modeled $\langle\theta\rangle$ immediately responded to rainfall, but depleted rather slowly. In contrast, simulated $\langle\theta\rangle$ drying processes tended to be faster than observed during August. VG performed better at the beginning of the vegetation season but delivered systematically lower $\langle\theta\rangle$ from the end of June onward. In SA, for S1 and S2a the CH approach underestimated $\langle\theta\rangle$ in spring and fall and significantly overestimated $\langle\theta\rangle$ during the summer drought. VG strongly underestimated the observed $\langle\theta\rangle$ during the entire observation period. In both regions, adding a site-specific parameterization of the hydraulic functions (S2b) significantly improved the model performance. Nevertheless, the topsoils of SA were always wetter than observed, except for certain time periods in spring and fall. Parameter $\langle\theta\rangle$ was overestimated during April drying periods and during summer drought (June–July) in KR. The underestimation of soil depletion during drying phases was greater when using CH than with VG. A further improvement was achieved by introducing heterogeneous vegetation (S3). This brought both simulated $\langle\theta\rangle$ dynamics closer to the measurements: EF and R^2 significantly increased, and RMSE and bias decreased (Table 2). In SA, however, Noah-MP continued to deliver systematically higher $\langle\theta\rangle$ than observed, except for one

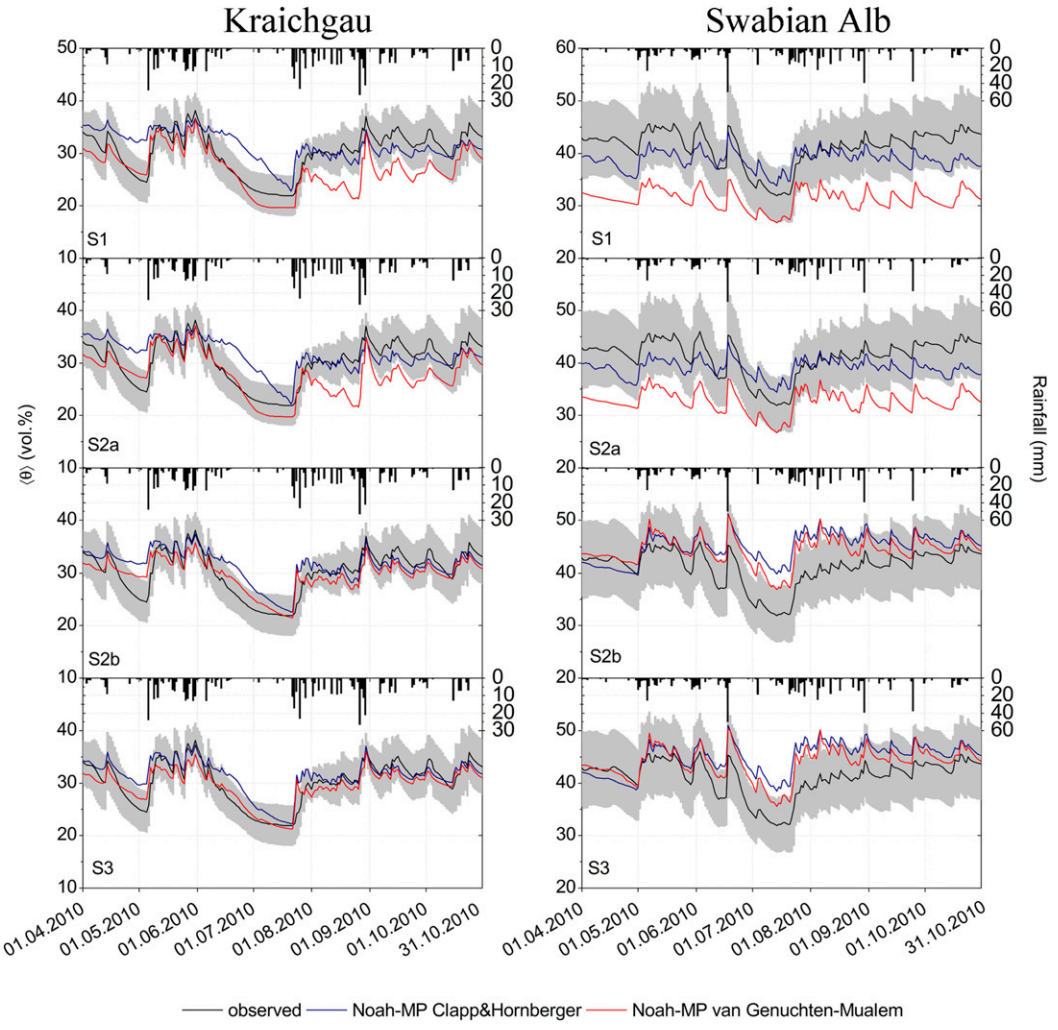

FIG. 4. Time series of spatial average SWC $\langle\theta\rangle$ and daily rainfall at the (left) KR and (right) SA sensor networks during the measuring period of April–October 2010 (214 days). Gray areas indicate the spatial standard deviation of observed SWC σ_θ. The results of the following simulation setup are presented from top to bottom: S1, spatially heterogeneous rainfall; S2a, spatially heterogeneous rainfall and soil texture class-specific soil hydraulic parameters; S2b, spatially heterogeneous rainfall and site-specific soil hydraulic parameters; and S3, spatially heterogeneous rainfall, site-specific soil hydraulic parameters, and vegetation dynamics.

month in spring. The highest R^2 and EF along with the lowest RMSE and bias were delivered by VG S3 in KR.

2) SPATIAL SWC VARIABILITY

Simulated and observed σ_θ–$\langle\theta\rangle$ data pairs are plotted in Fig. 5 against the constructed envelopes. The model performance statistics are given in Table 2. In both regions, S1 resulted in the poorest Noah-MP simulation. In KR, a great improvement was achieved by introducing spatially variable soil texture classes. The VG parameterization performed better than the CH approach. Moreover, VG S2a simulations delivered the highest fraction of modeled data points falling into the envelope, among all runs. It brought σ_θ–$\langle\theta\rangle$ on average slightly above the lower edge and greatly reduced the distance between two cluster centers (Table 2, Fig. 5; S2a). For KR, simulated σ_θ converged to the left anchor point during the long drying-out phase and showed the same pattern as the measurements. Parameter σ_θ increased as $\langle\theta\rangle$ decreased in the beginning of the drying period, reached the minimum point, and increased with further $\langle\theta\rangle$ decrease thereafter. Introducing station-specific soil texture (S2b) and spatially heterogeneous vegetation dynamics (S3) brought less data into the envelope than S2a, though the simulated and observed data clusters approached each other.

TABLE 2. Performance of Noah-MP land surface simulations of SWC and soil moisture heterogeneity at 0.15-m soil depth against observed data, based on spatial average SWC $\langle\theta\rangle$ and standard deviation of SWC σ_θ, respectively.

			Performance of Noah-MP simulations against observed $\langle\theta\rangle$				Performance of Noah-MP simulations against observed σ_θ		
Region	Simulation run	Description	R^2	RMSE (Vol.%)	Bias (Vol.%)	EF	Share of data points within envelope (%)	Mean distance between the data points and lower edge of envelope (Vol.%)[a]	Distance between the cluster center of observed data points and corresponding cluster center of simulated data points
KR	CH S1	Spatially variable rainfall, constant texture and vegetation	0.35	3.60	1.30	0.25	0.00	−1.39	3.60
	VG S1	Spatially variable rainfall, constant texture and vegetation	0.64	4.09	−3.18	0.02	2.34	−1.26	4.16
	CH S2a	Spatially variable rainfall and texture (class average), constant vegetation	0.42	3.47	1.39	0.30	0.00	−1.13	3.38
	VG S2a	Spatially variable rainfall and texture (class average), constant vegetation	0.62	3.66	−2.48	0.22	42.06	0.02	2.94
	CH S2b	Spatially variable rainfall and texture (parameters specified by station-specific soil analysis), constant vegetation	0.63	2.82	1.27	0.54	5.61	−0.64	2.88
	VG S2b	Spatially variable rainfall and texture (parameters specified by station-specific soil analysis), constant vegetation	0.77	2.14	−0.43	0.73	13.08	−0.36	2.30
	CH S3	Spatially variable rainfall, texture (parameters specified by station-specific soil analysis), and vegetation	0.78	2.30	1.15	0.69	4.67	−0.67	2.85
	VG S3	Spatially variable rainfall, texture (parameters specified by station-specific soil analysis), and vegetation	0.89	1.67	−0.63	0.84	11.22	−0.32	2.28
	VG S4a	Spatially variable rainfall and texture (parameters specified by station-specific soil analysis), constant vegetation, lognormally distributed K_s	—	—	—	—	19.63	0.23	2.20
	VG S4b	Spatially variable rainfall and texture (parameters specified by station-specific soil analysis), constant vegetation, variable weather parameters	—	—	—	—	31.31	2.12	1.73
SA	CH S1	Spatially variable rainfall, constant texture and vegetation	0.38	3.62	−2.33	−0.08	0.00	−3.27	5.96
	VG S1	Spatially variable rainfall, constant texture and vegetation	0.56	10.09	−9.81	−7.39	0.00	−4.25	11.44
	CH S2a	Spatially variable rainfall and texture (class average), constant vegetation	0.37	3.50	−2.09	−0.01	0.00	−3.12	5.74
	VG S2a	Spatially variable rainfall and texture (class average), constant vegetation	0.64	8.76	−8.48	−5.30	0.00	−2.80	9.65
	CH S2b	Spatially variable rainfall and texture (parameters specified by station-specific soil analysis), constant vegetation	0.23	5.13	3.99	−1.16	14.95	0.02	4.51
	VG S2b	Spatially variable rainfall and texture (parameters specified by station-specific soil analysis), constant vegetation	0.64	3.88	3.26	−0.24	4.21	0.09	3.86
	CH S3	Spatially variable rainfall, texture (parameters specified by station-specific soil analysis), and vegetation	0.30	4.87	3.76	−0.95	15.89	−0.01	4.32
	VG S3	Spatially variable rainfall, texture (parameters specified by station-specific soil analysis), and vegetation	0.65	3.53	2.85	−0.02	8.88	0.04	3.55

[a] For observed KR and SA σ_θ–$\langle\theta\rangle$ data points, this parameter is 1.79 and 2.21, respectively.

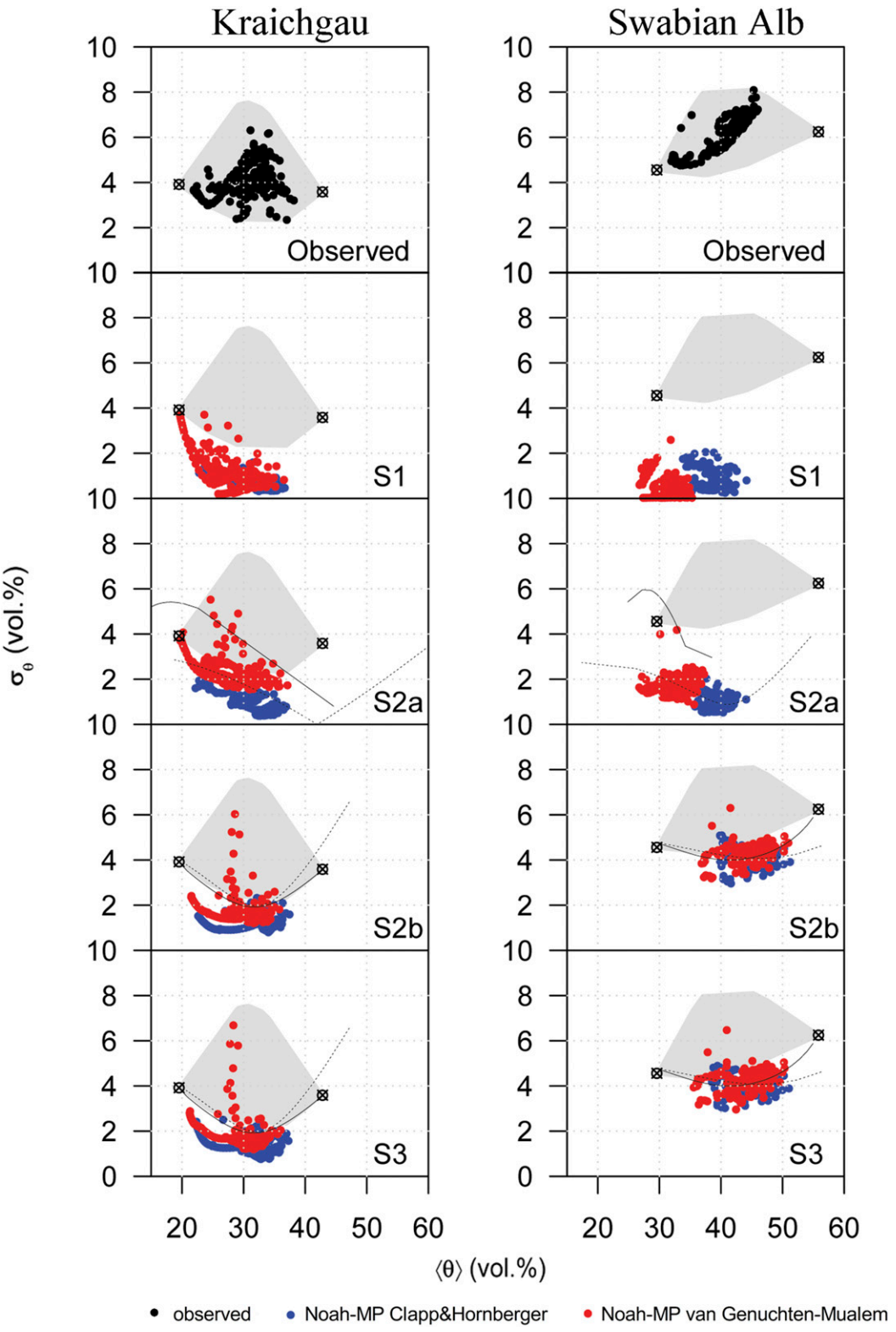

FIG. 5. Standard deviation σ_θ (spatial) of SWC vs spatial average SWC $\langle\theta\rangle$ for the (left) KR and (right) SA sensor networks. Black dots denote the observations, blue dots denote data simulations with the Noah-MP CH approach, and red dots denote data simulated with the Noah-MP VG approach. Gray areas indicate the contingent phase space of σ_θ and $\langle\theta\rangle$; solid and dashed lines denote the σ_θ–$\langle\theta\rangle$ over constant matric potentials, computed with CH and VG, respectively. From top to bottom, the observed and the S1, S2a, S2b, and S3 simulations are presented.

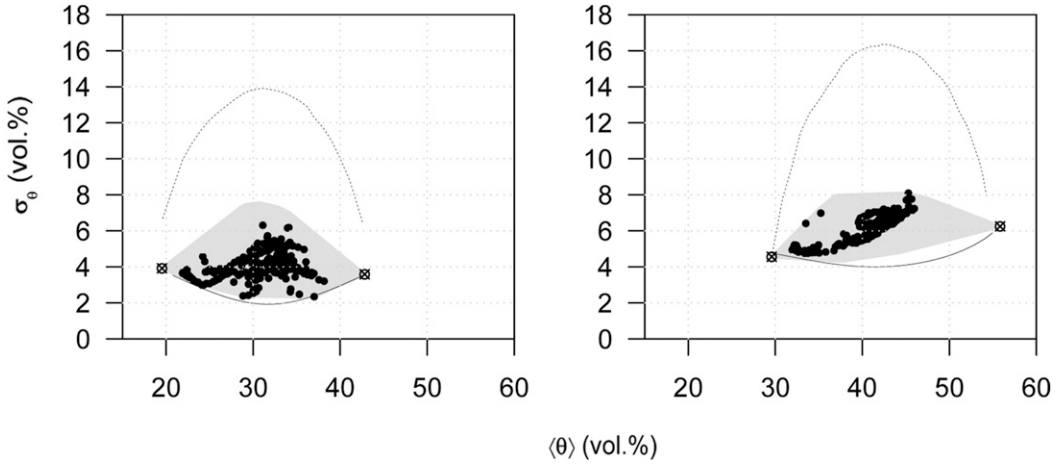

FIG. 6. Standard deviation of spatial average SWC σ_θ vs spatial average SWC $\langle\theta\rangle$ for the (left) KR and (right) SA sensor networks (2010 season). Solid and dashed lines indicate the σ_θ–$\langle\theta\rangle$ over constant matric potentials, computed with VG, and σ_θ–$\langle\theta\rangle$ over binary soil water content scenario, respectively.

In SA, the simulated data did not fall into the σ_θ–$\langle\theta\rangle$ envelope when the spatially heterogeneous soil texture was considered (Fig. 5, S2a). Considering station-specific soil texture (S2b) and, further, spatially variable dynamic vegetation (S3) positively influenced model performance. The maximum fraction of data points in the envelope was achieved with the CH S3 setup. S2b and S3 simulations formed a cloud of σ_θ–$\langle\theta\rangle$ data.

Both approaches could not adequately represent the SWC variability at the lower bound of the σ_θ–$\langle\theta\rangle$ envelope (black solid and dashed lines, Fig. 5; S2a). When a station-specific soil texture was introduced (S2b), the lines that reflect the variability within the water retention curve ensemble were located closer to the lower boundary of the σ_θ–$\langle\theta\rangle$ envelope.

The upper boundary of the σ_θ–$\langle\theta\rangle$ envelope had a top-closed convex shape, and the observed σ_θ values were positioned inside the polygon. Theoretically, however, measured values could be greater. The dashed curve in Fig. 6 indicates the maximum possible variability of SWC as estimated in the binary soil water scenario.

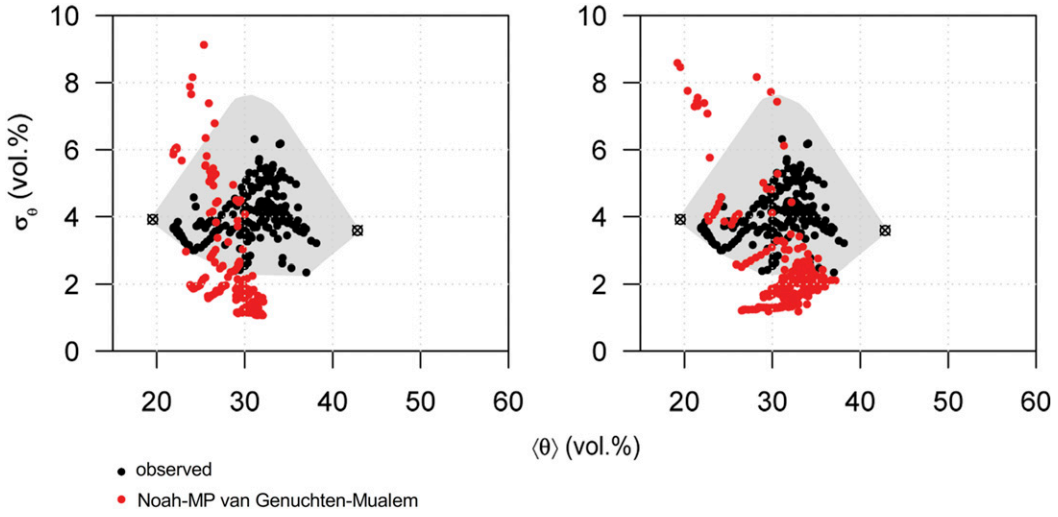

FIG. 7. Standard deviation σ_θ (spatial) of SWC vs spatially averaged SWC $\langle\theta\rangle$ for the KR sensor network (2010 season). The gray area indicates the contingent phase space of σ_θ and $\langle\theta\rangle$. The results of the following simulation setups are presented: (left) VG S4a—spatially variable rainfall, site-specific soil hydraulic parameters, and lognormally distributed K_s values; (right) VG S4b—spatially heterogeneous rainfall, site-specific soil hydraulic parameters, and variable atmospheric forcing.

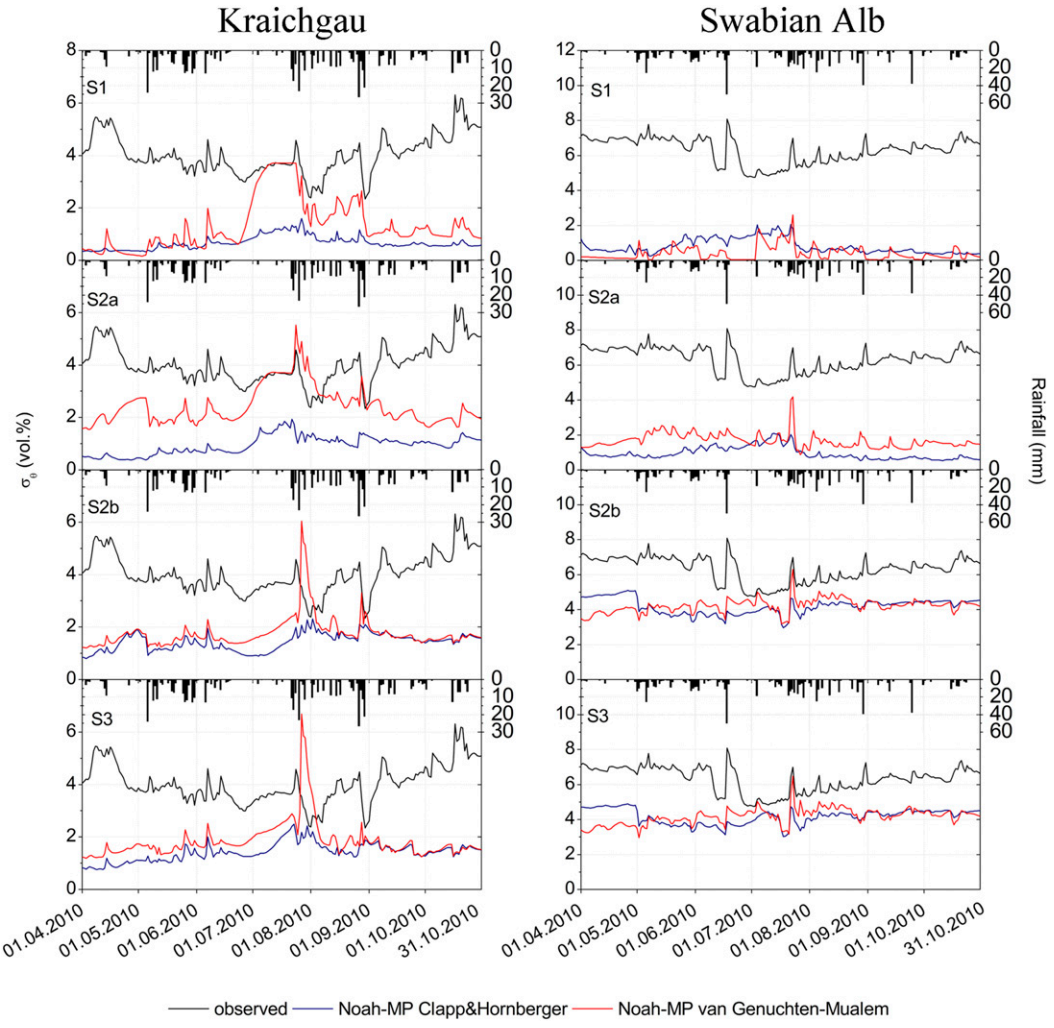

FIG. 8. Time series of the spatial standard deviation of SWC σ_θ and daily rainfall at the (left) KR and (right) SA sensor networks during the measuring period of April–October 2010 (214 days). The results of the following simulation setups are presented from top to bottom: S1, S2a, S2b, and S3.

The results of the sensitivity analyses are shown in Fig. 7 and are summarized in Table 2 (VG S4a,b). Each of VG S4 simulations brought more data points into the envelope than VG S2b (KR, Table 2). Among all runs, VG S4b yielded the highest positive mean distance between the data points and the lower envelope boundary and also the lowest distance between cluster centers of modeled and observed data.

The temporal dynamics of observed σ_θ versus σ_θ modeled with different Noah-MP setups are presented in Fig. 8. The statistical moments (temporal mean and σ) are given in Table 3. Based on the σ_θ–$\langle\theta\rangle$ relationships, the model generally failed to reproduce the observations. However, in KR the S2a and S3 variations yielded σ_θ values, the temporal variation of which was close to the σ of observed σ_θ (Table 3).

b. *S3 simulations from 2010 to 2012*

Figure 9 shows observed and simulated (S3 simulations) SWC dynamics in the 2010, 2011, and 2012 seasons. As expected, the response of the simulated $\langle\theta\rangle$ to rainfall was well pronounced in all three years. This led to frequent overestimation of wetting and $\langle\theta\rangle$ magnitude in both regions. In KR, VG tended to underestimate SWC in early April 2010 and April–May 2011 and 2012. Both CH and VG approaches repeatedly depleted the topsoil during the second half of July and August 2011 and 2012. The statistics show that the highest R^2 and EF values (Table 4) were observed in the season with positive SWB (2010, Table 5), while the lowest was found in the season with negative SWB (2012, Table 5). In SA, the best model fit was achieved in 2011, when the lowest

TABLE 3. Performance of different setups of Noah-MP in modeling soil moisture variability in the top 0.15-m soil layer against observed data, based on standard deviation of SWC σ_θ in the 2010 season.

Simulation run	Description	KR		SA	
		Mean	σ	Mean	σ
	Observed	4.02	0.75	6.29	0.73
CH S1	Spatially variable rainfall, constant texture and vegetation	0.67	0.25	0.80	0.42
VG S1	Spatially variable rainfall, constant texture and vegetation	1.33	0.97	0.40	0.40
CH S2a	Spatially variable rainfall and texture (class average), constant vegetation	0.95	0.35	0.95	0.36
VG S2a	Spatially variable rainfall and texture (class average), constant vegetation	2.43	0.71	1.67	0.41
CH S2b	Spatially variable rainfall and texture (parameters specified by station-specific soil analysis), constant vegetation	1.44	0.32	4.19	0.44
VG S2b	Spatially variable rainfall and texture (parameters specified by station-specific soil analysis), constant vegetation	1.77	0.60	4.22	0.40
CH S3	Spatially variable rainfall, texture (parameters specified by station-specific soil analysis), and vegetation	1.42	0.35	4.16	0.43
VG S3	Spatially variable rainfall, texture (parameters specified by station-specific soil analysis), and vegetation	1.83	0.71	4.17	0.46

SWB among the seasons occurred. In 2012, both approaches underestimated $\langle\theta\rangle$, particularly during the second half of the season.

The σ_θ–$\langle\theta\rangle$ pattern of the simulated SWC dynamics poorly reflected the observed SWC variability in all three years. This holds true for both regions (Fig. 10). In KR, VG performed better than CH in all three seasons (Table 6). The year 2011 was the year in which the largest fraction of modeled data points was within the envelope. In SA, the performance of VG and CH was different among the years. In 2010 and 2011, CH showed the best match and located more data points into the σ_θ–$\langle\theta\rangle$ envelope. In 2012, VG yielded a better match.

4. Discussion

In the present study, the best match between the mean spatial average of simulated and measured SWC values was achieved when the model used site-specific rainfall, soil texture, GVF, and LAI. Additionally, the choice of the hydraulic functions affected the performance of Noah-MP. The latter was best with VG. Gayler et al. (2013) suggested that one of the explanations for the better performance of VG parameterization in their work is that the VG model is more flexible than CH. It represents the inflection point of the retention curve better (data not shown). Moreover, with VG the unsaturated hydraulic function sloping was smoother than with CH (data not shown), which may have had a strong effect on SWC modeling. The same parameterization, however, performed less accurately for the seasons with neutral and negative SWB. During these seasons the observed $\langle\theta\rangle$ at 0.15-m depth often did not respond to a rainfall event, while the response of modeled $\langle\theta\rangle$ was well pronounced in all three years. One possible reason for this mismatch is that the modeled infiltration rate was too high, resulting in a sharp increase of SWC at 0.15 m. Noah-MP uses a simple water balance scheme (Schaake et al. 1996) to partition incoming rainfall into infiltration and runoff at the soil surface. Chen and Dudhia (2001) have pointed out that some of the parameters used in the simple water balance scheme are purely empirical. They depend on the precipitation climatology of a study region and have to be calibrated. Another reason for the mismatch may be a bias in simulated evapotranspiration, which controls the pace of dissipation of SWC. Ingwersen et al. (2011) compared latent heat flux, simulated by the Noah LSM, against the eddy covariance data measured in 2009 at a winter wheat stand in KR. The model underestimated latent heat flux in April–June and considerably overestimated it in July and August. The researchers could markedly improve the simulations by introducing a monthly varying minimum stomatal resistance into the Noah LSM.

The reasons for the better match of simulated and observed $\langle\theta\rangle$ in KR are twofold. First, the SA soils are usually shallow. The plowing horizon often directly overlies weathered lime rock. In Noah-MP, total soil thickness is set to 2 m by default. This unavoidably causes systematic errors, in particular with regard to the lower boundary condition. We applied a free drainage condition at the bottom of the soil column, precluding a possible influence of capillary rise on SWC. In the study areas, we can exclude capillary rise for the following reasons. SA is a karst region, so the groundwater is deeper than 25 m below the surface. In KR, the elevations of the soil moisture stations are about 10–15 m above the river basin level. In presimulations, we found that setting the soil column thickness to the observed one depleted the soil water profile in the simulations (data not shown).

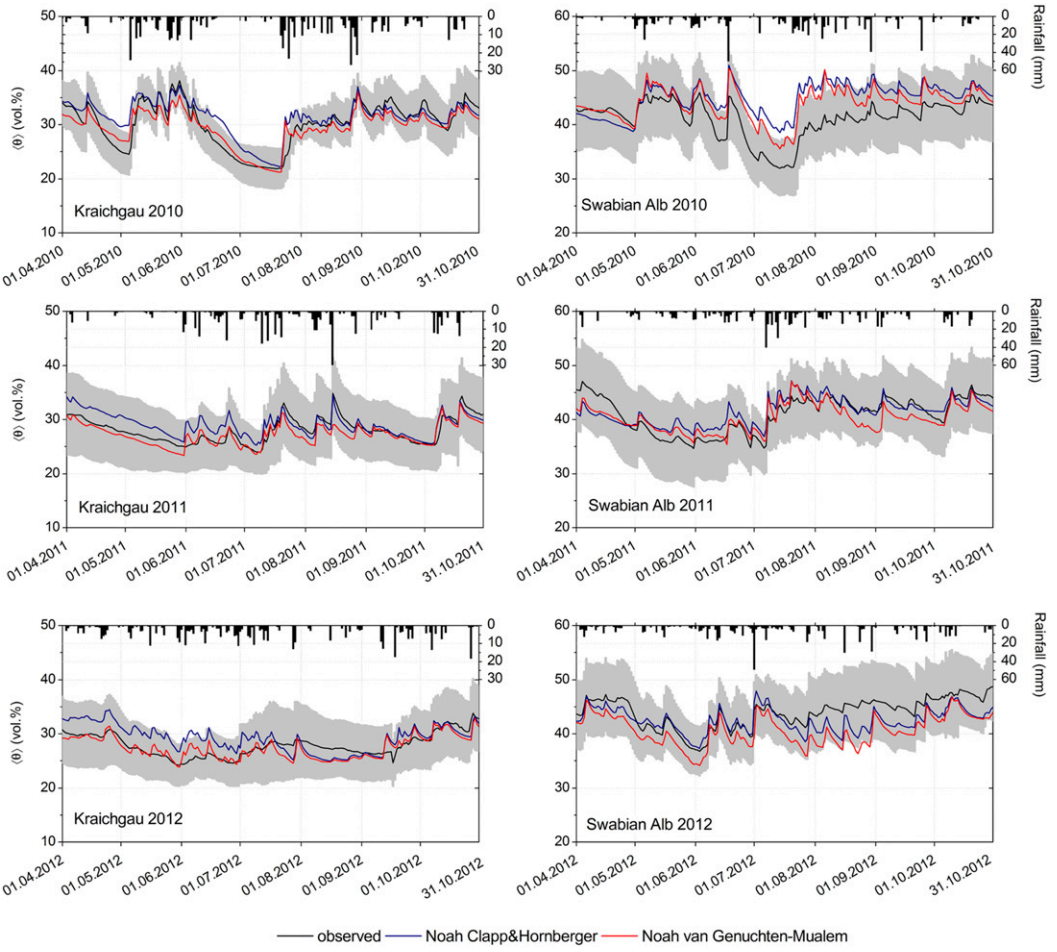

FIG. 9. Time series of spatially averaged SWC $\langle\theta\rangle$ and daily rainfall at the (left) KR and (right) SA sensor networks during measuring periods of April–October (214 days) in (top) 2010, (middle) 2011, and (bottom) 2012. Gray areas indicate the spatial standard deviation σ_θ of observed SWC. Shown are the results of S3 simulations (spatially heterogeneous rainfall, site-specific soil hydraulic parameters, and vegetation dynamics).

Therefore, we decided not to change the default setup. Second, SA soils are rich in clay and stones. VG is known to be less accurate in clay soils (van Genuchten 1980), and CH has known deficiencies in representing the hydraulic properties of rocky soils (Clapp and Hornberger 1978).

In both regions, Noah-MP poorly represented the spatial variability of SWC. In most cases, the greatest share of simulated σ_θ–$\langle\theta\rangle$ data points was located below the bottom edge of the envelope. The lower bound of the σ_θ–$\langle\theta\rangle$ phase space reflects the case of a spatially homogeneous matric potential. A position of σ_θ below the envelope indicates that Noah-MP smooths the spatial variability of SWC. Introducing site-specific parameters improved model performance, but the spatial variability of SWC was still systematically underestimated. The following factors contribute to the spatial variability of SWC. First, the model does not consider topography. It is well known that elevation, slope, and hillslope position (nonlocal controls) contribute considerably to SWC spatial variability (Grayson et al. 1997; Albertson and Montaldo 2003). Second, because of the restriction of a uniform root density profile, Noah-MP tends to uniformly deplete the soil column (Fan et al. 2006; Ingwersen et al. 2011). This results in weaker vertical SWC gradients compared to observations (Ingwersen et al. 2011). Gayler et al. (2014) have shown that including dynamic root growth may markedly improve the performance of Noah-MP. Third, K_s values observed in the field are lognormally distributed, while those calculated with pedotransfer functions are normally distributed (Wang et al. 2013). Using lognormally distributed K_s values increased the spatial variability of SWC. Fourth, the standard Richards equation as implemented in Noah-MP does not consider water movement along macropores or cracks. Wöhling et al. (2009) concluded in their HYDRUS-3D (Šimůnek et al. 2006) simulation study that model structural inadequacy is

TABLE 4. Performance of Noah-MP land surface simulations of SWC at 0.15-m soil depth, based on spatial averages SWC $\langle\theta\rangle$ of the 2010, 2011, and 2012 seasons.

	KR						SA					
	2010		2011		2012		2010		2011		2012	
Parameter	CH	VG	CH	VG	CH	VG	CH	VG	CH	VG	CH	VG
R^2	0.78	0.89	0.60	0.73	0.32	0.63	0.30	0.65	0.65	0.69	0.51	0.64
RMSE (Vol.%)	2.30	1.67	1.80	1.43	2.52	1.39	4.87	3.53	2.04	1.96	2.46	3.78
Bias (Vol.%)	1.15	−0.63	1.02	−0.78	1.35	−0.41	3.76	2.85	0.53	−0.62	−1.48	−3.33
EF	0.69	0.84	0.38	0.61	−0.46	0.56	−0.95	−0.02	0.62	0.65	0.22	−0.83

directly linked to the uniformity of modeled water flow, which is certainly not realistic (Wiekenkamp et al. 2016). Koch et al. (2016) also emphasized the systematic underestimation of spatial variability of SWC at the Wüstebach catchment site in Germany by three hydrologic distributed models that solve the Richards equation in three dimensions. They explained this failure mainly with the poor performance of the VG function during drought periods. This seems in contrast to our findings. Referring to Fig. 8, the temporal dynamics of σ_θ simulated with VG approaches the observed dynamics during the long dry period in July 2010 (when variability in SWC is mainly attributed to the variability in soil texture and residual water content), while Noah-MP tended to gradually decrease SWC variability during spring and fall. Fifth, spatially constant atmospheric forcing also leads to the homogenization of spatial SWC by the model (Albertson and Montaldo 2003). Monte Carlo simulations with variable weather conditions made more simulated σ_θ–$\langle\theta\rangle$ points fall into the envelopes. In the review paper by Crow et al. (2012), the meteorological forcing was also mentioned as one of the factors dominating large-scale soil moisture variability (observed at regional and larger scales). They stressed that the mean σ_θ for intermediate soil moisture conditions increases with increasing spatial extent. Sensor-to-sensor variability as well as sensor noise may also increase the overall variability of observed SWC. However, based on previous studies, sensor noise is usually much lower than sensor-to-sensor variability, and the latter is substantially decreased by sensor-specific calibration (Rosenbaum et al. 2010; Qu et al. 2013).

Huang and Margulis (2013) studied the impact of soil moisture variability on atmospheric boundary layer (ABL) characteristics, based on a coupled LSM–LES model. Introducing the SWC variability into the land–atmosphere system resulted in the formation of mesoscale circulations. Clouds and cloud-covered areas increased as soil moisture variability increased. The SWC variability length scale (extension of dry and wet regions) amplified this effect. The simulation design contained two configurations of dry–wet pixels, with initial SWC values set to 0.33–0.43 $cm^3\,cm^{-3}$ and 0.28–0.48 $cm^3\,cm^{-3}$. These dry–wet patterns were organized via chessboard-like surfaces with different length scales (1.25, 2.5, and 5 km) within a 10 km × 10 km domain. Using the input data, one can estimate that the minimum σ_θ of the domain is 5.0 Vol.%, corresponding to a variability length scale of 1.25 km. The maximum σ_θ was 11.6 Vol.% at the 5-km length scale (Huang and Margulis 2013). In our study the subgrid σ_θ of the middle domain (9 km × 9 km, including five stations of the inner domain and eight stations of the middle domain) of KR and SA networks were on average 4.4 and 7.0 Vol.%, respectively, in 2010.

The measuring volume of the TDT sensor used in our investigations is a 3-m-long cylinder with a diameter of several centimeters. The measurement is hence representative for a few square meters. Noah-MP, coupled with WRF, can be used down to the LES scale (Bauer et al. 2016). In most weather and climate simulations, however, Noah-MP has been used with a coarser horizontal grid spacing (12 km or more). On such a grid,

TABLE 5. Weather data for KR and SA in the April–October measuring periods in 2010, 2011, and 2012. Parameter ET_c is the cumulative evapotranspiration as assessed by the FAO Penman–Monteith approach (Allen et al. 1998). SD is standard deviation.

		KR			SA		
Parameter	Units	2010	2011	2012	2010	2011	2012
Total rainfall $R \pm$ SD	mm	509 ± 181	386 ± 157	415 ± 164	710 ± 250	615 ± 244	615 ± 224
Potential $ET_c \pm$ SD	mm	356 ± 73	383 ± 85	465 ± 63	343 ± 74	395 ± 94	388 ± 77
Seasonal water balance ($R - ET_c$) ± SD	mm	153 ± 108	3 ± 72	−50 ± 111	367 ± 176	220 ± 150	227 ± 147

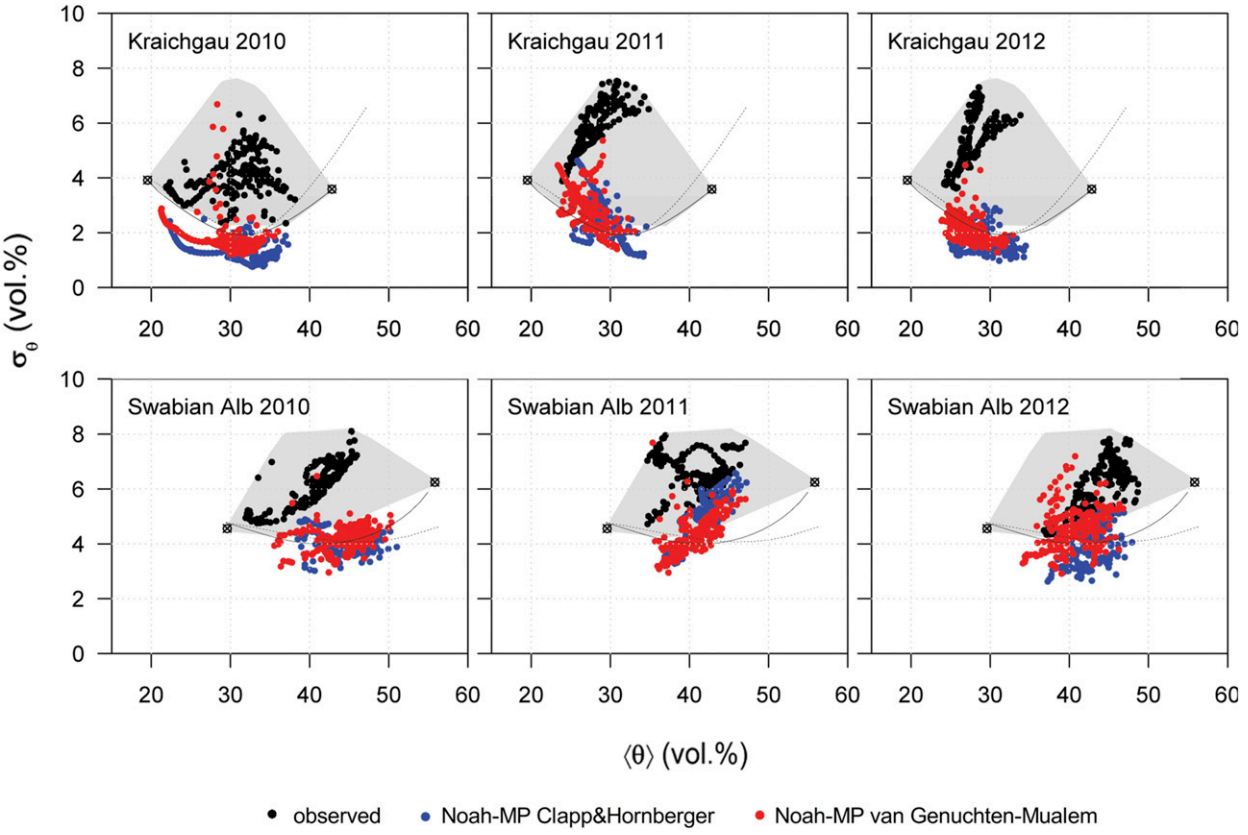

FIG. 10. Standard deviation σ_θ (spatial) of SWC vs spatially averaged SWC $\langle\theta\rangle$ of the (top) KR and (bottom) SA sensor networks in (left) 2010, (center) 2011, and (right) 2012. Gray areas indicate the contingent phase space of σ_θ and $\langle\theta\rangle$. Solid and dashed lines denote σ_θ–$\langle\theta\rangle$ over constant matric potentials computed with the VG and CH approach, respectively. Shown are the results of S3 simulations (spatially heterogeneous rainfall, site-specific soil hydraulic parameters, and vegetation dynamics).

σ_θ–$\langle\theta\rangle$ will take smaller values than at the square-meter scale. The performance of such simulations should be tested against measurements with larger support areas, employing remote sensing or hydrogeophysical techniques (e.g., Binley et al. 2015). Recently, high-resolution soil moisture products have gained significance and demand. Importantly, there is a branch of literature devoted to the development of downscaling methods that increase the

TABLE 6. Performance of Noah-MP land surface simulations of soil moisture heterogeneity for the top 0.15-m soil layer against observed data, based on the standard deviation of SWC σ_θ of the 2010, 2011, and 2012 seasons.

Parameter	2010			2011			2012		
	CH	VG	Obs.	CH	VG	Obs.	CH	VG	Obs.
					KR				
Share of data points within envelope (%)	4.67	11.22	100.00	53.27	64.95	100.0	7.94	14.02	100.00
Mean distance between data points and lower edge of envelope (Vol.%)	−0.67	−0.32	1.79	0.38	0.57	3.62	−0.54	−0.13	3.07
Distance between cluster center of observed data points and corresponding cluster center of simulated data points	2.85	2.28	0.00	3.52	3.07	0.00	3.97	3.18	0.00
					SA				
Share of data points within envelope (%)	15.89	8.88	100.00	70.56	37.38	100.00	30.84	55.14	100.00
Mean distance between data points and lower edge of envelope (Vol.%)	−0.01	0.04	2.21	0.94	0.29	2.46	0.02	0.49	1.99
Distance between cluster center of observed data points and corresponding cluster center of simulated data points	4.32	3.55	0.00	1.64	2.29	0.00	2.52	3.68	0.00

resolution of soil moisture within a coarse satellite pixel (Mohanty et al. 2017). In hydrology, for example, Mascaro and Vivoni (2012) demonstrated that disaggregation of remotely sensed soil moisture data (from 25.6 to 0.8 km) improved the performance of a hydrologic model within the Sierra Los Locos catchment in Sonora, Mexico. The downscaled high-resolution product delivered a more realistic spatial SWC distribution than the coarse product. This, in turn, positively influences the accuracy of the model prediction of surface fluxes, particularly evapotranspiration and runoff (Vivoni et al. 2010). Underestimation of (or leveling out) the spatial variability of soil moisture modeled by the Noah-MP needs to be further investigated, if one intends to use Noah-MP on finer scales.

5. Summary and conclusions

We evaluated the performance of Noah-MP against distributed time series from a topsoil water content measurement network in two regions in southwest Germany. The water content was measured by TDT and is representative for an area of a few square meters. With regard to the regional mean soil water content $\langle\theta\rangle$, Noah-MP performed fairly well for the loess soils of KR, but it has limitations as to the shallow, clayey, and stony soils of SA. The choice of hydraulic functions impacted the model output substantially. The best match was achieved with the VG approach and with site-specific rainfall, soil texture, GVF, and LAI input data. Simulation of $\langle\theta\rangle$ is the best in seasons with a positive water balance ($R > \mathrm{ET}_c$). However, the spatial variability of SWC is systematically underestimated by Noah-MP. The model tends to gradually eliminate the variability, particularly during the wet periods of a year (spring and autumn), but during long dry-down periods the observed σ_θ dynamics is represented considerably better (particularly the VG configuration). The majority of the modeled σ_θ–$\langle\theta\rangle$ pairs were located outside the envelopes of the measured data and below their lower bounds. The insufficient representation of the spatial SWC variability by Noah-MP can be mainly attributed to missing topography and terrain information, inadequate representation of the spatial variability of soil texture and hydraulic parameters, and the restriction to a uniform root distribution.

REFERENCES

Albertson, J. D., and N. Montaldo, 2003: Temporal dynamics of soil moisture variability: 1. Theoretical basis. *Water Resour. Res.*, **39**, 1275, https://doi.org/10.1029/2002WR001616.

Allen, R. G., L. S. Pereira, D. Raes, and M. Smith, 1998: Crop evapotranspiration: Guidelines for computing crop water requirements. FAO Irrigation and Drainage Paper 56, 300 pp., www.fao.org/docrep/X0490E/X0490E00.htm.

Bauer, H. S., and Coauthors, 2016: Multi-scale WRF simulations for atmospheric process understanding and boundary layer research. *Proc. Third bwHPC-Symp.*, Heidelberg, Germany, Universität Heidelberg, 65–69, https://doi.org/10.11588/heibooks.308.418.

Betts, A. K., and J. H. Ball, 1998: FIFE surface climate and site-average dataset 1987–89. *J. Atmos. Sci.*, **55**, 1091–1108, https://doi.org/10.1175/1520-0469(1998)055<1091:FSCASA>2.0.CO;2.

Binley, A., S. S. Hubbard, J. A. Huisman, A. Revil, D. A. Robinson, K. Singha, and L. D. Slater, 2015: The emergence of hydrogeophysics for improved understanding of subsurface processes over multiple scales. *Water Resour. Res.*, **51**, 3837–3866, https://doi.org/10.1002/2015WR017016.

Cai, X., Z.-L. Yang, C. H. David, G.-Y. Niu, and M. Rodell, 2014: Hydrological evaluation of the Noah-MP land surface model for the Mississippi River Basin. *J. Geophys. Res. Atmos.*, **119**, 23–38, https://doi.org/10.1002/2013JD020792.

Chen, F., and J. Dudhia, 2001: Coupling an advanced land surface–hydrology model with the Penn State–NCAR MM5 modelling system. Part I: Model implementation and sensitivity. *Mon. Wea. Rev.*, **129**, 569–585, https://doi.org/10.1175/1520-0493(2001)129<0569:CAALSH>2.0.CO;2.

Clapp, R. B., and G. M. Hornberger, 1978: Empirical equations for some soil hydraulic properties. *Water Resour. Res.*, **14**, 601–604, https://doi.org/10.1029/WR014i004p00601.

Cosby, B. J., G. M. Hornberger, R. B. Clapp, and T. R. Ginn, 1984: A statistical exploration of the relationships of soil moisture characteristics to the physical properties of soil. *Water Resour. Res.*, **20**, 682–690, https://doi.org/10.1029/WR020i006p00682.

Crow, W. T., and Coauthors, 2012: Upscaling sparse ground-based soil moisture observations for the validation of coarse-resolution satellite soil moisture products. *Rev. Geophys.*, **50**, RG2002, https://doi.org/10.1029/2011RG000372.

Dirmeyer, P. A., 1995: Problems in initializing soil wetness. *Bull. Amer. Meteor. Soc.*, **76**, 2234–2240.

——, and J. Shukla, 1994: Albedo as a modulator of climate response to tropical deforestation. *J. Geophys. Res.*, **99**, 20 863–20 877, https://doi.org/10.1029/94JD01311.

——, R. D. Koster, and Z. Guo, 2006: Do global models properly represent the feedback between land and atmosphere? *J. Hydrometeor.*, **7**, 1177–1198, https://doi.org/10.1175/JHM532.1.

Famiglietti, J. S., D. Ryu, A. A. Berg, M. Rodell, and T. J. Jackson, 2008: Field observations of soil moisture variability across scales. *Water Resour. Res.*, **44**, W01423, https://doi.org/10.1029/2006WR005804.

Fan, Y., H. M. van den Dool, D. Lohmann, and K. Mitchell, 2006: 1948–98 U.S. hydrological reanalysis by the Noah land data assimilation system. *J. Climate*, **19**, 1214–1237, https://doi.org/10.1175/JCLI3681.1.

Gantner, L., and N. Kalthoff, 2010: Sensitivity of a modelled life cycle of a mesoscale convective system to soil conditions over West Africa. *Quart. J. Roy. Meteor. Soc.*, **136**, 471–482, https://doi.org/10.1002/qj.425.

Gayler, S., J. Ingwersen, E. Priesack, T. Wöhling, V. Wulfmeyer, and T. Streck, 2013: Assessing the relevance of subsurface processes for the simulation of evapotranspiration and soil moisture dynamics with CLM3.5: Comparison with field data

and crop model simulations. *Environ. Earth Sci.*, **69**, 415, https://doi.org/10.1007/s12665-013-2309-z.

——, and Coauthors, 2014: Incorporating dynamic root growth enhances the performance of NOAH-MP at two contrasting winter wheat field sites. *Water Resour. Res.*, **50**, 1337–1356, https://doi.org/10.1002/2013WR014634.

Goodrich, D. C., T. J. Schmugge, T. J. Jackson, C. L. Unkrich, T. O. Keefer, R. Parry, L. B. Bach, and S. A. Am, 1994: Runoff simulation sensitivity to remotely sensed initial soil water content. *Water Resour. Res.*, **30**, 1393–1405, https://doi.org/10.1029/93WR03083.

Grayson, R. B., A. W. Western, F. H. S. Chiew, and G. Bloschl, 1997: Preferred states in spatial soil moisture patterns: Local and nonlocal controls. *Water Resour. Res.*, **33**, 2897–2908, https://doi.org/10.1029/97WR02174.

Hauck, C., C. Barthlott, L. Krauss, and N. Kalthoff, 2011: Soil moisture variability and its influence on convective precipitation over complex terrain. *Quart. J. Roy. Meteor. Soc.*, **137**, 42–56, https://doi.org/10.1002/qj.766.

Heathman, G. C., M. Larose, M. H. Cosh, and R. Bindlish, 2009: Surface and profile soil moisture spatio-temporal analysis during an excessive rainfall period in the southern Great Plains, USA. *Catena*, **78**, 159–169, https://doi.org/10.1016/j.catena.2009.04.002.

——, M. H. Cosh, V. Merwade, and E. Han, 2012: Multi-scale temporal stability analysis of surface and subsurface soil moisture within the upper Cedar Creek Watershed, Indiana. *Catena*, **95**, 91–103, https://doi.org/10.1016/j.catena.2012.03.008.

Hollinger, S. E., and S. A. Isard, 1994: A soil moisture climatology of Illinois. *J. Climatol.*, **7**, 822–833, https://doi.org/10.1175/1520-0442(1994)007<0822:ASMCOI>2.0.CO;2.

Huang, H. Y., and S. A. Margulis, 2013: Impact of soil moisture heterogeneity length scale and gradients on daytime coupled land-cloudy boundary layer interactions. *Hydrol. Processes*, **27**, 1988–2003, https://doi.org/10.1002/hyp.9351.

Imukova, K., J. Ingwersen, and T. Streck, 2015: Determining the spatial and temporal dynamics of the green vegetation fraction of croplands using high-resolution RapidEye satellite images. *Agric. For. Meteor.*, **206**, 113–123, https://doi.org/10.1016/j.agrformet.2015.03.003.

Ingwersen, J., and Coauthors, 2011: Comparison of Noah simulations with eddy covariance and soil water measurements at a winter wheat stand. *Agric. For. Meteor.*, **151**, 345–355, https://doi.org/10.1016/j.agrformet.2010.11.010.

Koch, J., T. Cornelissen, Z. Fang, H. Bogena, B. Diekkruger, S. Kollet, and S. Stisen, 2016: Inter-comparison of three distributed hydrological models with respect to seasonal variability of soil moisture patterns at a small forested catchment. *J. Hydrol.*, **533**, 234–249, https://doi.org/10.1016/j.jhydrol.2015.12.002.

Koster, R. D., and Coauthors, 2004: Regions of strong coupling between soil moisture and precipitation. *Science*, **305**, 1138–1140, https://doi.org/10.1126/science.1100217.

Leib, B. G., J. D. Jabro, and G. R. Matthews, 2003: Field evaluation and performance comparison of soil moisture sensors. *Soil Sci.*, **168**, 396–408, https://doi.org/10.1097/01.ss.0000075285.87447.86.

Mascaro, G., and E. R. Vivoni, 2012: Utility of coarse and downscaled soil moisture products at L-band for hydrologic modeling at the catchment scale. *Geophys. Res. Lett.*, **39**, L10403, https://doi.org/10.1029/2012GL051809.

Meier, U., 2001: Growth stages of mono- and dicotyledonous plants. BBCH Monograph, Federal Biological Research Centre for Agriculture and Forestry, 158 pp.

Mohanty, B. P., M. H. Cosh, V. Lakshmi, and C. Montzka, 2017: Soil moisture remote sensing: State-of-the-Science. *Vadose Zone J.*, **16**, https://doi.org/10.2136/vzj2016.10.0105.

Morari, F., and L. Giardini, 2002: Irrigation automation with heterogeneous vegetation: The case of the Padova botanical garden. *Agric. Water Manage.*, **55**, 183–201, https://doi.org/10.1016/S0378-3774(01)00192-5.

Moriasi, D. N., J. G. Arnold, M. W. Van Liew, R. L. Bingner, R. D. Harmel, and T. L. Veith, 2007: Model evaluation guidelines for systematic quantification of accuracy in watershed simulations. *Trans. ASABE*, **50**, 885–900, https://doi.org/10.13031/2013.23153.

Nash, J. E., and J. V. Sutcliffe, 1970: River flow forecasting through conceptual models. Part I. A discussion of principles. *J. Hydrol.*, **10**, 282–290, https://doi.org/10.1016/0022-1694(70)90255-6.

Niu, G.-Y., and Coauthors, 2011: The community Noah land surface model with multiparameterization options (Noah-MP): 1. Model description and evaluation with local-scale measurements. *J. Geophys. Res.*, **116**, D12109, https://doi.org/10.1029/2010JD015139.

Noma, E., 2013: Package PlotRegionHighlighter, version 1.0. R package, accessed 28 April 2016, https://cran.r-project.org/web/packages/PlotRegionHighlighter/index.html.

Pebesma, E. J., and R. S. Bivand, 2005: Classes and methods for spatial data in R. *R News*, No. 5 (2), R Foundation, Vienna, Austria, 9–13, https://cran.r-project.org/doc/Rnews/Rnews_2005-2.pdf.

Poltoradnev, M., J. Ingwersen, and T. Streck, 2015: Calibration and application of Aquaflex TDT soil water probes to measure the soil water dynamics of agricultural topsoil in southwest Germany. *J. Irrig. Drain. Eng.*, **141**, https://doi.org/10.1061/(ASCE)IR.1943-4774.0000838.

——, ——, and ——, 2016: Spatial and temporal variability of soil water content in two regions of southwest Germany during a three-year observation period. *Vadose Zone J.*, **15**, https://doi.org/10.2136/vzj2015.11.0143.

Qu, W., H. R. Bogena, J. A. Huisman, and H. Vereecken, 2013: Calibration of a novel low-cost soil water content sensor based on a ring oscillator. *Vadose Zone J.*, **12**, https://doi.org/10.2136/vzj2012.0139.

Roger, S., R. S. Bivand, E. J. Pebesma, and V. Gomez-Rubio, 2013: *Applied Spatial Data Analysis with R*. 2nd ed. Springer, 405 pp.

Rosenbaum, U., J. A. Huisman, A. Weuthen, H. Vereecken, and H. R. Bogena, 2010: Sensor-to-sensor variability of the ECH2O EC-5, TE, and 5TE sensors in dielectric liquids. *Vadose Zone J.*, **9**, 181–186, https://doi.org/10.2136/vzj2009.0036.

Schaake, J. C., V. I. Koren, Q.-Y. Duan, K. Mitchell, and F. Chen, 1996: Simple water balance model for estimating runoff at different spatial and temporal scales. *J. Geophys. Res.*, **101**, 7461–7475, https://doi.org/10.1029/95JD02892.

Schaap, M. G., F. J. Leij, and M. Th. van Genuchten, 2001: Rosetta: A computer program for estimating soil hydraulic parameters with hierarchical pedotransfer functions. *J. Hydrol.*, **251**, 163–176, https://doi.org/10.1016/S0022-1694(01)00466-8.

Schaefer, G. L., M. H. Cosh, and T. J. Jackson, 2007: The USDA Natural Resources Conservation Service Soil Climate Analysis Network (SCAN). *J. Atmos. Oceanic Technol.*, **24**, 2073–2077, https://doi.org/10.1175/2007JTECHA930.1.

Scheffer, F., and P. Schachtschabel, 2008: *Lehrbuch der Bodenkunde*. 15th ed. Spektrum Akademischer Verlag, 593 pp.

Seneviratne, S. I., T. Corti, E. L. Davin, M. Hirschi, E. B. Jaeger, I. Lehner, B. Orlowsky, and A. J. Teuling, 2010: Investigating soil moisture–climate interactions in a changing climate: A

review. *Earth-Sci. Rev.*, **99**, 125–161, https://doi.org/10.1016/j.earscirev.2010.02.004.

Šimůnek, J., M. Th. van Genuchten, and M. Šejna, 2006: The HYDRUS software package for simulating the two- and three-dimensional movement of water, heat, and multiple solutes in variably-saturated media. Tech. Manual, 213 pp., https://www.pc-progress.com/downloads/Pgm_Hydrus3D/HYDRUS3D%20Technical%20Manual.pdf.

Skamarock, W. C., and Coauthors, 2008: A description of the Advanced Research WRF version 3. NCAR Tech. Note NCAR/TN-475+STR, 113 pp., https://doi.org/10.5065/D68S4MVH.

Soil Survey Division Staff, 1993: *Soil Survey Manual.* U.S. Department of Agriculture, 375 pp.

van Genuchten, M. Th., 1980: A closed-form equation for predicting the hydraulic conductivity of unsaturated soils. *Soil Sci. Soc. Amer. J.*, **44**, 892–898, https://doi.org/10.2136/sssaj1980.03615995004400050002x.

Vivoni, E. R., J. C. Rodríguez, and C. J. Watts, 2010: On the spatiotemporal variability of soil moisture and evapotranspiration in a mountainous basin within the North American monsoon region. *Water Resour. Res.*, **46**, W02509, https://doi.org/10.1029/2009WR008240.

Wang, Y., M. Shao, Z. Liu, and R. Horton, 2013: Regional-scale variation and distribution patterns of soil saturated hydraulic conductivities in surface and subsurface layers in the loessial soils of China. *J. Hydrol.*, **487**, 13–23, https://doi.org/10.1016/j.jhydrol.2013.02.006.

Wiekenkamp, I., J. A. Huisman, H. R. Bogena, H. S. Lin, and H. Vereecken, 2016: Spatial and temporal occurrence of preferential flow in a forested headwater catchment. *J. Hydrol.*, **534**, 139–149, https://doi.org/10.1016/j.jhydrol.2015.12.050.

Wizemann, H.-D., J. Ingwersen, P. Högy, K. Warrach-Sagi, T. Streck, and V. Wulfmeyer, 2015: Three year observations of water vapor and energy fluxes over agricultural crops in two regional climates of southwest Germany. *Meteor. Z.*, **24**, 39–59, https://doi.org/10.1127/metz/2014/0618.

Wöhling, T., N. Schütze, B. Heinrich, J. Šimůnek, and G. F. Barkle, 2009: Three-dimensional modeling of multiple automated equilibrium tension lysimeters to measure vadose zone fluxes. *Vadose Zone J.*, **8**, 1051–1063, https://doi.org/10.2136/vzj2009.0040.

Wraith, J. M., D. A. Robinson, S. B. Jones, and D. S. Long, 2005: Spatially characterizing apparent electrical conductivity and water content of surface soils with time domain reflectometry. *Comput. Electron. Agric.*, **46**, 239–261, https://doi.org/10.1016/j.compag.2004.11.009.

WRB, 2006: World reference base for soil resources 206. World Soil Resources Rep. 103, 128 pp., http://www.fao.org/tempref/docrep/fao/009/a0510e/a0510e00.pdf.

Yang, Z.-L., and Coauthors, 2011: The community Noah land surface model with multiparameterization options (Noah-MP): 2. Evaluation over global river basins. *J. Geophys. Res.*, **116**, D12110, https://doi.org/10.1029/2010JD015140.

Yeh, T., R. T. Wetherald, and S. Manabe, 1984: The effect of soil moisture on the short-term climate and hydrology change—A numerical experiment. *Mon. Wea. Rev.*, **112**, 474–490, https://doi.org/10.1175/1520-0493(1984)112<0474:TEOSMO>2.0.CO;2.

7. General Discussion

The TDT method is one of the most suitable instruments for continuous real-time in-situ soil moisture measurements (Robinson et al., 2008). The results of my thesis agree with the conclusions of Schwartz et al. (2008) in that the site-specific calibration should be used over the default in order to obtain unbiased measurements of SWC. As a compromise between the labour-intensive effort and reading accuracy, an alternative approach is suggested. It is based on easily measured soil properties and is applicable to soils characterized by the same properties as in KR and SA. The KR pedotransfer-based calibration was impacted by the soil bulk density and electrical conductivity. On SA, total nitrogen content, bulk density and silt fraction influenced the regression. The physical and chemical soil properties, indicated in my thesis as those that affect the TDT readings, have been recognized and discussed by various researchers (Robinson et al. 2003; Gong et al. 2003; Schwartz et al. 2008; Stangl et al. 2009; Rosenbaum et al. 2011; Qu et al. 2013).

The three-year observation period captured very distinct seasons in terms of the balance between rainfall and evapotranspiration. The differences between the seasonal water balance (SWB) were particularly pronounced for KR. The SWB was highly positive in 2010, neutral in 2011 and negative in 2012. The 2010 season was very special compared to 2011 and 2012. It was characterized by a wet spring and fall and a very dry summer. On SA the SWB was always positive. The results showed that the relation between rainfall and $\langle\theta\rangle$ time series is the strongest during the period with positive SWB and weakens with decreasing SWB. Various authors (Famiglietti et al., 1998; Albertson and Montaldo, 2003; De Lannoy et al., 2006; Rosenbaum et al., 2012; Mittelbach and Seneviratne, 2012) noted that the response time of $\langle\theta\rangle$ and σ_θ to a rainfall event depends on precipitation amount, antecedent SWC, and rainfall intensity, among other factors.

Qu et al. (2015) concluded that spatial variability of soil hydraulic parameters exerts a strong control on the σ_θ-$\langle\theta\rangle$ relationship. The findings of my thesis agree with this statement. The seasonal variability of $\langle\theta\rangle$ and σ_θ, expressed through the σ_θ-$\langle\theta\rangle$ phase-space diagrams, is limited by the variability of the soil water retention curves at the bottom of the envelope. The theoretical maximum σ_θ-$\langle\theta\rangle$ was estimated based on the binary soil water scenario – variability in soil texture and structure. The σ_θ-$\langle\theta\rangle$ envelope is the broadest in the intermediate state of SWC. Its

upper and lower bounds collapse at the left and right hand-sides, which reflect the variability of SWC at the permanent wilting point and porosity, respectively. The proximity of σ_θ to the edge of the σ_θ-$\langle\theta\rangle$ envelope and the anchor point considerably determine whether σ_θ will increase or decrease. The shape of the envelope indicates that, under very wet conditions, rainfall may even reduce the spatial variability of SWC if σ_θ approaches the right anchor point from a starting point above σ_θ-$\langle\theta_s\rangle$. Under dry conditions, evapotranspiration may generate spatial variability of SWC if the initial position of σ_θ is at a starting point below σ_θ-$\langle\theta_{wp}\rangle$. In the literature, variation in soil hydraulic properties, water availability for root water uptake and evapotranspiration were indicated to be among the factors that lead to a re-increase of σ_θ during long periods without rainfall, as was the case in July 2010 (Mittelbach and Seneviratne, 2012; Rosenbaum et al., 2012; Fatichi et al., 2015). Implicit evidence for this statement is the result of the Noah-MP simulation run for the same time period, when spatially variable soil texture was introduced, although the modeled σ_θ values were significantly lower than observed (discussed below).

At the event scale, the hysteretic σ_θ-$\langle\theta\rangle$ loops were found to be triggered by rainstorms exceeding a threshold value of rainfall intensity, i.e. 1.1 ± 0.6 mm/h for KR and 2.9 ± 2.8 mm/h for SA. This finding agrees with Rosenbaum et al. (2012) in that the convective (advective) rainfall determines hysteretic (nonhysteretic) σ_θ-$\langle\theta\rangle$ behavior. The loop in σ_θ-$\langle\theta\rangle$ might be a result of non-uniform saturation of the upper 0.15 m soil layer and involve the preferential flow occurrence (Wiekenkamp et al., 2016). On the other hand, it might also be related to the hysteresis of soil water retention curves, but its role remains to be quantified.

My thesis echoes recent findings of Kishne et al. (2017) in that the default soil hydraulic parameterization of Noah-MP needs to be tuned based on on-site measurements. The best match between simulated and observed $\langle\theta\rangle$ values was achieved for the loess soils of KR in 2010, when site-specific rainfall, GVF, LAI and soil texture, specified by VG hydraulic function, were introduced into the Noah-MP model. The same parameterization, however, performed less accurately for those seasons with neutral and negative SWB. During such seasons the observed $\langle\theta\rangle$ at 0.15 m depth often did not respond to a rainfall event, whereas the response of modelled $\langle\theta\rangle$ was well pronounced in all three years. Among the possible reasons for the discrepancy between simulations and measurements is an overestimation of infiltration rates by the model and biases in the simulated evapotranspiration (Chen and Dudhia, 2001; Ingwersen et al., 2011).

The Noah-MP has limitations in modelling the SWC dynamics on SA. These limitations are linked to the shallow soil profile and high stone content of SA soils. Pre-simulations revealed that Noah-MP unavoidably depletes a thin soil column. Therefore, column thickness should have been extended to 2 m, used by default. Unlike KR, none of two hydraulic functions could significantly improve the model performance on SA. Although the VG model is more flexible than CH (Gayler et al., 2013), VG is known to be less accurate in clay soils (van Genuchten, 1980). Moreover, CH has deficiencies in representing the hydraulic properties of rocky soils (Clapp and Hornberger, 1978).

Noah-MP systematically underestimated the spatial variability of SWC in both regions. Introducing site-specific parameters improved the model performance, but in most cases most of the σ_θ-$\langle\theta\rangle$ data points were located below the bottom edge of the envelope. Among the factors that lead to insufficient representation of spatial SWC variability, the following are considered: missing topography and terrain information, inadequate representation of the spatial variability of soil texture and hydraulic parameters, and the model assumption of a uniform root distribution. Individual effects of these factors on model outcomes have been observed in various studies (e.g. Wöhling et al., 2009; Ingwersen et al., 2011; Kishne et al., 2017). On one hand, it is expected that the σ_θ is greater at point scale measurements than at the coarse grid spacing usually employed in weather and climate simulations. On the other hand, several simulation studies (Gantner and Kalthoff, 2010; Huang and Margulis, 2013) and observational case studies (Taylor et al., 2007) have shown that spatial SWC variability strongly influences the structure of the turbulence in the boundary layer, the formation and distribution of clouds, as well as location of convective rainfall on much finer scales. Huang and Margulis (2013) report that the amount of clouds and cloud-covered areas increases with increasing soil moisture variability. Estimations based on the input data published in Huang and Margulis (2013) show that the minimum and maximum σ_θ of a 10 km × 10 km domain corresponds to 5.0 Vol.% (the soil moisture variability length scale is 1.25 km) and 11.6 Vol.% (the soil moisture variability length scale is 5 km), respectively. As a reference, in my thesis the average σ_θ of the middle domain (9 km x 9 km, including 5 stations of the inner domain and 8 stations of the middle domain) of KR and SA networks was 4.4 and 7.0 Vol.%, respectively, for the data set of the 2010 season. Finally, Mascaro and Vivoni (2012) demonstrated that downscaling satellite-based soil moisture delivers a more realistic spatial SWC distribution. This might help to improve the simulation of

hydrological processes and surface fluxes, particularly evapotranspiration and runoff (Vivoni et al., 2010).

8. Final Conclusions

In my thesis, the regional average SWC ($\langle\theta\rangle$) and its spatial variability (σ_θ) were analyzed based on the data obtained from two regional soil moisture networks. High-leverage soil properties affecting the TDT readings in KR and SA were determined, and both pedotransfer and site-specific calibrations were developed. When soils have similar textures and properties, as in KR and SA, the pedotransfer-based approach might be used over the factory Aquaflex TDT calibration, especially when many sensors are available and the time and resources are lacking to perform on-site calibrations. The latter delivered the best agreement between gravimetrically determined SWCs and TDT-sensed SWCs. Sensor calibrations in the KR region were affected by soil bulk density and electrical conductivity. Total nitrogen content, soil bulk density and silt content entered the SA pedotransfer calibration.

The evaluation of a three-year data set of topsoil SWC and rainfall record revealed the factors that control the σ_θ-$\langle\theta\rangle$ relationship at seasonal and event scales. The anchor points in the σ_θ-$\langle\theta\rangle$ phase-space are determined by the regional variability of soil texture and soil structure. The lower and the upper bounds of the envelope reflect, respectively, the regional variability of soil water retention curves and the binary variability of SWC at the saturation and wilting point. The σ_θ-$\langle\theta\rangle$ envelope is the broadest in the intermediate SWC state and narrows towards the two anchor points. At the edges of the envelope the momentary location of σ_θ in relation to the anchor points and the upper and lower bounds of the σ_θ-$\langle\theta\rangle$ envelope determines whether SWC variability increases or decreases upon a change in $\langle\theta\rangle$. At the event scale, most hysteretic σ_θ-$\langle\theta\rangle$ loops occurred in the intermediate and intermediate/wet state. The initiation of clockwise hysteretic loops is triggered by rainstorms with spatially highly variable intensities.

Noah-MP delivered fairly accurate $\langle\theta\rangle$ for the loess soils of KR, but had limitations for the shallow, clayey and stony soils of SA. The best match was achieved with the VG representation of soil hydraulic functions and with site-specific rainfall, soil texture, GVF and LAI input data. The simulation of $\langle\theta\rangle$ is the best in seasons with positive water balance ($R>ET_c$).

Noah-MP systematically underestimated the spatial variability of SWC at the point scale (representing few square meters). This issue needs to be further investigated if Noah-MP is to be used on finer (e.g. LES) scales. Most of the modelled σ_θ-$\langle\theta\rangle$ pairs were located outside the envelope of measurements and below the lower bound. The insufficient representation of spatial

SWC variability by Noah-MP can be mainly attributed to missing topography and terrain information, inadequate representation of spatial variability of soil texture and hydraulic parameters, and the model assumption of a uniform root distribution. The results of my thesis underline the potential utility for various disciplines of further validating the Noah-MP simulation of regional SWC variability against high-resolution remotely sensed soil moisture data. This would be all the more important considering the recent scientific and practical interest in downscaling of satellite-based soil moisture and improvements in the spatial representation of SWC reported by a number of studies.

Acknowledgments

My PhD thesis was a part of the German Research Foundation (DFG) in the frame of PAK 346 “Structure and functions of agricultural landscapes under climate change – processes and projections on a regional scale” and the research unit FOR 1695 “Regional climate change”. I also acknowledge the Iamonet Erasmus Mundus Scholarship Program and personally Dr. Heinrich Schüle for giving me the opportunity to begin studies in Hohenheim University.

I am thankful for all those, who contributed to my work: Prof. Dr. Thilo Streck – for being kind to let me take part in the project from the very beginning, openness for discussions and criticism; Dr. Joachim Ingwersen – literary for everything, starting from the field, teaching how to solder wires of a sensor, and finishing with endless patience in guiding me through the process of data evaluation to the final manuscript submission; Thilo and Joachim, thank you for your support and your time; Elke Feiertag and Erhard Strohm – for helping with laboratory tests and equipment; Sybille Schulz – for clarifying numerous administrative questions; 38 farmers of Kraichgau and Swabian Alb regions – for driving their vehicles around the sensor area, thus letting the measurements run permanently; the teams of the car park and mechanics workshop of Hohenheim University – the former, for being patient to sometimes accept dirty cars, the latter, for fixing the sensors, that were accidently ploughed; Michael Stachovitsch – for reading out my manuscripts and present thesis.

I thank Prof. Dr. Andreas Fangmeier and Prof. Dr. Volker Wulfmeyer for investing their time.

I am also grateful to those, without whom it is impossible to imagine myself where I am now: mom and dad, thank you for bringing me up the person I am; grandma, thank you for pushing me to study and broaden my mind; bro, thank you for your emotional support, it always encourages me to keep on going. I am especially thankful to my destiny and the spring of my inspiration – Olga, my lovely wife, and Vladislav, my boy – thank you for the support and light during gloomy days, as well as numerous moments of joy. Since the time we began our walk hand in hand, you give me strengths to make a step and lighten my breath. All my friends in Hohenheim – Robert, Fetewei, Tasso, Sebastian, Zorica, Basanta and many others (I am sorry not to mention everyone, well, you know, cheers!) – big hug! One goes to my friend Slava. Ivanich, without your commitment and realism our longstanding conversation behind the desk in MSU would

have ended up just a conversation. Thank you for putting me on the ground sometimes and shaping a vector out of my impulse, turning it to an effort. Special thanks goes to Konstantin Müller for his kind heart and support.

References

Albertson, J.D., and N. Montaldo. 2003. Temporal dynamics of soil moisture variability: 1. Theoretical basis. *Water Resources Research*, 39(10), 1274.

Avissar, R., and Y. Liu. 1996. Three-dimensional numerical study of shallow convective clouds and precipitation induced by landsurface forcing. *Journal of Geophysical Research*, 101, 7499-7518.

Barthlott, C. and N. Kalthoff. 2011. A numerical sensitivity study on the impact of soil moisture on convection-related parameters and convective precipitation over complex terrain. *Journal of Atmospheric Sciences*, 68, 2971-2987.

Brocca, L., Tullo, T., Melone, F., Moramarco, T., and R. Morbidelli. 2012. Catchment scale soil moisture spatial-temporal variability. *Journal of Hydrology*, 422-423, 63-75.

Chen, F., and J. Dudhia. 2001. Coupling an advanced land surface-hydrology model with the Penn-State-NCAR MM5 modelling system. Part I. Model implementation and sensitivity. *Monthly Weather Review*, 129(4), 569-585.

Clapp, B.R., and G.M. Hornberger. Empirical equations for some soil hydraulic properties. *Water Resources Research*, 14(4), 601-604.

Cosby, B.J., Hornberger, G.M., Clapp, R.B., and T.R. Ginn. 1984. A statistical exploration of the relationships of soil moisture characteristics to the physical properties of soil. *Water Resources Research*, 20, 682-690.

De Lannoy, G.J.M., Verhoest, N.E.C., Houser, P.R., Gish, T.J., and M. Van Meirvenne. 2006. Spatial and temporal characteristics of soil moisture in an intensively monitored agricultural field (OPE3). *Journal of Hydrology*, 331, 719-730.

Dirmeyer, P.A., and K.L. Brubaker. 1999. Contrasting evaporative moisture sources during the drought of 1988 and the flood of 1993. *Journal of Geophysical Research*, 104, 19383-19397.

Dorigo, W.A., Wagner, W., Hohensinn, R., Hahn, S., Paulik, C., Xaver, A., Gruber, A., Drusch, M., Mecklenburg, S., van Oevelen, P., Robock, A., and T. Jackson. 2011. The international soil moisture network: a data hosting facility for global in situ soil moisture measurements. Hydrological Earth Systems Sciences, 15(5), 1675-1698.

Ek, M., and A.A.M. Holtslag. 2004. Impact of soil moisture on boundary-layer cloud development. *Journal of Hydrometeorology*, 5, 86-99.

Eltahir, E. 1998. A soil moisture–rainfall feedback mechanism. 1: Theory and observations. *Water Resources Research*, 34, 765-776.

Famiglietti, J.S., Rudnicki, J.W., and M. Rodell. 1998. Variability in surface moisture content along a hillslope transect: Rattlesnake hill, Texas. *Journal of Hydrology*, 210, 259-281.

Famiglietti, J.S., Ryu, D., Berg, A.A., Rodell, M., and T.J. Jackson. 2008. Field observations of soil moisture variability across scales. *Water Resources Research*, 44, W01423.

Fatichi, S., Katul, G.G., Ivanov, V.Y., Pappas, C., Paschalis, A., Consolo, A., Kim, J., and P. Burlando. 2015. Abiotic and biotic controls of soil moisture spatiotemporal variability and the occurrence of hysteresis. *Water Resources Research*, 51, 3505-3524.

Fischer, E.M., S.I. Seneviratne, Luethi, D., and C. Schaer. 2007. Contribution of land-atmosphere coupling to recent European summer heat waves. *Geophysical Research Letters*, 34, L06707.

Gantner, L., and N. Kalthoff. 2010. Sensitivity of a modelled life cycle of a mesoscale convective system to soil conditions over West Africa. *Quarterly journal of the royal meteorological society*, 136(s1), 471-482.

Gayler, S., Ingwersen, J., Priesack, E., Wöhling, T., Wulfmeyer, V., and S. Thilo. 2013. Assessing the relevance of subsurface processes for the simulation of evapotranspiration and soil moisture dynamics with CLM3.5: comparison with field data and crop model simulations. *Environmental Earth Sciences*.

van Genuchten, M. Th. 1980. A closed-form equation for predicting the hydraulic conductivity of unsaturated soils. *Soil Science Society of America Journal*, 44, 892-898.

Georgakakos, K.P., Bae, D.-H., and D. R. Cayan. 1995. Hydroclimatology of continental watersheds, 1, Temporal analyses. *Water Resources Research*, 31(3), 655-675.

Gong, Y., Cao, Q., and Z. Sun. 2003. The effects of soil bulk density, clay content and temperature on soil water content measurement using time-domain reflectometry. *Hydrological Processes*, 17, 3601-6314.

Grayson, R.B., Western, A.W., Chiew, F.H.S., and G. Bloschl. 1997. Preferred states in spatial soil moisture patterns: Local and nonlocal controls, *Water Resources Research*, 33(12), 2897-2908.

Hauck, C., Barthlott, C., Krauss, L., and N. Kalthoff. 2011. Soil moisture variability and its influence on convective precipitation over complex terrain. *Quarterly Journal of the Royal Meteorological Society*, 137, 42-56.

Heathman, G.C., Cosh, M.H., Merwade, V., and E. Han. 2012. Multi-scale temporal stability analysis of surface and subsurface soil moisture within the upper Cedar Creek watershed, Indiana. *Catena*, 95, 91-103.

Hohenegger, C., Brockhaus, P., Bretherton, C.S., and C. Schar. 2009. The soil moisture–precipitation feedback in simulations with explicit and parameterized convection. *Journal of Climate*, 22, 5003-5020

Huang, J., van den Dool, H.M., and K.P. Georgakakos. 1996. Analysis of model-calculated soil moisture over the United States (1931-1993) and applications to long-range temperature forecasts. *Journal of Climate*, 9, 1350-1362.

Huang, H. Y., and S. A. Margulis. 2013. Impact of soil moisture heterogeneity length scale and gradients on daytime coupled land-cloudy boundary layer interactions. *Hydrological Processes*, 27, 1988-2003.

Ingwersen, J., Steffens, K., Högy, P., Warrach-Sagi, K., Zhunusbayeva, D., Poltoradnev, M., Gäbler, R., Wizemann, H.-D., Fangmeier, A., Wulfmeyer, V., and T. Streck. 2011. Comparison of Noah simulations with eddy covariance and soil water measurements at a winter wheat stand. *Agriculture and Forest Meteorology*, 151, 345-355.

Kishne, A.Sz., Tadasse Yimam, Y., Morgan, L.S.C., and B.C. Dornblaser. 2017. Evaluation and improvement of the default soil hydraulic parameters for the Noah Land Surface Model. *Geoderma*, 285, 247-259.

Koch J., Cornelissen T., Fang Z., Bogena H., Diekkruger B., Kollet S., Stisen S. 2016. Inter-comparison of three distributed hydrological models with respect to seasonal variability of soil moisture patterns at a small forested catchment. *Journal of Hydrology*, 533, 234-249.

Koster, R.D., et al. 2004. Regions of strong coupling between soil moisture and precipitation, *Science*, 305, 1138-1140.

Leib, B.G., Jabro, J.D., and G.R. Matthews. 2003. Field evaluation and performance comparison of soil moisture sensors. *Soil Science*, 168, 396-408.

Mascaro, G., and E.R. Vivoni. 2012. Utility of coarse and downscaled soil moisture products at L-band for hydrologic modeling at the catchment scale. *Geophysical Research Letters*, 39, L1043.

Mittelbach, H., and S.I. Seneviratne. 2012. A new perspective on the spatio-temporal variability of soil moisture: Temporal dynamics versus time-invariant contributions. *Hydrology and Earth System Sciences*, 16, 2169-2179.

Morari, F., and L. Giardini. 2002. Irrigation automation with heterogeneous vegetation: The case of the Padova botanical garden. *Agricultural Water Management*, 55, 183-201.

Niu, G.-Y., Yang, Z.-L., Mitchell, K.E., Chen, F., Ek, M.B., Barlage, M., Kumar, A., Manning, K., Niyogi, D., Rosero, E., Tewari, M., and Y. Xia. 2011. The community Noah land surface model with multiparameterization options (Noah-MP): 1. Model description and evaluation with local-scale measurements. *Journal of Geophysical Research*, 116, D12109.

Pan, F., and C.D. Peters-Lidard. 2008. On the Relationship Between Mean and Variance of Soil Moisture Fields. *Journal of the American Water Resources Association*, 44(1), 235-242.

Patton, E., Sullivan, P., and C. Moeng. 2005. The influence of idealized heterogeneity on wet and dry planetary boundary layers coupled to the land surface. *Journal of Atmospherical Sciences*, 62, 2078-2097.

Qu, W., Bogena, H.R., Huisman, J.A., Vanderborght, J., Schuh, M., Priesack, E., and H. Vereecken. 2015. Predicting subgrid variability of soil water content from basic soil information. *Geophysical Research Letters*, 42, 789-796.

Robinson, D.A., Campbell, C.S., Hopmans, J.W., Hornbuckle, B.K., Jones, S.B., Knight, R., Ogden, F., Selker, J., and O. Wendroth. 2008. Soil moisture measurement for ecological and hydrological watershed-scale observatories: A review. *Vadose Zone Journal*, 7, 358-389.

Robock, A., Luo, L., Wood, E.F., Wen, F., Mitchell, K.E., Houser, P.R., Schaake, J.C., Lohmann, D., Cosgrove, B.A., Sheffield, J., Duan, Q., Higgins, R.W., Pinker, R.T., Tarpley, J.D., Basara, J.B., and K.C. Crawford,. 2003. Evaluation of the North American land data assimilation system over the southern Great Plains during the warm season. *Journal of Geophysical Research*, 108, GCP 7-GCP 21.

Rosenbaum, U., Huisman, J.A., Vrba, J., Vereecken, H., and H.R. Bogena. 2011. Correction of temperature and electrical conductivity effects on dielectric permittivity measurements with ECH2O sensors. *Vadose Zone Journal*, 10, 582-593.

Rosenbaum, U., Bogena, H.R., Herbst, M., Huisman, J.A., Peterson, T.J., Weuthen, A., Western, A.W., and H. Vereecken. 2012. Seasonal and event dynamicsof spatial soil moisture patterns at the small catchment scale. *Water Resources Research*, 48, 10544-10566.

Seneviratne, S.I., Corti, T., Davin, E.L., Hirschi, M., Jaeger, E.B., Lehner, I., Orlowsky, B., and A.J. Teuling. 2010. Investigating soil moisture–climate interactions in a changing climate: A review. *Earth Sciences Review*, 99(3-4), 125-161.

Schwartz, B.F., Schreiber, M.E., Pooler, P.S., and J.D. Rimstidt. 2008. Calibrating access-tube time domain reflectometry soil water measurements in deep heterogeneous soils. *Soil Science Society of America Journal*, 72, 917-930.

Stangl, R., Buchan, G.D., and W. Loiskandl. 2009. Field use and calibration of a TDR-based probe for monitoring water content in a high-clay landslide soil in Austria. *Geoderma*, 150, 23-31.

Taylor, C.M., Parker, D.J., and P.P. Harris. 2007. An observational case study of mesoscale atmospheric circulations induced by soil moisture. *Geophysical research letters*, 34, L15801.

Vereecken, H., Kamai, T., Harter, T., Kasteel, R., Hopmans, J., and J. Vanderborght. 2007. Explaining soil moisture variability as a function of mean soil moisture: A stochastic unsaturated flow perspective. *Geophysical Research Letters*, 34, L22402.

Vivoni, E.R., Rodrı´guez, J.C., and C.J. Watts. 2010. On the spatiotemporal variability of soil moisture and evapotranspiration in a mountainous basin within the North American monsoon region. *Water Resources Research*, 46, W02509.

Weaver, C.P., and R. Avissar. 2001. Atmospheric disturbances caused by human modification of the landscape. *Bulletin of the American Meteorological Society*, 82, 269-281.

Wiekenkamp, I., Huisman, J.A., Bogena, H.R., Lin, H.S., and H. Vereecken. 2016. Spatial and temporal occurrence of preferential flow in a forested headwater catchment. *Journal of Hydrology*, 534, 139-149.

Wöhling, T., Schütze, N., Heinrich, B., Šimůnek, J., and G.F. Barkle. 2009. Three-dimensional modeling of multiple automated equilibrium tension lysimeters to measure vadose zone fluxes. *Vadose Zone Journal*, 8, 1051-1063.

Wraith, J.M., Robinson, D.A., Jones, S.B., and D.S. Long. 2005. Spatially characterizing apparent electrical conductivity and water content of surface soils with time domain reflectometry. *Computers and Electronics in Agriculture*, 46, 239-261.

Yang, Z.-L., Niu, G.-Y., Mitchell, K. E., Chen, F., Ek, M. B., Barlage, M., Manning, K., Niyogi, D., Tewari, M., and Y. Xia. 2011. The community Noah land surface model with multiparameterization options (Noah-MP): 2. Evaluation over global river basins. *Journal of Geophysical Research*, 116, D12110.

Zreda, M., Desilets, D., Ferre, T.P.A., and R.L. Scott. 2008. Measuring soil moisture content non-invasively at intermediate spatial scale using cosmic-ray neutrons. *Geophysical Research Letters*, 35, L21402.

Curriculum vitae

Name:	Poltoradnev Maxim
Date of Birth:	03/09/1986
Place of Birth:	Tula, Russia
Marital status:	Married, 1 kid

Education

Since 11/2008	**Universität Hohenheim, Stuttgart, Germany** PhD student, Biogeophysics
05/2008 – 10/2008	**Universität Hohenheim, Stuttgart, Germany** Erasmus Mundus External Cooperation Window 2008, one semester Master of Science Program, specialization in Agriculture
09/2003 – 06/2008	**Moscow Lomonosov State University, Moscow, Russia** Soil Science institute, faculty of Soil Physics and Land Reclamation, Bachelor and Master Diploma, graduated with high honors

Professional Expertise

Soil science, soil physics, plant nutrition, agronomy

Publications

Ingwersen, J., Steffens, K., Högy, P., Warrach-Sagi, K., Zhunusbayeva, D., Poltoradnev, M., Gäbler, R., Wizemann, H.-D., Fangmeier, A., Wulfmeyer, V., and T. Streck (2011). "Comparison of Noah simulations with eddy covariance and soil water measurements at a winter wheat stand." *Agricultural and Forest Meteorology*, 151, 345.

Mirzaeitalarposhti, R., Scott Demyan, M., Rasche, F., Poltoradnev, M., Cadisch, G., and T. Müller (2015). "MidDRIFTS-PLSR-based quantification of physico-chemical soil properties across two agroecological zones in Southwest Germany: generic independent validation surpasses region specific cross-validation." *Nutrient cycling in agroecosystems*, 102(2).

Publications, included in the doctoral thesis:

Poltoradnev, M., Ingwersen, J., and T. Streck (2015). "Calibration and application of Aquaflex TDT soil water probes to measure the soil water dynamics of agricultural topsoil in Southwest Germany." *Irrigation and Drainage Engineering*, 141(6), 04014072.

Poltoradnev, M., Ingwersen, J., and T. Streck (2016). "Spatial and Temporal Variability of Soil Water Content in Two Regions of Southwest Germany during a Three-Year Observation Period." *Vadose Zone Journal*, 15(6).

Poltoradnev, M., Ingwersen, J., Imukova, K., and T. Streck (2017). "How well does Noah-MP simulate the regional mean and spatial variability of topsoil water content in two agricultural landscapes in southwest Germany?" *Journal of Hydrology* (submitted).